THE USE OF FINITE TRANSMISSION LINE ELEMENTS IN NUMERICAL ANALYSIS.

GEOFFREY FERGUSON SLATER, B.Sc.

Thesis submitted to the University of Nottingham
for the degree of Doctor of Philosophy, October, 1973.

Department of Electrical and Electronic Engineering
University of Nottingham.

SUMMARY.

The complex nature of solving microwave circuit problems with their many varied boundary conditions, precludes direct analysis utilising the basic laws involved. This thesis describes methods that have been developed to determine the defining parameters of such problems. The methods are based on numerical techniques, using a digital computer to perform the calculations.

The finite difference and element techniques are reviewed briefly and extensions made into the analysis of three dimensional configurations. The difficulties of such methods are also discussed. The evolution of the steady state transmission line element method from the finite difference/element techniques is shown to possess many distinct advantages over the more conventional techniques, notably that of the ease in which it is formulated.

Examples of rectangular, circular and elliptical wave guide analysis are shown, and comparisons formed with finite difference/element analysis where necessary. Proposals are also introduced whereby the method may be utilised to provide a wide range of microwave characteristics, with little or no alterations to existing procedures. The adaptation to other fields of interest, such as those associated with structural or fluid dynamics was also briefly noted.

ACKNOWLEDGEMENTS.

The author wishes to extend his thanks to

Mr. P. B. Johns for his continual advice, encouragement and interest throughout this project.

Professor J. E. Parton for extending to him the facilities of the Electrical and Electronic Engineering Department.

The Science Research Council for providing financial assistance.

Mrs. Marilyn Slater, the author's wife, for her patience and understanding.

Parts of this thesis have been submitted for publication as

(i) Slater, G. F., and Johns, P.B. :

Solution of waveguide problems by steady state analysis of a transmission-line matrix.

Submitted to Proc. IEE.

(ii) Johns, P.B., and Slater, G. F. :

Transient analysis of waveguides with curved boundaries.

Submitted to Electronic Letters.

TABLE OF CONTENTS.

CHAPTER 1.

INTRODUCTION.

The area of microwave circuits is a branch of electromagnetic field theory and must therefore involve the physical laws, described by Maxwells equations, for such a theory. Since these equations are essentially partial differential equations, their solution must depend heavily on initial and boundary conditions. The large variety of such possible conditions eliminates any hope of obtaining simple analytical solutions for some parameter or field descriptions for the structure involved. Consequently the engineer developing such circuitry largely resorts to computer orientated numerical techniques enabling the circuit's performance and characteristics to be examined.

The propagation of electromagnetic waves are governed by the now classical Maxwells equations

$$\begin{aligned} \nabla \wedge \underline{H} &= \frac{\partial \underline{D}}{\partial t} + \underline{J} \\ \nabla \wedge \underline{E} &= -\frac{\partial \underline{B}}{\partial t} \\ \nabla . \underline{D} &= \rho \\ \nabla . \underline{B} &= 0 \end{aligned} \tag{1.1}$$

together with the relationships that concern the medium in which propagation occurs

$$\begin{aligned} \underline{D} &= \epsilon_o \epsilon_r \underline{E} \\ \underline{B} &= \mu_o \mu_r \underline{H} \\ \underline{J} &= \sigma \underline{E} \end{aligned} \tag{1.2}$$

where $\epsilon_o, \epsilon_r, \mu_o, \mu_r, \sigma,$ describe the permittivity, permeability and conductivity of the medium, which is assumed to be homogeneous, isotropic and source free.

For propagation in a perfect dielectric, containing no charges and conduction currents, it can be shown that

$$\nabla^2 \underline{E} = \mu_o \mu_r \epsilon_o \epsilon_r \frac{\partial^2 \underline{E}}{\partial t^2}$$

$$\nabla^2 \underline{H} = \mu_o \mu_r \epsilon_o \epsilon_r \frac{\partial^2 \underline{H}}{\partial t^2} \qquad (1.3)$$

Equations (1.3) are the vector wave equations and by considering the field components of either the electric or magnetic field vectors, the vector wave equation reduces to that of the scalar wave equation

$$\nabla^2 \phi = \mu\epsilon \frac{\partial^2 \phi}{\partial t^2} \qquad (1.4)$$

where ϕ represents any field component; $\mu = \mu_o \mu_r$ and $\epsilon = \epsilon_o \epsilon_r$

If it is assumed that the electric or magnetic fields possess periodic variations in time such that they may be analysed in terms of the complex exponential function e^{jwt}, and also if a field dependence in one direction is also assumed to be of the form $e^{-\gamma z}$, where γ is a constant which typifies propagation and z is the direction where knowledge of the propagation is assumed, then the scalar wave equation (1.4) becomes

$$\nabla_{xy}^2 \phi + k^2 \phi = 0 \qquad (1.5)$$

where

$$k^2 = \omega^2 \mu\epsilon - \gamma^2$$

Equation (1.5) is an elliptic partial differential equation[1] and is known as the two dimensional Helmholtz equation. It is this equation which is widely used to determine the propagating characteristics and field descriptions of electromagnetic waves for a vast range of microwave circuits and configurations.

Most of the present methods of solving equation (1.5) is to consider a region R bounded by a closed boundary S, over which equation (1.5) is assumed to hold, and is applicable to most of the present day microwave circuitry applications. A number of techniques are available to solve the two dimensional Helmholtz equation. Apart from the analytical methods which become restrictive due to the many boundary conditions that may be imposed on S, the development of high speed digital computers have enabled recourse to numerical procedures for evaluation of the particular parameters which are defined by the structure under analysis.

The finite difference technique was applied to electromagnetic waveguides and cavities as early as 1946 by Motz[2] and entails dividing the region under investigation into a net of small but finite mesh size. At each intersection of the net or node, the potential existing at that node is expressed as a function of the potentials existing at the immediate neighbouring nodes. In this manner a difference equation is formed at each node in the region considered, resulting in the replacement of the scalar Helmholtz equation by a large number of simultaneous linear algebraic equations. Subsequent investigations closely followed, Collins and Daly[3], Davies and Muilwyk[4] and more recently Sinnott[5] and Corr[6] applied themselves to the development of the method to include various arbitrary waveguide structures.

A similar approach to the finite difference technique, the finite element technique, was developed by Zienkiewicz[7,8] for use in structural mechanics, but was also applied to vibrating membrane problems, which is a boundary value problem and for which Helmholtz's equation can be used to describe the particular modes of vibrations and displacements. Silvester[9], Arlett[10], and Daly[11] applied this form of

solution to the wave equation to similar regions as those investigated by finite difference techniques. The finite element method relies on a variational approach, which is based on the concept that the integral of some function typical of a system has a smaller value for the actual performance than it would have for any other assumed performance. The method approximates the region under consideration by polygonal sub domains or elements randomly orientated. Within such sub domains the fields are approximated by piecewise plane functions uniquely defined over each element. Use of these elements give rise to vertices across the region at each of which the appropriate finite element equation is derived. As in the finite difference approximation a large number of simultaneous linear equations arise.

The two methods briefly described above are by no means the only ones available for solving the scalar Helmholtz equation, but are those most commonly employed. There has, however, been a flourish of new techniques and adaptive procedures to provide solutions to the wave equation and have been reviewed briefly by Davies[12] who proposes in answer to the question 'Which is the best method of solving our wave guide problem?' that it is dependent on the requirements of the user; viz., as to what region is being analysed, the suitability of the particular method to various waveguide geometries, the possibility of requiring dominant and higher modes, or field values, and also the main influential factor, computer running time and available store. This reasoning is essentially valid, but one factor not considered by many, is the degree of ease with w hich any particular method is formulated for computational use.

It is proposed here to develop a method which incorporates most if not all the points Davies raises, and which is basically simple in conception and use, a method to which an engineer can readily adapt himself, since it contains no detailed mathematical procedures inherent in such techniques described before, other than that of basic transmission line theory.

The first part of the investigations concerned reviewing the salient points of the finite difference/element techniques, the difficulties encountered and the accuracy of solutions for several spatial discretizations of the regions analysed in two dimensions.

The feasibility of analysing three dimensional structures by the finite element technique utilising a simple cubic element, derived in the text, was studied and initially applied to a homogeneous rectangular cavity producing results to a good degree of accuracy. The three dimensional analysis and element was also applied to a homogeneous rectangular cavity containing an axially continuous stripline. By minimizing the stored electrostatic energy between the two conductors the characteristic impedance of the structure could be calculated. The continuous microstrip structure also examined necessitated the inclusion of a dielectric slab. Because of the inhomogeneity of the cavity and lacking a formal variational expression for such a configuration, a quasi-static approach was assumed and again the characteristic impedance of the system calculated. Both configurations gave reasonable solutions. The final part of this section investigated the possibility of adapting the variational expression utilised in two dimensional analysis to describe propagation in a three dimensional in homogeneous rectangular cavity. The derived expression, although an incomplete one, yielded surprisingly accurate

solutions for the structure, but the limitations produced by the derivation of the variational expression did not warrant further analysis for the general purpose of this investigation.

Subsequent chapters producedan entirely new numerical technique of solving microwave problems evolved from the methods of finite differences/elements and consisted of modelling the cross-section of various waveguide structures by a mesh of intersecting transmission lines. Identities were formed between the voltages and currents on the mesh of transmission lines with the field components that exist within a waveguiding system governed by Maxwells field equations. Essentially the method (the steady state transmission line element method) replaced the linear potential function between mesh intersections in the finite difference/element methods by a circular function and could thus describe the field variations in waveguides of a rectangular geometry exactly and provide a much improved solution, (than those of the finite difference/element techniques) to those geometries which are non-rectangular.

The method possesses the advantages of providing solutions, characterizing the cut-off of the dominant and higher ordered modes, to a good degree of accuracy for any shape of waveguide, together with the field descriptions throughout the structure. The method is easily formulated since only basic transmission line theory is utilised and the solution to a large system of simultaneous linear algebraic equations is avoided. The computational store is minimal, all calculations being performed on a machine of immediate access store 12 kbyte and no backing store. No attempt was made to form a generalised program to deal with

configurations of arbitrary shape, due to the store limitations imposed by the computer used; most of the store being used to accommodate the description of the structure under investigation. Naturally, however, no difficulty is foreseen if a generalised program is to be written. The disadvantage of this method is the relatively long machine run time that is required to obtain the solutions, because of the numerous trigonometrical calculations that have to be performed, and as yet no procedure has been produced to minimize the run time necessary.

However, it must be appreciated that the steady state transmission line element method as it stands is still in a very early stage of development and is capable of affording a vast quantity of further interesting, absorbing and worthwhile research.

C H A P T E R 2 .

FINITE DIFFERENCE/FINITE ELEMENT FORMULATION OF THE HELMHOLTZ EQUATION.

Previous discussion implied that the most commonly used techniques to solve the two dimensional Helmholtz equation were those of finite difference and finite element approximations. It is accepted that the Helmholtz equation is that which governs the propagation of electromagnetic waves and since a dependence of $e^{-\gamma z}$ was assumed for propagation in the z co-ordinate direction, it is only necessary to restrict subsequent investigations to those concerning the cross-section of the particular structure to be analysed i.e. two dimensional regions R bounded by closed contours S. Two methods of investigation are considered; finite difference approximation of the Helmholtz equation using a Taylor series expansion, and an analysis using finite elements. Both methods are applied to a general multiply connected two dimensional region R, consisting of two subregions R_1 R_2; R_1 being bounded by C_1 and C_2 and R_2 by C_3 as shown in fig. (2.1.). Regions R_1 and R_2 consist of uniform, sectionally constant, isotropic, source free dielectric media of relative permittivities ϵ_{r_1}, ϵ_{r_2} respectively. The analysis for both methods is performed over the rectangular cartesian system of co-ordinates.

The mode of propagation in such a structure is governed by Maxwell's field equations, which in terms of their field components become

$$\frac{\partial E_z}{\partial y} + \gamma E_y = -j\omega\mu_0 H_x \quad ; \quad \frac{\partial H_z}{\partial y} + \gamma H_y = j\omega\epsilon_0\epsilon_{ri} E_x$$

$$-\frac{\partial E_z}{\partial x} - \gamma E_x = -j\omega\mu_0 H_y \quad ; \quad -\frac{\partial H_z}{\partial x} - \gamma H_x = j\omega\epsilon_0\epsilon_{ri} E_y \qquad (2.1)$$

$$\frac{\partial E_y}{\partial x} - \frac{\partial E_x}{\partial y} = -j\omega\mu_0 H_z \quad ; \quad \frac{\partial H_y}{\partial x} - \frac{\partial H_x}{\partial y} = j\omega\epsilon_0\epsilon_{ri} E_z$$

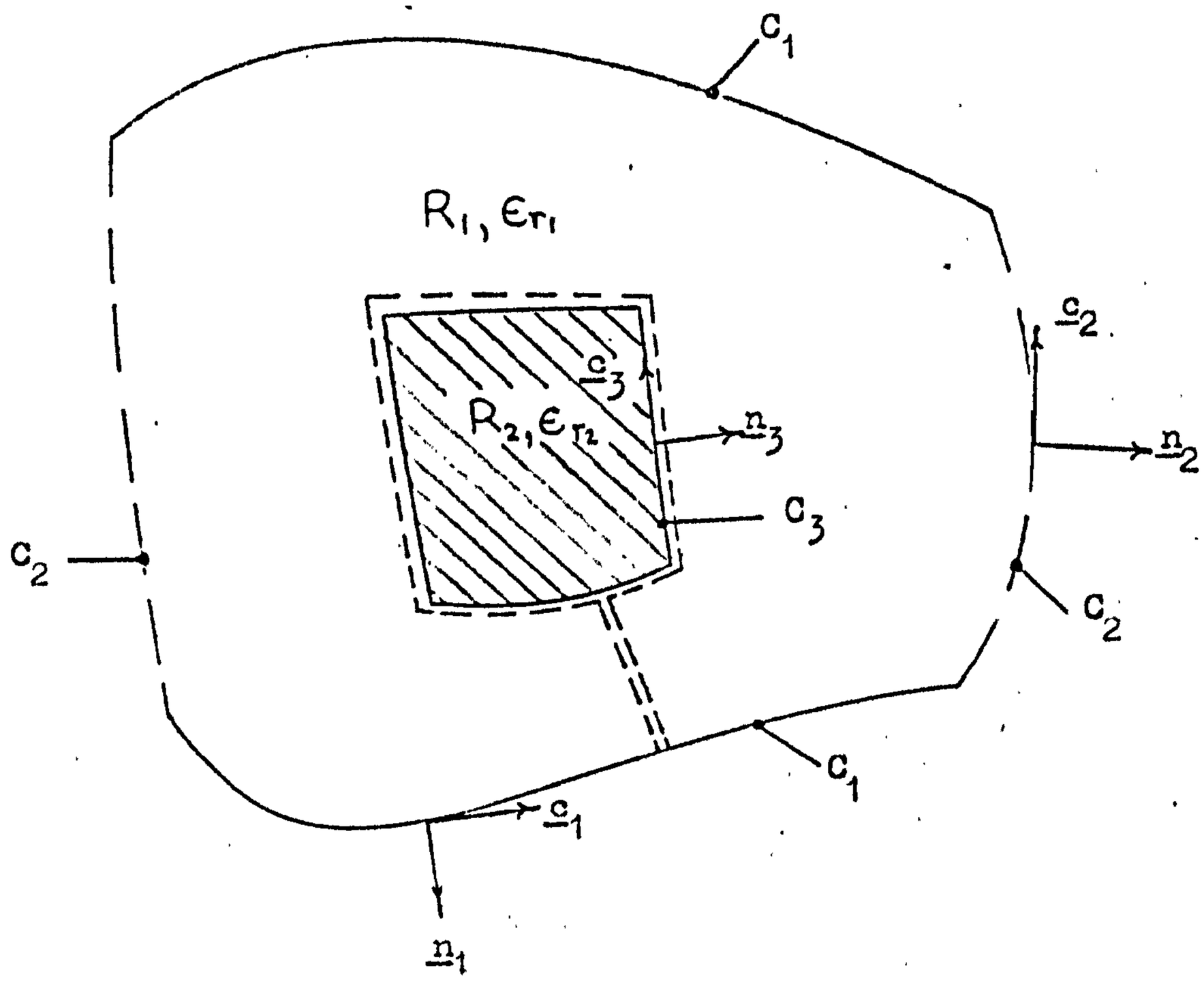

Fig.(2.1.) General multiply connected two dimensional region.

The transverse field components can however be expressed in terms of the axially directed field components, by suitable manipulation of equation (2.1.) yielding

$$E_x = \frac{-1}{k_i^2}\left[\gamma \frac{\partial E_z}{\partial x} + j\omega\mu_o \frac{\partial H_z}{\partial y}\right]$$

$$E_y = \frac{-1}{k_i^2}\left[\gamma \frac{\partial E_z}{\partial y} - j\omega\mu_o \frac{\partial H_z}{\partial x}\right] \qquad (2.2)$$

$$H_x = \frac{-1}{k_i^2}\left[-j\omega\epsilon_o\epsilon_{ri} \frac{\partial E_z}{\partial y} + \gamma \frac{\partial H_z}{\partial x}\right]$$

$$H_y = \frac{-1}{k_i^2}\left[j\omega\epsilon_o\epsilon_{ri} \frac{\partial E_z}{\partial x} + \gamma \frac{\partial H_z}{\partial y}\right]$$

with $k_i^2 = \omega^2\mu_o\epsilon_o\epsilon_{ri} + \gamma^2$ = cut-off wave number

and further manipulation yields the pair of Helmholtz equations

$$\nabla_{xy}^2 H_z + k_i^2 H_z = 0 \qquad (2.3a)$$

$$\nabla_{xy}^2 E_z + k_i^2 E_z = 0 \qquad (2.3b)$$

thus E_z and H_z must satisfy equation (2.3) together with the necessary boundary conditions.

$$E_z = 0 \;;\; \frac{\partial H_z}{\partial n_1} = 0 \;;\; \frac{\partial E_z}{\partial c_1} = 0 \quad \text{on } C_1 \text{ (electric walls)} \qquad (2.4)$$

$$\frac{\partial E_z}{\partial n_2} = 0 \;;\; H_z = 0 \;;\; \frac{\partial H_z}{\partial c_2} = 0 \quad \text{on } C_2 \text{ (magnetic walls)}$$

where $\frac{\partial}{\partial c_i}$ = spatial derivative tangential to the contour C_i and $\frac{\partial}{\partial n_i}$ = spatial derivative in the direction of the outward normal to C_i.

On the contour C_3; i.e. the interface between the two media;

(1) E_z, H_z must be continuous

(2) Tangential components of $\underline{E}$, $\underline{H}$ must be continuous

(3) Normal components of $\underline{D}$, $\underline{B}$ must be continuous

Continuity of the tangential components of $\underline{E}$ across the interface C_3 requires

$$\tau_1 \left\{ \frac{\beta}{\omega\mu_0} \frac{\partial E_z}{\partial c_1} - \left(\frac{\partial H_z}{\partial n_1} \right) \right\}_{R_1} = -\tau_2 \left\{ \frac{\beta}{\omega\mu_0} \frac{\partial E_z}{\partial c_3} - \left(\frac{\partial H_z}{\partial n_3} \right) \right\}_{R_2} \qquad (2.5)$$

whilst continuity of the normal components of $\underline{D}$ across the interface C_3 requires

$$\tau_1 \epsilon_{r_1} \left\{ \frac{\partial H_z}{\partial c_1} + \frac{\beta}{\omega\mu_0} \left(\frac{\partial E_z}{\partial n_1} \right) \right\}_{R_1} = -\tau_2 \epsilon_{r_2} \left\{ \frac{\partial H_z}{\partial c_3} + \frac{\beta}{\omega\mu_0} \left(\frac{\partial E_z}{\partial n_3} \right) \right\}_{R_2} \qquad (2.6)$$

where $\gamma = j\beta$, a loss free system

and $$\tau_i = \frac{\omega^2\mu_0\epsilon_0 - \beta^2}{\omega^2\mu_0\epsilon_0\epsilon_{r_i} - \beta^2} = \frac{\underline{k}^2}{k_i^2}$$

Thus for an inhomogeneous region R, the axially directed field components must in addition to satisfying equations (2.3) and (2.4), satisfy equations (2.5) and (2.6) and the propagating mode is said to be hybrid due to the coexistence of E_z and H_z field components.

For the case of a homogeneous region i.e. $\epsilon_{r_1} = \epsilon_{r_2}$ in fig. (2.1), interfacial boundary conditions do not exist and the problem reduces to that of seeking a solution to either equation (2.3a) (TE modes) or (2.3b) (TM modes) subject to the conditions of equation (2.4)

2.1. Finite difference formulation using a Taylor Series expansion.

This method is already well documented[3,13] but will be reviewed briefly, such that the salient points may emerge. The structure to be examined is shown in fig.(2.2.). A regular cartesian mesh is imprinted on the region, such that the boundaries of the structure lie on the mesh lines. The mesh intersections or nodes are numbered in some ordered sequence and with each node i, there is an associated scalar magnetic potential $\phi_i (= H_{zi})$ and a scalar electric potential $\psi_i \left(= \frac{\omega\epsilon_0}{\beta} E_{zi}\right)$ such that ϕ and ψ are dimensionally compatible, Fig. (2.3.) shows a typical interior node with its four immediate neighbours, each a distance h, the mesh pitch, away from the centrally located node. In this manner the actual continuous field is represented by the discretized field at each node on the cross sectional region R.

Using Taylors series to expand the derivatives in equations (2.3a), (2.3b) and assuming that $\phi(x,y)$ and $\psi(x,y)$ and their derivatives are single valued, finite, and piecewise continuous functions at each node, then

$$2(\tau_1+\tau_2)\phi_0 - \tfrac{1}{2}(\tau_1+\tau_2)(\phi_1+\phi_3) - \tau_1\phi_4 - \tau_2\phi_2$$

$$+\tfrac{1}{2}(\tau_2\epsilon_2 - \tau_1\epsilon_1)(\psi_1-\psi_3) = h^2k^2\phi_0 \qquad (2.7a)$$

$$2(\tau_1\epsilon_1+\tau_2\epsilon_2)\psi_0 - \tfrac{1}{2}(\tau_1\epsilon_1+\tau_2\epsilon_2)(\psi_1+\psi_3) - \tau_1\epsilon_1\psi_4 - \tau_2\epsilon_2\psi_2$$

$$+\tfrac{1}{2}(\tau_2-\tau_1)(\phi_3-\phi_1) = \tfrac{1}{2}h^2k^2(\epsilon_1+\epsilon_2)\psi_0 \qquad (2.7b)$$

represent the finite difference form of the potentials ϕ_0, ψ_0 at a typical interior interfacial node on the boundary CF, fig. (2.2). In their derivation the concept of 'image' nodes is utilised such that the boundary conditions at the interface may be written into the formulation, yielding the coupling terms

$$\tfrac{1}{2}(\tau_2\epsilon_2-\tau_1\epsilon_1)(\psi_1-\psi_3) \;;\; \tfrac{1}{2}(\tau_2-\tau_1)(\phi_3-\phi_1)$$

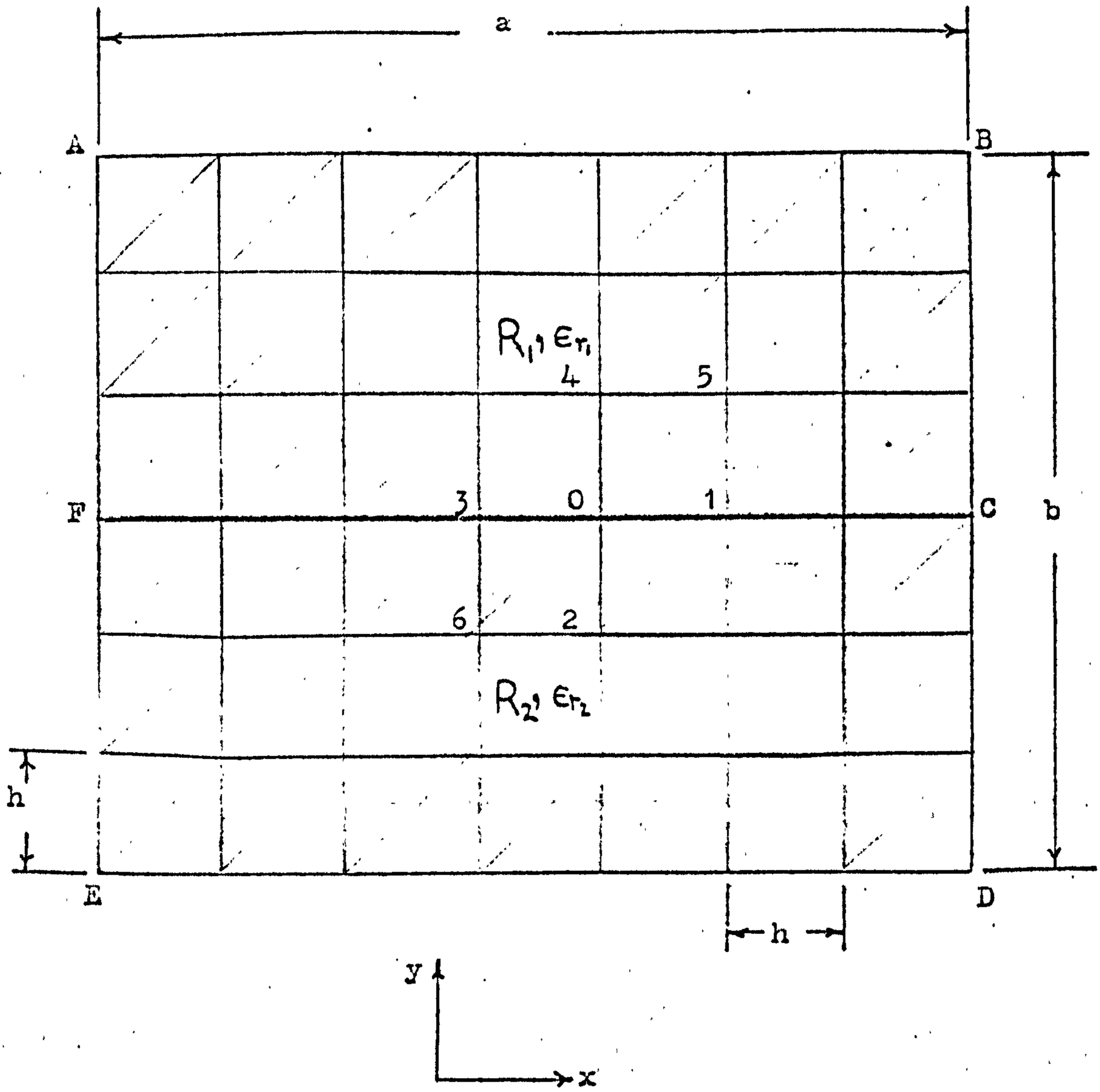

Fig. (2.2.) Structure to be analysed using finite difference/element techniques.

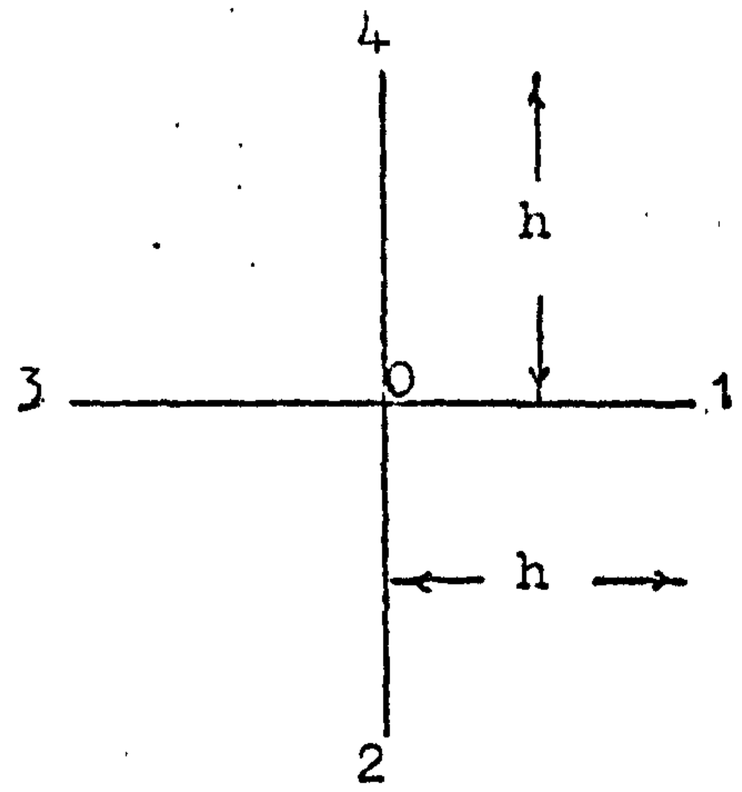

Fig. (2.3.) Typical interior node, with immediate neighbouring nodes.

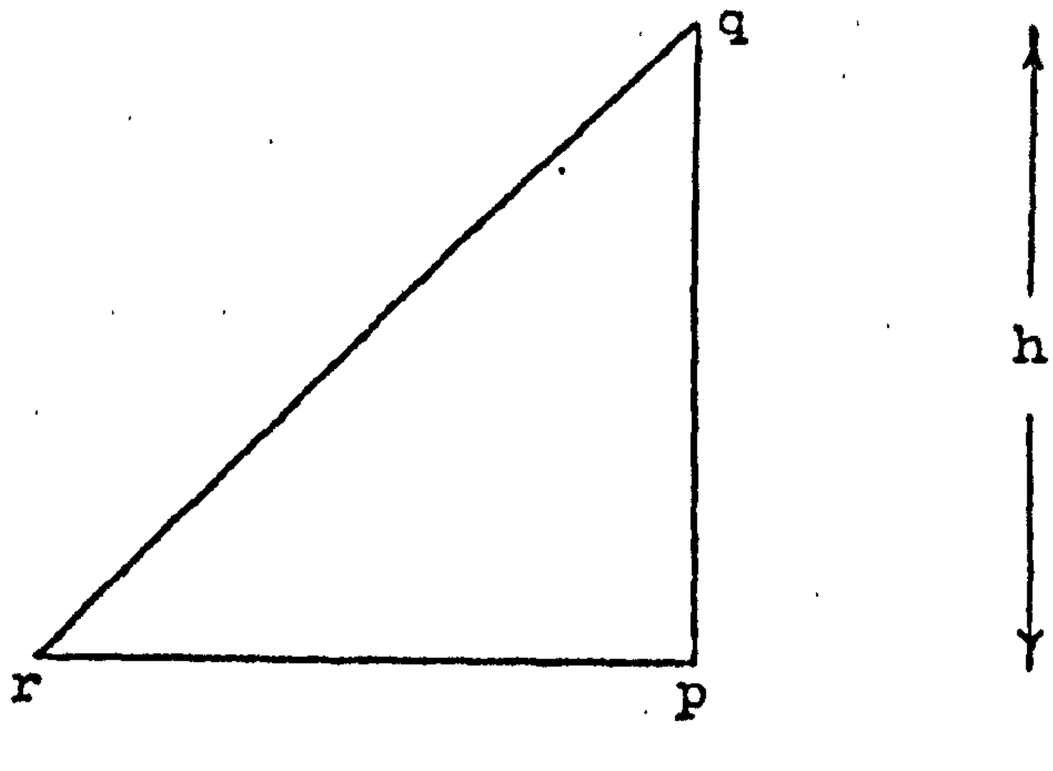

Fig. (2.4.) Right triangular element.

The finite difference form of the potentials ϕ_o and ψ_o at a node situated wholely in one of the homogeneous regions, can be obtained from equation (2.7) directly, by allowing

$$\tau_2 \rightarrow \tau_1 \quad , \quad \epsilon_2 \rightarrow \epsilon_1 \quad \text{for node in region 1.}$$

$$\tau_1 \rightarrow \tau_2 \quad , \quad \epsilon_1 \rightarrow \epsilon_2 \quad \text{for node in region 2.}$$

and equation (2.7) reduces to the familiar 5 point finite difference formulation of Helmholtz's equation, with the coupling terms automatically vanishing.

Nodes on the boundaries, however need special treatment, yielding slight modifications to the generalised interior situated nodal equations. For a node on an electric wall C_1 (ABCDE - fig. 2.2), $\psi = 0$ and an equation is unnecessary to describe the variation of the electric potential, further $\frac{\partial \phi}{\partial y} = 0$ on the contour AB, and this condition is written into equation (2.7a) by stipulating $\phi_3 = \phi_1$.

In a similar manner nodes situated on the contours BD, DE give rise to modified versions of the generalised equation.

The magnetic wall conditions on C_2 (AFE - fig. 2.2) require $\frac{\partial \psi}{\partial x} = \phi = 0$ and the identical dual procedure to that for electric walls is performed.

Discussion, so far, has been restricted to the analysis of the propagation of hybrid modes such that the system of equations represented by equation (2.7) taken over all the nodes in the structure with the necessary boundary modifications must be solved simultaneously. If the case where variation of the axially directed magnetic field in the x direction is zero is considered, $\left(\frac{\partial \phi}{\partial x} = 0\right)$ then a TM mode can exist within such a structure satisfying the boundary conditions on the interface, viz.

$$\tau_1 \left(\frac{\partial \phi}{\partial y}\right)_{R_1} = \tau_2 \left(\frac{\partial \phi}{\partial y}\right)_{R_2}$$

in fig. (2.2).

The problem is then reduced to replacing the one dimensional Helmholtz operator by the appropriate finite difference operator at nodes along any one mesh line in the y direction, the generalised equation for the finite difference form of the magnetic potential ϕ_o at the interface node being

$$(\tau_1 + \tau_2)\,\phi_o - \tau_1\,\phi_4 - \tau_2\,\phi_2 = k^2 h^2 \phi_o \qquad (2.8)$$

with the modifications described previously being performed for nodes situated on electric or magnetic walls.

Most structural problems to be analysed do not usually possess boundaries which lie on mesh lines parallel to the co-ordinate directions, for example, a circular boundary. Two main alternatives are then open to the user (a) to approximate the true boundary by mesh lines, with a much finer mesh pitch, thus allowing the boundary to become deformed or (b) to allow the mesh arm lengths - fig. (2.3) - to be corrected so that nodes lie on the boundary, but the mesh is no longer regular everywhere[1,14].

The repeated application of equations (2.7) at each node in the region, with due consideration for nodes at the boundaries, results in approximating the Helmholtz equations (2.3a, 2.3b) by a series of algebraic equations in ϕ and ψ which must be solved simultaneously. This may be written as a matrix eigenvalue problem of the form

$$(\underline{A} - \lambda \underline{B})\,\underline{\theta} = \underline{0} \qquad (2.9)$$

Where $\underline{A}$ has as its components, the coefficients of the ϕ's and ψ's defined by the left hand side of equation (2.7), whilst $\underline{B}$ is similarly defined for the right hand side of equations (2.7), λ is representative of the structures wave number k^2, and dependant on the mesh pitch.

$\underline{A}$ is a square, sparse banded matrix and $\underline{B}$ a diagonal matrix, both of order $2m$, where m is the number of nodes defining the structure. Providing a regular mesh is used everywhere over the region, A will be symmetric for electric walls completely surrounding the region, but this condition does not hold for the presence of a magnetic wall due to the presence of image points in this type of boundary. $\underline{\theta}$ is a column matrix of order 2m whose elements consist of the potentials ϕ, ψ at each node in the structure.

Since τ_i is frequency dependant, the eigenvalue equation is solved for discrete values of τ_i corresponding to investigations performed over a selected frequency band yielding a dispersion curve. The properties of $\underline{A}$ are further influenced by the choice of τ_i for in the range $\tau_i > 0$, (corresponding to the velocity of the propagating wave exceeding that of light in free space), $\underline{A}$ is at least positive semidefinite, thus assuring $\underline{A}$ possesses real, nonnegative eigenvalues. For $\tau_i < 0$ (corresponding to the velocity of the propagating wave being less than that of light in free space), the eigenvalues associated with $\underline{A}$ can either be positive and negative or all negative, since $\underline{A}$ may no longer be positive definite and the eigenvalue corresponding to the dominant mode is normally taken as the least negative one[6].

The homogeneous system ($\epsilon_{r_1} = \epsilon_{r_2}$) requires the solution to either (2.3a) or (2.3b) together with the boundary conditions at an electric or magnetic wall, since the absence of interface conditions in effect decouples the equations represented in equation (2.3). Thus $\tau_1 = \tau_2 = 1$ $\epsilon_{r_1} = \epsilon_{r_2} = \epsilon_r$, in either equation (2.7a) or (2.7b) yields the generalised finite difference form of the potential ϕ_o or ψ_o at a typical interior node, and application of this operator again forms a matrix eigenvalue equation similar to that of (2.9), with the properties of $\underline{A}$, $\underline{B}$ as described above.

$\underline{\theta}$ represents the scalar magnetic (TE modes) or scalar electric (TM modes) potentials and λ becomes proportional to the cut off wave number of the structure. However since τ_i is no longer frequency dependant, the eigenvalue equation has only to be solved once to obtain the desired information regarding the fields and cut-off wave numbers of the propagating modes.

Although discussion has been restricted to the 5 point finite difference operator, improved accuracy can be obtained under certain conditions, by approximating the Laplacian operator by a 9 point or even higher ordered difference operators.[1,3].

2.2. FINITE ELEMENT FORMULATION.

Unlike finite differences, which depends on constructing a set of difference equations involving field values at mesh points, to replace the differential operator, the theory of finite elements allows the two dimensional region to be divided into a finite number of polygons or elements over each of which the field is expressed as a function of the fields at the vertices of the elements. A variational expression is constructed for some parameter of the problem and minimization of the variational expression with respect to the field values existing at each vertex is performed.

The principle behind variational methods is based on the concept that the integral of some function, typical of a system has a smaller value for the actual performance of the system than it would have for any other assumed performance. A variational expression which is stationary in k^2, the wave number of the system, for the structure of fig. (2.1.) is given by[15]

$$J(\phi,\psi) = \int_R \beta^2 \tau_i \epsilon_{ri} |\nabla_{xy}\psi|^2 dR + \int_R \tau_i |\nabla_{xy}\phi|^2 dR$$

$$+ 2\int_R \underline{e}_z \cdot \beta^2 \tau_i (\nabla_{xy}\psi \wedge \nabla_{xy}\phi) dR - k^2 \int_R (\beta^2 \epsilon_{ri}\psi^2 + \phi^2) dR \qquad (2.10)$$

where $\bar{\beta}^2 = \left(\frac{\beta c}{\omega}\right)^2$, $k^2 = \frac{\omega^2}{c^2}(1-\bar{\beta}^2)$

and thus $$\tau_i = \frac{\omega^2\mu_o\epsilon_o - \beta^2}{\omega^2\mu_o\epsilon_o\epsilon_{ri} - \beta^2} = \frac{1-\bar{\beta}^2}{\epsilon_{ri} - \bar{\beta}^2}$$

the variational expression $J(\phi,\psi)$ can be shown to have as its Euler equations[16]

$$\tau_i \nabla_{xy}\phi + k^2\phi = 0 \qquad (2.11a)$$

and $$\beta^2\tau_i\epsilon_{ri}\nabla_{xy}\psi + \beta^2\epsilon_{ri}k^2\psi = 0 \qquad (2.11b)$$

over each region R_i, which are satisfied because of the two dimensional Helmholtz equations, equation (2.3).

By taking a branch cut as shown in fig. (2.1) such that region R_1 is simply connected, it can be shown that the natural boundary conditions automatically satisfied by $J(\phi,\psi)$ when stationary are

$$\tau_1\left\{\bar{\beta}^2\frac{\partial\psi}{\partial c} - \left(\frac{\partial\phi}{\partial n}\right)_{c_3}\right\}_{R_1} = -\tau_2\left\{\bar{\beta}^2\frac{\partial\psi}{\partial c} - \left(\frac{\partial\phi}{\partial n}\right)_{c_3}\right\}_{R_2} \qquad (2.12a)$$

and

$$\tau_1\bar{\beta}^2\left\{\epsilon_{r_1}\left(\frac{\partial\psi}{\partial n}\right)_{c_3} + \frac{\partial\phi}{\partial c}\right\}_{R_1} = -\tau_2\bar{\beta}^2\left\{\epsilon_{r_2}\left(\frac{\partial\psi}{\partial n}\right)_{c_3} + \frac{\partial\phi}{\partial c}\right\}_{R_2} \qquad (2.12b)$$

at the interface of the two media, which are the boundary conditions for the continuity of the tangential electric and magnetic fields across the interface, providing that the fields ϕ and ψ satisfy

$\phi = \frac{\partial\phi}{\partial c} = 0$ on a magnetic wall

$\psi = \frac{\partial\psi}{\partial c} = 0$ on an electric wall

If $\phi(x,y)$, $\psi(x,y)$ are the trial solutions of the scalar magnetic and electric potentials over the region represented itself by a finite number of elements, the values of $\phi(x,y)$ and $\psi(x,y)$ which yields the smallest possible $J(\phi,\psi)$ will be the correct values satisfying equation (2.3).

Over a triangular element fig. (2.4), $\phi(x,y)$ and $\psi(x,y)$ are represented by

$$\phi^{e}(x,y) = \sum_{k=p,q,r,} N_k^e (x,y)\, \phi_k^e \quad ; \tag{2.13a}$$

$$\psi^{e}(x,y) = \sum_{k=p,q,r.} N_k^e (x,y)\, \psi_k^e \tag{2.13b}$$

Where ϕ_k, ψ_k are the values of the fields ϕ, ψ at the k_{th} vertex, and $N_i(x,y)$ is a function of the spatial co-ordinates, uniquely defined and differentiable over each element and reducing to zero outside it. The substitution of equation (2.13) into the functional form of $J(\phi,\psi)$ then reduces $J(\phi,\psi)$ to a function of the variables ϕ_k and ψ_k. The optimum sets of ϕ_k, ψ_k and thus the optimum fields ϕ, ψ are then obtained by minimising $J(\phi,\psi)$ with respect to each of the parameters ϕ_k, ψ_k viz.

$$\frac{\partial J(\phi,\psi)}{\partial \phi_k} = \frac{\partial J(\phi,\psi)}{\partial \psi_k} = 0 \qquad k = p,\ q,\ r,$$

The minimisation of $J(\phi,\psi)$ over R is equivalent to the minimisation of $J(\phi,\psi)$ over each element providing the fields are continuous across the element interface[8], which is assured since at least two nodes must be common to adjacent elements, and if each vertex k of the element , e, is common to P elements, then

$$\frac{\partial J(\phi,\psi)}{\partial \phi_k} = 2\sum_{e=1}^{R}\Bigg[\int_{el.}\tau_i\left\{\frac{\partial}{\partial x}[\underline{G}]\,\underline{\phi}^e\,\frac{\partial N_k^e}{\partial x}+\frac{\partial}{\partial y}[\underline{G}]\,\underline{\phi}^e\,\frac{\partial N_k^e}{\partial y}\right\}dx\,dy$$

$$+\bar{\beta}^2\int_{el.}\tau_i\left\{\frac{\partial}{\partial y}[\underline{G}]\,\underline{\psi}^e\,\frac{\partial N_k^e}{\partial x}-\frac{\partial}{\partial x}[\underline{G}]\,\underline{\psi}^e\,\frac{\partial N_k^e}{\partial y}\right\}dx\,dy$$

$$-K^2\int_{el.}[\underline{G}]\;\underline{\phi}_k^e\,.\,N_k^e\;dx\,dy\Bigg] \qquad (2.14a)$$

$$\frac{\partial J(\phi,\psi)}{\partial \psi_k} = 2\sum_{e=1}^{R}\Bigg[\int_{el}\bar{\beta}^2\tau_i\epsilon_{ri}\left\{\frac{\partial}{\partial x}[\underline{G}]\,\underline{\psi}^e\,\frac{\partial N_k^e}{\partial x}+\frac{\partial}{\partial y}[\underline{G}]\,\underline{\psi}^e\,\frac{\partial N_k^e}{\partial y}\right\}dx\,dy$$

$$-\bar{\beta}^2\int_{el}\tau_i\left\{\frac{\partial}{\partial y}[\underline{G}]\,\underline{\phi}^e\,\frac{\partial N_k^e}{\partial x}-\frac{\partial}{\partial x}[\underline{G}]\,\underline{\phi}^e\,\frac{\partial N_k^e}{\partial y}\right\}dx\,dy$$

$$-K^2\bar{\beta}^2\int_{el}\epsilon_{ri}\;[\underline{G}]\;\underline{\psi}^e\,.\,N_k^e\;dx\,dy\Bigg] \qquad (2.14b)$$

represents the minimization of $J(\phi,\psi)$ with respect to ϕ and ψ at the k_{th} vertex, where $\underline{G}$ is the row matrix

$$\begin{bmatrix} N_p^e & N_q^e & N_r^e \end{bmatrix}$$

and $\underline{\phi}^e$, $\underline{\psi}^e$ are column matrices

$$\begin{bmatrix}\phi_p^e & \phi_q^e & \phi_r^e\end{bmatrix}^T \qquad \begin{bmatrix}\psi_p^e & \psi_q^e & \psi_r^e\end{bmatrix}^T$$

with reference to the triangular element fig. (2.4).

Over one such element, the functional dependance of ϕ and ψ can be written as in equation (2.13) where

$$N_p^e = (a_p + b_p x + c_p y) \;/\; 2\Delta$$

$$a_p = x_q y_r - x_r y_q$$

$$b_p = y_q - y_r$$

$$c_p = x_r - x_q$$

Δ = area of the triangle

with the other parameters being obtained by cyclic rotation of the suffices p, q, r, and this minimization of $J(\phi, \psi)$ over the element may be written compactly as

$$\frac{\partial J^e(\phi,\psi)}{\partial \underline{\phi}^e} = \left(\tau_i \underline{S}^e \underline{\phi}^e + \bar{\beta}^2 \tau_i \underline{C}^e \underline{\psi}^e \right) - K^2 \underline{F}^e \underline{\phi}^e$$

$$\frac{\partial J^e(\phi,\psi)}{\partial \underline{\psi}^e} = \left(\bar{\beta}^2 \tau_i \epsilon_{ri} \underline{S}^e \underline{\psi}^e - \bar{\beta}^2 \tau_i \underline{C}^e \underline{\phi}^e \right) - K^2 \bar{\beta}^2 \epsilon_{ri} \underline{\psi}^e$$

where

$$\underline{S}^e = \begin{bmatrix} S_{pp} & S_{pq} & S_{pr} \\ S_{qp} & S_{qq} & S_{qr} \\ S_{rp} & S_{rq} & S_{rr} \end{bmatrix} \qquad \underline{C}^e = \begin{bmatrix} C_{pp} & C_{pq} & C_{pr} \\ C_{qp} & C_{qq} & C_{qr} \\ C_{rp} & C_{rq} & C_{rr} \end{bmatrix}$$

$$\underline{F}^e = \begin{bmatrix} F_{pp} & F_{pq} & F_{pr} \\ F_{qp} & F_{qq} & F_{qr} \\ F_{rp} & F_{rq} & F_{rr} \end{bmatrix}$$

and $$S_{pq} = \frac{1}{4\Delta^2} \int_{el.} \left[\frac{\partial N_p}{\partial x} \frac{\partial N_q}{\partial x} + \frac{\partial N_p}{\partial y} \frac{\partial N_q}{\partial y} \right] dx\, dy$$

$$C_{pq} = \frac{1}{4\Delta^2} \int_{el.} \left[\frac{\partial N_p}{\partial y} \frac{\partial N_q}{\partial x} - \frac{\partial N_p}{\partial x} \frac{\partial N_q}{\partial y} \right] dx\, dy$$

$$F_{pq} = \frac{1}{4\Delta^2} \int_{el.} N_p N_q \; dx\, dy$$

Evaluation of these integrals over the right triangular element in fig. (2.4) results in the final form for $\underline{S}^e$, $\underline{C}^e$, $\underline{F}^e$ as

$$\underline{S}^e = \frac{1}{2}\begin{bmatrix} 2 & -1 & -1 \\ -1 & 1 & 0 \\ -1 & 0 & 1 \end{bmatrix} \qquad \underline{C}^e = \frac{1}{2}\begin{bmatrix} 0 & +1 & -1 \\ -1 & 0 & +1 \\ +1 & 1 & 0 \end{bmatrix} \qquad \underline{F}^e = \frac{\Delta}{12}\begin{bmatrix} 2 & 1 & 1 \\ 1 & 2 & 1 \\ 1 & 1 & 2 \end{bmatrix}$$

Thus the finite element representation of the potentials ϕ_o and ψ_o at a typical interior interfacial node on the boundary CF - fig. (2.2) common to six right triangular elements, as in fig. (2.5) becomes

$$2(\tau_1+\tau_2)\phi_0 - \tfrac{1}{2}(\tau_1+\tau_2)(\phi_1+\phi_3) - \tau_1\phi_4 - \tau_2\phi_2 + \tfrac{\bar{\beta}^2}{2}(\tau_2-\tau_1)(\psi_3-\psi_1) = \tfrac{K^2}{12}h^2\left[6\phi_0 + \sum_{i=1}^{6}\phi_i\right] \qquad (2.15a)$$

$$2(\tau_1\epsilon_1+\tau_2\epsilon_2)\psi_0 - \tfrac{1}{2}(\tau_1\epsilon_1+\tau_2\epsilon_2)(\psi_1+\psi_3) - \tau_1\epsilon_1\psi_4 - \tau_2\epsilon_2\psi_2 - \tfrac{\bar{\beta}^2}{2}(\tau_2-\tau_1)(\phi_3-\phi_1) = \tfrac{K^2}{12}h^2\left[3(\epsilon_1+\epsilon_2)\psi_0 + \tfrac{1}{2}(\epsilon_1+\epsilon_2)(\psi_1+\psi_3) + \epsilon_1(\psi_4+\psi_5) + \epsilon_2(\psi_2+\psi_6)\right] \qquad (2.15b)$$

after the condition for stationarity i.e. $\frac{\partial J(\phi,\psi)}{\partial \underline{\phi}^e / \partial \underline{\psi}^e} = 0$ has been performed. In a similar manner to that of finite differences, the finite element formulation for nodes situated entirely in one of the homogeneous regions can be obtained directly from equation (2.15) by allowing the parameters τ_i, ϵ_i to possess the same values for that region R_i, and noting that the coupling terms vanish.

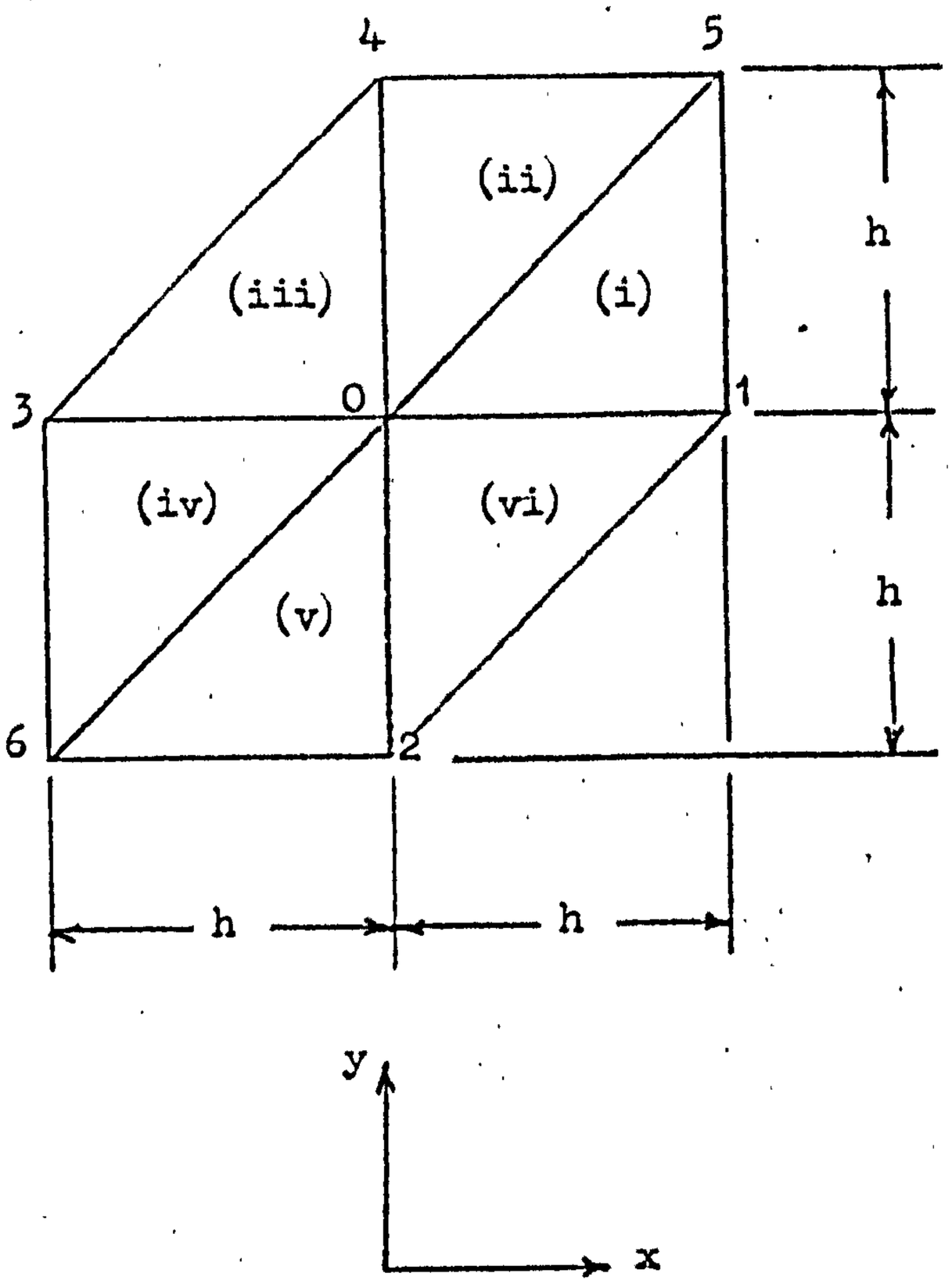

Fig. (2.5.) Interior interfacial node, common to six right triangular elements.

For nodes on an electric wall $\psi = 0$ and a nodal formulation of the potential is unnecessary. On the same wall, for example AB in fig. (2.2), $\frac{\partial \Phi}{\partial y} = 0$ but it can be seen that for a typical node on this wall there is at most three right triangular elements associated with this node, and by summing the contributions to $\frac{\partial T(\Phi,\psi)}{\partial \Phi / \partial \psi}$ over the triangles, the finite element representation of the potential Φ existing at this node can be derived, automatically satisfying the required boundary condition. Identical arguments are valid for the dual case of magnetic walls.

The propagating mode, that can be solved using one spatial dimension can be found in a similar manner, by utilising a line element[17] joining two nodes, each node therefore being common to at most two such elements and the finite element formulation of the potential ϕ_0 existing at the boundary between the two media yields,

$$(\tau_1 + \tau_2)\phi_0 - \tau_1 \phi_4 - \tau_2 \phi_2 = \frac{k^2 h^2}{6}(4\phi_0 + \phi_2 + \phi_4) \qquad (2.16)$$

with modifications being made where the node under consideration is situated entirely within either of the homogeneous media, or placed on an electric or magnetic wall. This can be seen to be identical to equation (2.8) if the weighting on the right hand side is thrown entirely onto the central node.

Application of equation (2.15) over each node in the region, with due regard for the modifications at the boundaries, again results in approximating the simultaneous equations (2.3) together with their boundary conditions, by a set of linear algebraic equations in Φ, ψ; the set forming the matrix eigenvalue problem

$$(\underline{A}_1 - \lambda \underline{B}_1)\underline{\Theta} = \underline{0} \qquad (2.17)$$

with $\underline{A}_1$ being the matrix of the coefficients of the ϕ's and ψ's defined by the left hand side of equation (2.15), whilst $\underline{B}_1$ is defined by the right hand side of equation (2.15). λ is the eigenvalue proportional to the wave number k^2 and the mesh pitch. $\underline{A}_1$ and $\underline{B}_1$ are now both symmetric, even under magnetic wall conditions, due to the symmetry of the matrices $\underline{S}^e$, $\underline{F}^e$ and $\underline{C}^e$, further they are sparse and banded and $\underline{B}_1$ is positive definite. $\underline{A}_1$ is positive or negative semi definite according as to the values of τ_i discussed previously. $\underline{\Theta}$ is the column matrix representing the values of the fields ϕ, ψ at each node or element vertex. Other than these exceptions, the examination of the dispersive properties of the structure together with the effect of varying τ_i on the matrix $\underline{A}_1$ and the investigation of the fields within a totally homogeneous structure, follow those discussed previously for the finite difference analysis of the same structure.

Although it has been briefly shown here, the development of the finite element formulation for triangular elements, the approach can be applied to other elemental shapes which serve to increase the accuracy of the approximation. This increase in accuracy can be brought about in two ways.

(a) using a higher order polygonal element e.g. a rectangular element, these however produce additional difficulties when approximating a structure whose boundaries do not lie parallel to one of the co-ordinate directions, such as the perimeter of the circle, and thus use of the simplest two dimensional region - the triangle is advisable.

(b) using a higher order polynomial approximation[18,19] of the function describing the variation of the fields across an element. This approach is the favoured one, even though it does give rise to more complicated elemental subregions such as 6 point, 10 point triangles etc. The advantages are such that one higher ordered polynomial element can replace a few lower ordered polynomial elements in defining the region, but it must be appreciated that a large number of the simpler elements is clearly advantageous when modelling a complicated boundary shape.

2.3. METHODS OF SOLUTION OF THE DERIVED MATRIX EIGENVALUE PROBLEMS.

The methods of solution of the generalised matrix eigen value problem

$$(\underline{A}-\lambda\underline{B})\underline{\theta} = \underline{0} \tag{2.18}$$

fall into two well defined categories viz; (i) by relaxation of the fields at each node within the system - indirect methods and (ii) by direct matrix manipulation. Each method possesses its characteristic advantages and disadvantages, according to the size of the matrices, solutions for all eigenvalues and the properties of the individual matrices. It is to be observed that the methods involved in the solution of the particular equations are many for both the above categories and discussion of the relevant techniques is beyond the scope of this thesis.

Since the system of linear equations from which the matrix eigenvalue problem is derived are usually large, they must be solved using numerical techniques with high speed digital computers.

2.3.1. Indirect Methods.

Indirect or relaxation methods base their mode of operations on the principle of repeated application of a simple algorithm. The advantage of this method is that the non-zero elements of the rows of the matrices $\underline{A}$, $\underline{B}$ need only be generated when required, and thus storage of the complete matrices which are sparse , is obviated. Further since there are only a few different types of node structures within the region of Fig. (2.2) and hence few different types of rows of the matrices, only a small number of sub-algorithms need to be written for the complete algorithm. The algorithm that has received most attention over previous years is that of successive point over-relaxation[1,14] (SOR) and it is proposed to use this powerful technique here for the solution of derived matrix eigen value problem.

Consider the implementation of SOR on equation (2.18). An approximation is made to the required eigenvector, $\underline{\Theta}'$ and eigenvalue λ', then for each element of $\underline{\Theta}$, $\underline{\Theta}_i$, the residual R_i at that element is found by

$$R_i = \left(\underline{A}_i - \lambda' \underline{B}_i\right) \underline{\Theta}'$$

where $\underline{A}_i$ denotes the i_{th} row of matrix A.

Ideally the residual should be zero at each element for a solution and thus the i_{th} component of $\underline{\Theta}'$ should be over relaxed by a factor wR_i i.e.

$$\underline{\Theta}_i \rightarrow \underline{\Theta}_i + w R_i$$

where w is known as the accelerating factor and affects the rate of convergence to the correct solution. The eigenvector is scanned systematically several times in this manner.

The eigenvalue estimate, however will not usually be the correct one, and in this case for an estimated eigenvalue greater (or smaller) than the correct eigenvalue the eigenvector grows (or diminishes) and cannot converge as the determinant of $(A-\lambda B)$ is non zero. However the elements of $\underline{\theta}$ tend to assume their correct shape, and after several iterations, the incorrect although 'shaped' eigenvector is substituted into the Rayleigh quotient,[14]

$$\lambda_{new} = \frac{\underline{\theta}^T \underline{A}\, \underline{\theta}}{\underline{\theta}^T \underline{B}\, \underline{\theta}}$$

which gives an improved eigenvalue estimate λ_{new} and is also stationary for the true solution. Using this new estimate, the SOR process is reverted to with the most recent eigenvector and an improved $\underline{\theta}$ found. Alternate usage of the SOR process and the Rayleigh quotient causes convergence to the correct eigenvalue and eigenvector within the accuracy required.

The disadvantage of the SOR method is that it cannot be used with convergence guaranteed on an arbitrary matrix. The convergence theorem[1] states that convergence is guaranteed only on symmetrical and positive semidefinite matrices, with diagonal terms greater than zero, and off diagonal terms less than or equal to zero, and for $0 < w < 2$. For example this means that the SOR process can only calculate the dominant eigenvalue.

The finite element formulation of Helmholtz's two dimensional equations yields $\underline{A}$ and $\underline{B}$ as symmetrical and positive definite matrices for $\tau_i > 0$ and thus convergence occurs. For $\tau_i < 0$ the matrix $\underline{A}$ is indefinite whilst still retaining its symmetry and thus convergence to the correct eigenvector is in no way guaranteed, and recourse has to be

made to other techniques notably that of Peters and Wilkinson[20], which is a semi-iterative technique and although permitting $\underline{A}$ to be indefinite has the added advantages of utilising the band structures of $\underline{A}$ and $\underline{B}$ and calculating higher ordered eigenvalues.

The finite difference formulation of the same problem does not necessarily produce a symmetric matrix $\underline{A}$ and only when the structure is devoid of magnetic walls will $\underline{A}$ be symmetric. For the general case $\underline{A}$ will only be slightly non-symmetric, but is sufficient to waive the convergence criterion for coarse meshes when the non symmetry is most pronounced, but for finer meshes $\underline{A}$ will tend to a more symmetrical nature and convergence can be optimistically thought of. Again the definiteness of indefiniteness of $\underline{A}$ is of importance and the discussion held in the previous paragraph is equally applicable here.

The matrix eigenvalue equation derived for the totally homogeneous structures, have both $\underline{A}$ and $\underline{B}$ symmetrical or 'near' symmetrical, and positive definite and thus a guarantee of cenvergence. It is worthy to note that for TE modes in a structure being bounded solely by electric walls that the trivial solution $\underline{\Theta}$ = constant to equation (2.18) exists, this can be eliminated by using magnetic walls of symmetry such that the fundamental mode also satisfies these boundary conditions.

The method of successive overrelaxation applied to equation (2.18) yields the dominant eigenvalue, since an attempt to seek the next ordered eigenvalue would result in $\underline{A}$ becoming negative definite and hence the loss of convergence.

Silvester[21] and Beaubien and Wexler[22] have developed biharmonic operators to make the relevant matrices positive definite so as to compute higher order eigenvalues and to use SOR for the inhomogeneous problem. The disadvantage is that the value of the next lowest eigenvalue has to be known for the computation of any eigenvalue to be successful. This is suitable for empty waveguides as Beaubien and Wexler have noted, but for the inhomogeneous system, since the dominant mode can correspond to a negative eigenvalue[6] the choice of the 'next lowest' eigenvalue is a difficult one to estimate. The introduction of the biharmonic operator also gives rise to a 13 point or 25 point operator and this must give additional complexity in formulating the necessary boundary conditions.

Successive over-relaxation was applied to the matrix formulation of fig. (2.2) using 5 point, 9 point finite difference operators and right triangular and square finite element operators to describe the field variations. The totally homogeneous case being considered initially, with electric walls an AB, BCD, DE and a magnetic wall on AFE thus seeking the cut-off wave numbers of the TM_{11} mode. These results are shown in Table (2.1) with $b = 2a$.

Table (2.1) indicates that analysis using square elements is as accurate as for the five point finite difference formulation, which further are an improvement on the accuracies obtained by the triangular element subdivision of the mesh and using a nine point finite difference operator. The greater errors incurred in the triangular element formulation is due to the non symmetry[19] of the description of the potential at a typical node - fig. (2.5) where the images of points 5 and 6 in the planes defined by 103 and 204 are absent; whilst the nine

TABLE (2.1).

Cut-off wave number $(kb)^2$ for the TM_{11} mode in a wave guide of square cross-section of side b.

h/b	Triangular elements $(kb)^2$	error %	Square elements $(kb)^2$	error %	5 point finite differences $(kb)^2$	error %	9 point finite differences $(kb)^2$	error %
1/6	21.1090	6.94	20.1942	2.31	19.2920	2.26	18.8615	4.65
1/8	20.5056	3.88	19.9942	1.29	19.4867	1.28	19.2390	2.60
1/10	20.278	2.48	19.9020	0.82	19.5770	0.82	19.4170	1.66
1/14	19.9881	1.26	19.8215	0.42	19.6549	0.42	19.5743	0.84

$(kb)^2$ anal $= 2\pi^2 = 19.7392.$

point finite difference's errors are caused by the introduction of more nodal potentials to describe the potential at the central node and thus at the magnetic wall, where modifications have to be made to the relevant difference equation, a less symmetrical matrix than that for the set of five point difference equations is produced.

The one dimensional TE_{10} was also investigated, by using one mesh line of fig. (2.2), BD with a magnetic wall at D and an electric wall at B. Table (2.2) records the results of the cut off wave number for several values of the discretisation of the line, using the finite difference and finite element formulations, equations (2.8) and (2.16) respectively, with $\tau_1 = \tau_2 = 1$ for the completely homogeneous system. Examination of Table (2.2) indicates that there is little difference in accuracy, but, as in Table (2.1), the finite element formulation yields an upper bound to the correct solution whilst the finite difference formulation yields a lower bound.

Table (2.3) represents the wave lengths of the propagating wave for the inhomogeneous structure of fig.(2.2) for the dominant longitudinal section magnetic (LSM) mode[23] at cut-off. Square finite element and five point finite difference formulations were used, as these were the most accurate of all the formulations discussed for the homogeneous region. The dispersive properties although readily obtained by the SOR process for the range $\tau_i > 0$ are not recorded as these are well documented elsewhere.[6,15] Region 1 possesses a relative permittivity of unity and region 2 has relative permittivities of 2.45, 9.0, 50.0, and 100.0.

TABLE (2.2)

Cut-off wave number $(kb)^2$ for the TE_{10} mode, in a waveguide of width 2b.

h/b	Finite elements $(kb)^2$	error %	Finite Difference $(kb)^2$	error %
1/4	2.4992	1.29	2.4359	1.29
1/8	2.4753	0.32	2.4595	0.32
1/16	2.4694	0.08	2.4655	0.08

$$(kb)^2 \text{ anal} = \left(\frac{\pi}{2}\right)^2 = 2.4674$$

ABCDE - fig. (2.2) again represents an electric wall whilst AFE represents a magnetic wall of symmetry, the discretization employed $h/b = \frac{1}{8}$, with the dielectric interface situated at $y = b/2$. The analytical results are obtained from Marcuvitz[24]. Again there is little or no difference in the accuracies between the two methods.

The dominant longitudinal section electric (LSE) mode[23] was investigated, utilising its one dimensional representation or model. Table (2.4) shows the cut-off wavelengths of this dominant mode, for the same values of relative permittivities as those in the LSM investigations. The mesh line BCD was utilised for the modes together with an electric wall at B and a magnetic wall at D, the discretization $h/b = 1/4$ is utilised so as to provide compatibility with the dimensions of the structure analysed for LSM mode-type propagation. The accuracy of the finite element formulation is now far better than that of the finite difference formulation, comparing the results with the analytical ones obtained from Marcuvitz[24]. This must be due to the formulation of the matrix $\underline{B}$ in the eigenvalue equation, where for the finite element representation of matrix $\underline{B}$ the potential existing at any one node is replaced by a linear function of the potential at that node and also of the potentials existing at the neighbouring nodes, whilst the finite difference representation of the same matrix weights the potentials existing at the surrounding nodes and 'throws' them on to the central node, and is clearly disadvantageous when a relatively large variation in the field exists such as that at a dielectric boundary.

TABLE (2.3)

Cut-off wavelengths (b/λ_c) of the dominant LSM mode in a waveguide of square cross-section of side b.

ϵ_r	Finite element b/λ_c	error %	Finite difference b/λ_c	error %	b/λ_c analytic (see text).
2.45	0.3875	0.66	0.3831	0.49	0.3850
9.0	0.2278	0.66	0.2251	0.51	0.2263
50.0	0.09992	0.62	0.09864	0.66	0.09930
100.0	0.07088	0.59	0.07001	0.65	0.07047

TABLE (2.4)

Cut-off wavelengths (b/λ_c) of the dominant LSE mode in a waveguide of width 2b.

ϵ_r	Finite element b/λ_c	error %	Finite Difference b/λ_c	error %	b/λ_c analytic (see text)
2.45	0.3385	0.38	0.3334	0.98	0.3372
9.0	0.1812	0.25	0.1785	1.19	0.1807
50.0	0.07748	0.20	0.07631	1.30	0.07732
100.0	0.05483	0.20	0.05400	1.31	0.05472

2.3.2. Direct Methods.

For direct matrix manipulation of the eigenvalue problem most computing centres possess large matrix routine packages and it is on these that the user normally relies. The algorithms employed in most cases, are those noted by Wilkinson and Reinsch,[25] who recommend certain algorithms for the numerical solution of equation (2.18) where matrices $\underline{A}$,$\underline{B}$ can be symmetric or nonsymmetric, sparse or dense, real or complex and $\underline{B}$ can take the value of $\underline{I}$, the identity matrix. Further the authors record (and have tested rigorously) the algorithms in a fully readable programmable form to enable the user to incorporate the required solution technique into the relevant program.

For the generalised symmetric eigenvalue problem represented in equation (2.18) where $\underline{A}$ is a real symmetric or 'near' symmetric matrix and $\underline{B}$ is a real symmetric positive definite matrix, $\underline{B}$ can be factorised by Cholesky's method, $\underline{B} = \underline{L}\underline{L}^T$ where $\underline{L}$ is a lower triangular matrix. Hence equation (2.18) can be written

$$\{ \underline{L}^{-1} \underline{A} (\underline{L}^{-1})^T - \lambda \underline{I} \} \{ \underline{L}^T \underline{\theta} \} = \underline{0}$$

so that symmetry is still guaranteed for $\{\underline{L}^{-1} \underline{A} (\underline{L}^{-1})^T\}$ but the banded structure is destroyed, and the transformed matrix is now dense. In the finite difference formulation $\underline{B}$ is or can be arranged to be the identity matrix and the Cholesky decomposition is not required, therefore the eigenvalues are sought of the real symmetric, sparse banded matrix $\underline{A}$.

Wilkinson recommends the methods of Jacobi or Householder (ref. 25 pp 202-270) to solve the matrix eigenvalue problem for real, symmetric matrices, but these methods suffer from the fact the whole of $\underline{A}$ and $\underline{B}$ or at least one of their symmetrical halves must be stored and no advantage of their respective sparseness is taken. The sparseness must be of paramount importance especially when manipulating and storing large order matrices and Peters and Wilkinson[20] indicate the manner in which the property of sparseness may be utilised in deriving solutions to equation (2.18) whilst Schwarz (ref.25, p 273) reports the method of solution for the generalised matrix eigenvalue problem where $\underline{B}$ is the identity matrix and again full advantage is taken of the sparseness of $\underline{A}$.

The alternative approach of premultiplying equation (2.18) by the inverse of $\underline{B}$, $\underline{B}^{-1}$ is to be avoided, for although both $\underline{A}$, $\underline{B}$ are symmetric and sparse the product $\underline{B}^{-1}\ \underline{A}$ is not necessarily symmetric and is dense, thus reducing the methods of solution for which the complete nonsymmetrical matrix is stored and these methods Wilkinson[25] has noted tend to be numerically unstable.

The direct approach was applied to the homogeneous configuration of fig. (2.2), ($\epsilon_{r_1} = \epsilon_{r_2} = 1$), with electric walls at AB, BCD, DE and a magnetic wall at AFE, and thus seeking the cut-off wave numbers of the TM modes that satisfy these boundary conditions. These are recorded in Table (2.5) with $b=2a$ and using the finite element formulation over square elements, and solving the resultant matrix eigenvalue equation by the method of Householder. Two discretisations, h/b, are employed with modes whose computed cut-off wave numbers differ from the analytic ones by at least 10% being rejected.

TABLE (2.5)

Cut-off wavenumbers $(kb)^2$ of TM_{nm} modes in a waveguide of square cross-section of side b.

$\frac{h}{b}$	Mode	$(kb)^2$ comp.	$(kb)^2$ anal.	Error%
1/8	TM_{11}	19.9942	19.7392	1.29
	TM_{12}	51.5437	49.3480	4.45
1/10	TM_{11}	19.9020	19.7392	0.82
	TM_{12}	50.7450	49.3480	2.83
	TM_{31}	105.5300	98.6960	6.92
	TM_{13}	105.5300	98.6960	6.92
	TM_{32}	136.3700	128.3049	6.28
	TM_{33}	189.5000	177.6529	6.67

TABLE (2.6)

Cut-off wavenumber $(kb)^2$ of TE_{no} modes in a waveguide of width 2b.

$\frac{h}{b}$	Mode	$(kb)^2$ comp.	$(kb)^2$ anal.	Error %
1/4	TE_{10}	2.4992	2.4674	1.29%
1/8	TE_{10}	2.4753	2.4674	0.32
	TE_{30}	22.8557	22.2066	2.92
	TE_{50}	66.7776	61.6850	8.26
1/16	TE_{10}	2.4694	2.4674	0.08
	TE_{30}	22.3675	22.2066	0.72
	TE_{50}	62.9325	61.6850	2.02
	TE_{70}	125.7318	120.9027	3.99
	TE_{90}	213.1686	199.8595	6.66

The errors in Table (2.5) are the same for the corresponding entries in Table (2.1), but it can be seen that a slight decrease in discretisations not only produces an improved accuracy but also introduces far more results concerning the higher order modes below the imposed 10% error level. Note, also, that errors incurred in the computation of the TM_{13}, and TM_{31} cut-off wave numbers are larger than that of the next two higher modes, this is due to the degeneracy of the two modes, thus allowing the matrix eigenvalue problem to possess at least one set of multiple eigenvalues but with differing eigenvectors between which the Householder routine is incapable of distinguishing.

The one dimensional model of TE_{ho} mode propagation was also investigated for various values of discretization and the results recorded in Table (2.6) for the same range of error. Again it can be seen that the results in Table (2.6) are identical to the corresponding entries in Table (2.2).

2.4. THREE DIMENSIONAL FINITE ELEMENTS.

Previous discussion has been restricted to those two dimensional problems where the field dependance in the direction of propagation, z, has been assumed to be of the form $e^{-\gamma z}$, where γ is the constant of propagation. This situation is ideal for structures possessing an axial continuity, as has been shown. However modern microwave communication applications require, for example, the use of sophisticated microstrip circuitry where the strip is seldom axially continuous (change in strip width, terminations etc.,) and where variations in field components exist in each spatial direction, necessitating the utilisation of three dimensional analysis.

To date there has been no formal proposal of such analysis and it is at this point that the feasibility of such studies is considered.

Although, as has been shown, there is little difference between the finite element and finite difference formulations for the same configuration, it is felt that the assertion of a symmetrical matrix operator and the weighting process of nodal potentials exhibited in the derivation of matrix $\underline{B}$, makes the finite element technique slightly more favourable, and thus the finite element approach is considered throughout all further analysis.

2.4.1. Solution of Homogeneous Cavities.

Considering the configuration of fig. (2.6), a rectangular prismatic cavity V consisting of two subregions V_1, V_2. Regions V_1, V_2 consist of uniform, sectionally constant, isotropic, source free dielectric media of relative permittivities ϵ_{r_1}, ϵ_{r_2}, respectively and unity permeabilities.

In a similar manner to that of the two dimensional structure, a set of equations to be satisfied by the field components over a homogeneous subsection of fig. (2.6) are

$$\nabla^2 H_z + k_i^2 H_z = 0 \qquad (2.19a)$$

$$\nabla^2 E_z + k_i^2 E_z = 0 \qquad (2.19b)$$

where $k_i^2 = \omega^2 \mu_o \epsilon_o \epsilon_{r_i}$

subject to the boundary conditions

$E_z = 0$; $\frac{\partial E_z}{\partial s} = 0$; $\frac{\partial H_z}{\partial n} = 0$ on an electric wall

$H_z = 0$; $\frac{\partial H_z}{\partial s} = 0$; $\frac{\partial E_z}{\partial n} = 0$ on a magnetic wall

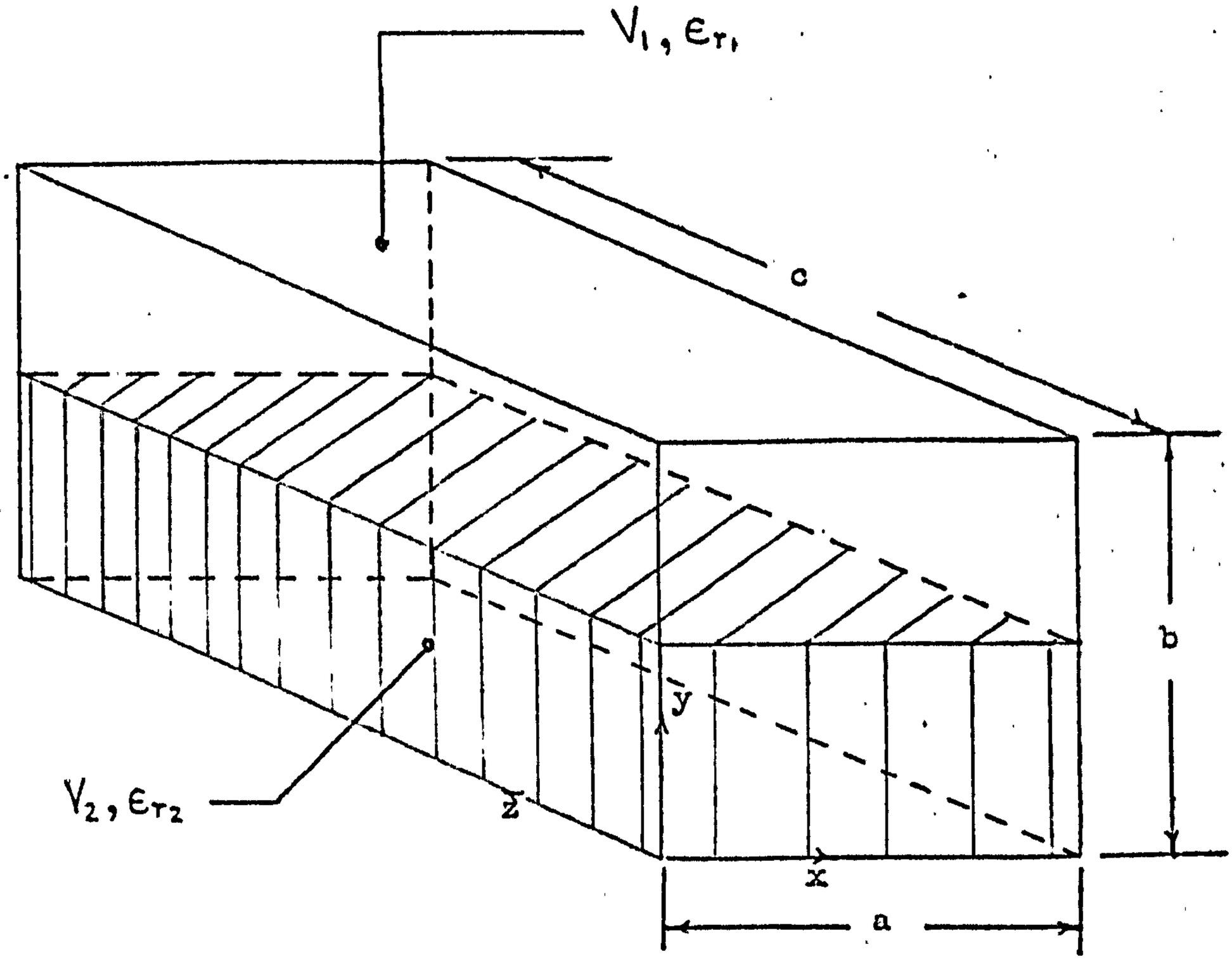

Fig. (2.6.) Rectangular prismatic cavity.

where $\frac{\partial}{\partial n}$ is as before, and $\frac{\partial}{\partial s}$ is the spatial derivative tangential to the surface S, together with continuity of the tangential components of $\underline{E}$ and $\underline{H}$, and normal components of $\underline{D}$ and $\underline{B}$ asserted across the interface.

For a completely homogeneous cavity ($\epsilon_{r_1} = \epsilon_{r_2} = \epsilon_r$), either of equations (2.19) defines a spectrum of possible propagating modes as in the two dimensional configuration. These likewise are classified as TE_{mnp} type if a scalar field ϕ is found such that it satisfies equation (2.19a) and the boundary conditions

$$\frac{\partial \phi}{\partial n} = 0 \qquad \text{on an electric wall}$$

$$\phi = 0 \; ; \quad \frac{\partial \phi}{\partial s} = 0 \qquad \text{on a magnetic wall}$$

and TM_{mnp} type if a scalar field ψ is found such that it now satisfies equation (2.19b) with the dual boundary conditions

$$\frac{\partial \psi}{\partial n} = 0 \qquad \text{on a magnetic wall}$$

$$\psi = 0 \; ; \quad \frac{\partial \psi}{\partial s} = 0 \qquad \text{on an electric wall}$$

A variational expression which is stationary in k^2 ($k^2 = \omega^2 \mu_0 \epsilon_0$), for the homogeneous rectangular prismatic cavity described above can be shown to be

$$J(\phi) = \int_V \frac{1}{\epsilon_r} |\nabla \phi|^2 \, dV - R^2 \int_V \phi^2 \, dV \qquad (2.20)$$

which has as its Euler equations [16]

$$\frac{1}{\epsilon_r} \nabla^2 \phi + R^2 \phi = 0$$

and is satisfied by the three dimensional scalar Helmholtz equation, equation (2.19a). $J(\phi)$ is stationary providing, also, that the fields ϕ satisfy the boundary conditions. Similarly, a variational functional of the form of equation (2.20) can be derived for the electric field scalar, which has its Euler equation the form of equation (2.19b) and is stationary providing the field scalar satisfies the necessary boundary conditions.

The region V is subdivided into a finite number of elements and the value of $\phi(x,y,z)$ which yields the smallest possible $J(\phi)$ will be the correct solution to the three dimensional scalar Helmholtz equation, subject to the boundary conditions. The element chosen for analysis being the cubic prism fig. (2.7).

Over such a typical prism which possesses 8 vertices the field $\phi(x,y,z)$ can thus be represented by

$$\phi^e(x,y,z) = \sum_{r=i,j,k....}^{p} N_r^e(x,y,z)\,\phi_r^e$$

where the shape function N_r^e is [19]

$$N_r^e = a_r + b_r x + c_r y + d_r z + e_r xz + f_r yz + g_r xy + h_r xyz$$

which is uniquely defined and differentiable over each element, and where the coefficients $a_r, b_r \ldots\ldots h_r$ are defined in Table (2.7) with reference to fig. (2.7.).

ϕ_r^e is the value of the scalar magnetic field at the r_{th} vertex of the element.

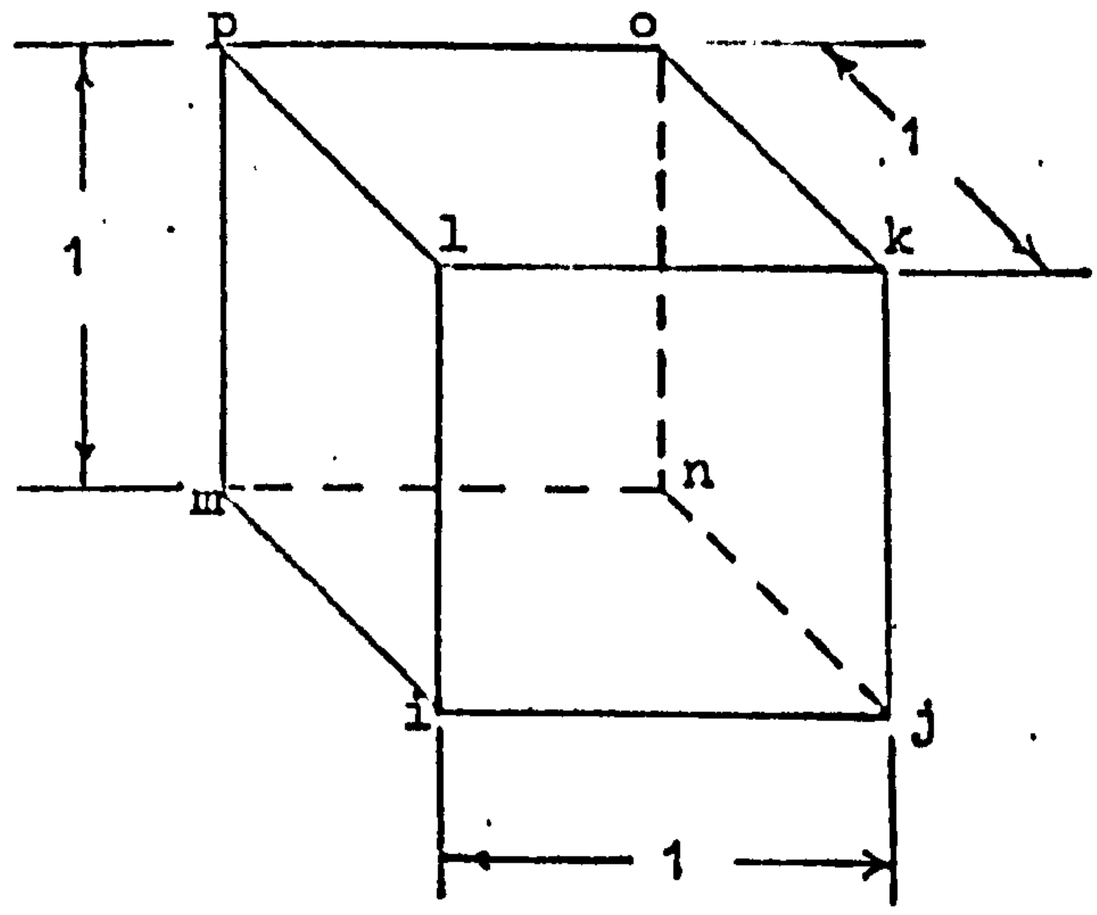

Fig. (2.7.) Cubic element.

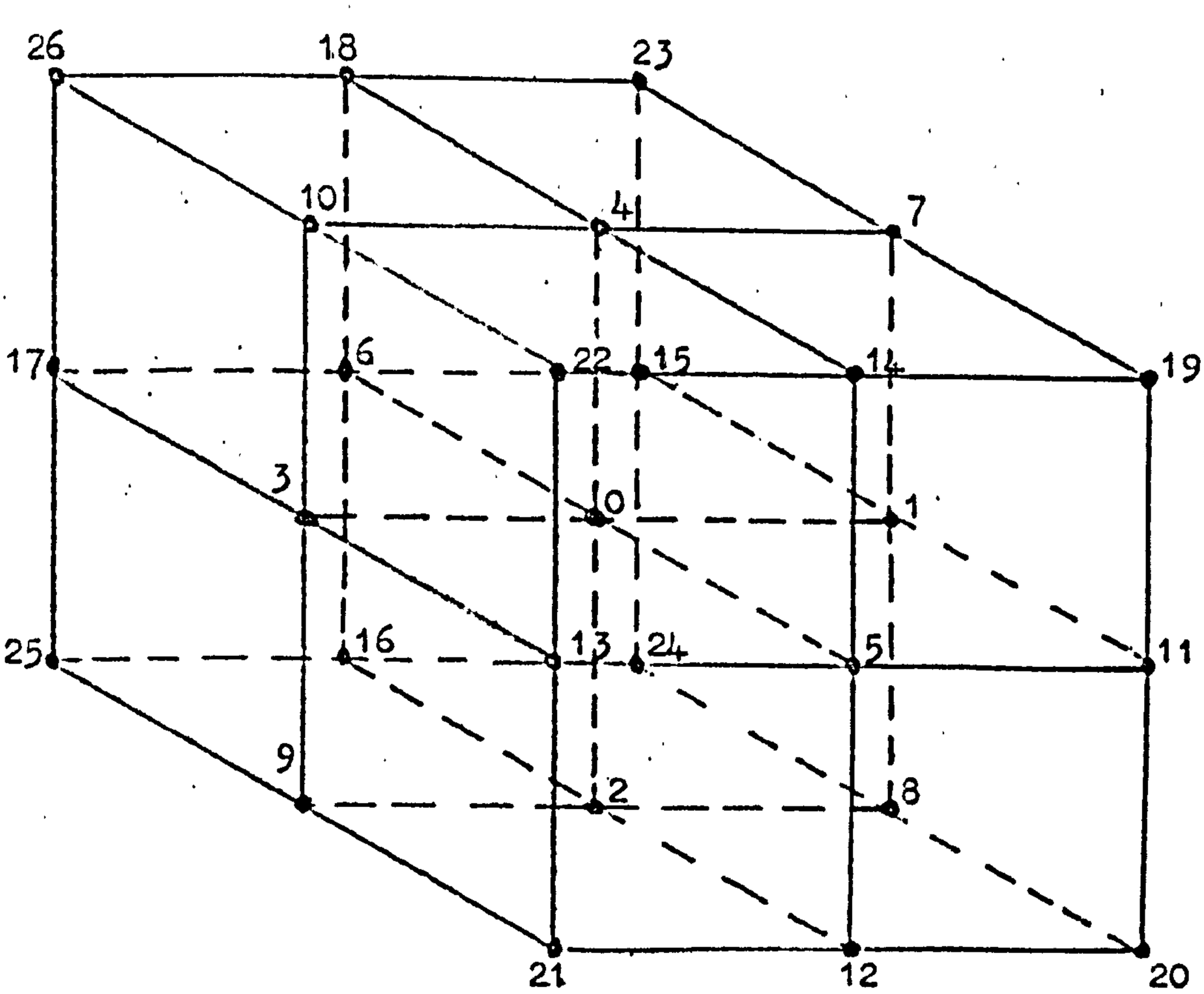

Fig. (2.8.) Interior node common to eight cubic elements.

The substitution of the expression defining the field over each element into the variational functional, yields $J(\phi)$ as a function of the field potentials ϕ_r existing at each vertex of every element describing the structure, and minimization of this function with respect to each ϕ_r will give the correct field configuration and cut-off wave number. Again minimization of $J(\phi)$ over the entire volume is equivalent to minimising $J(\phi)$ over each element providing the field is continuous across the element interfaces,[8] which is assured, and thus if each vertex r of the element, e , is common to P elements, ($\leqslant 8$)

$$\frac{\partial J(\phi)}{\partial \phi_r} = 2 \sum_{e=1}^{R} \left[\frac{1}{\epsilon_r} \int_{el} \left\{ \frac{\partial}{\partial x} [\underline{G}] \underline{\phi}^e \frac{\partial N_r^e}{\partial x} + \frac{\partial}{\partial y} [\underline{G}] \underline{\phi}^e \frac{\partial N_r^e}{\partial y} + \frac{\partial}{\partial z} [\underline{G}] \underline{\phi}^e \frac{\partial N_r^e}{\partial z} \right\} dV - k^2 \int_{el} [\underline{G}] \underline{\phi}^e N_r^e \, dV \right]$$

where

$$[\underline{G}] = [N_i^e \; N_j^e \ldots . \; N_p^e]$$

$$\underline{\phi}^e = [\phi_i^e \; \phi_j^e \ldots . \; \phi_p^e]^T$$

Over one such element, the minimization of $J(\phi)$ may be written more compactly as

$$\frac{\partial \underline{J}(\phi)}{\partial \underline{\phi}^e} = \frac{1}{\epsilon_r} \underline{\underline{S}}^e \underline{\phi}^e - k^2 \underline{F}^e \underline{\phi}^e$$

where

$$\underline{S}^e = \begin{bmatrix} S_{ii} & S_{ij} & \cdots\cdots & S_{ip} \\ S_{ji} & S_{jj} & \cdots\cdots & S_{jp} \\ \vdots & \vdots & & \vdots \\ S_{pi} & S_{pj} & \cdots\cdots & S_{pp} \end{bmatrix} \qquad \underline{F}^e = \begin{bmatrix} F_{ii} & F_{ij} & \cdots\cdots & F_{ip} \\ F_{ji} & F_{jj} & \cdots\cdots & F_{jp} \\ \vdots & \vdots & & \vdots \\ F_{pi} & F_{pj} & \cdots\cdots & F_{pp} \end{bmatrix}$$

and

$$S_{ij} = \int_v \left\{ \frac{\partial \underline{N}_i^e}{\partial x} \frac{\partial \underline{N}_j^e}{\partial x} + \frac{\partial \underline{N}_i^e}{\partial y} \frac{\partial \underline{N}_j^e}{\partial y} + \frac{\partial \underline{N}_i^e}{\partial z} \frac{\partial \underline{N}_j^e}{\partial z} \right\} dx\, dy\, dz$$

$$= (b_i b_j + c_i c_j + d_i d_j) + \frac{1}{6}(g_i g_j + e_i e_j + f_i f_j) + \frac{1}{48} h_i h_j$$

$$F_{ij} = \int_v N_i^e\, N_j^e\, dx\, dy\, dz$$

$$= a_i a_j + \frac{1}{12}(b_i b_j + c_i c_j + d_i d_j) + \frac{1}{144}(e_i e_j + f_i f_j + g_i g_j) + \frac{1}{1728} h_i h_j$$

by suitable integration over the volume and noting that S_{ij}, F_{ij} remain invariant to a change of origin.

The components of $\underline{S}^e$ and $\underline{F}^e$ have been evaluated, for the element discussed and are shown in Table (2.8) where because of symmetry only the upper triangular half of $\underline{S}^e$ and the lower triangular half of $\underline{F}^e$ are quoted, the leading diagonal terms being identical.

For a typical interior vertex, o, fig. (2.8) within the volume V, minimization of $J(\phi)$ with respect to the potential existing at that vertex implies, with the aid of Table (2.8)

TABLE (2.7.)

Coefficients of shape functions Ni, Nj, --- Np over a cubic element

	a	b	c	d	e	f	g	h
i	1	-2	-2	-2	4	4	4	-8
j	1	2	-2	-2	-4	4	-4	8
k	1	2	2	-2	-4	-4	4	-8
l	1	-2	2	-2	4	-4	-4	8
m	1	-2	-2	2	-4	-4	4	8
n	1	2	-2	2	4	-4	-4	-8
o	1	2	2	2	4	4	4	8
p	1	-2	2	2	-4	4	-4	-8

All coefficients have a common divisor of 8.

TABLE (2.8.)

Components of the matrices $\underline{S}^e$, $\underline{F}^e$ for a cubic element, fig. (2.7.)

$\underline{F}^e \diagdown \underline{S}^e =$

	i	j	k	l	m	n	o	p
i	4	0	-1	0	0	-1	-1	-1
j	2	4	0	-1	-1	0	-1	-1
k	1	2	4	0	-1	-1	0	-1
l	2	1	2	4	0	-1	-1	0
m	2	1	$\frac{1}{2}$	1	4	0	-1	0
n	1	2	1	$\frac{1}{2}$	2	4	0	-1
o	$\frac{1}{2}$	1	2	1	1	2	4	0
p	1	$\frac{1}{2}$	1	2	2	1	2	4

Common divisor of $\underline{S}^e$ = 12

Common divisor of $\underline{F}^e$ = 108

$$\frac{1}{12}\left[32\phi_0 - 2\sum_{i=7}^{18}\phi_i - \sum_{i=19}^{26}\phi_i \right]$$

$$= \epsilon_r \frac{R^2}{108}\left[32\phi_0 + 8\sum_{i=1}^{6}\phi_i + 2\sum_{i=7}^{18}\phi_i + \frac{1}{2}\sum_{i=19}^{26}\phi_i\right] \qquad (2.21)$$

and a similar treatment to that for the two dimensional formulation, is required for nodes situated on magnetic and electric walls.

The repeated application of equation (2.21) or a similarly derived equation to each vertex in the system, results in approximating equation (2.19a) together with the relevant boundary conditions by a system of linear algebraic equations in ϕ, the system forming the familar eigenvalue equation

$$(\underline{A} - \lambda \underline{B})\underline{\phi} = \underline{0}$$

with $\underline{A}$, $\underline{B}$ being real, symmetric, banded, sparse, positive definite matrices.

The method of solution must now be restricted to those involving iterative procedures, due to the large number of vertices or nodes generated within the volume. Successive over-relaxation was used to calculate the resonant frequencies of various sizes of cavities, for both TE and TM type modes and are tabulated in Table (2.9). Using most of the lines of symmetry available only a quarter of the rectangular cavity was analysed with the appropriate magnetic and electric walls surrounding the volume.

Table (2.9) indicates that the errors incurred in three dimensional analysis are identical to those for two dimensional analysis by comparison with Table (2.1.).

TABLE (2.9)

Resonant frequencies ($k^2 = \omega^2 \mu_o \epsilon_o$) of rectangular cavities represented by fig. (2.6.) with $\epsilon_{r_1} = \epsilon_{r_2} = 1$ using the unit cubic element.

Mode	a, b, c	(ka) comp.	(ka) anal.	Error. %
TM_{111}) TE_{111})	10, 5, 10	7.7907	7.6953	1.24
TM_{111}) TE_{111})	12, 12, 12	5.4570	5.4414	0.29
TM_{111}) TE_{111})	16, 16, 16	5.4510	5.4414	0.16
TE_{101}	10, 5, 10	4.4618	4.4429	0.43
TE_{101}	12, 12, 12	4.556	4.4429	0.29
TE_{101}	16, 16, 16	4.4503	4.4429	0.17

The TE_{101} mode is a mode which can be analysed in two dimensions, but the inclusion was necessary so as to provide the relevant comparison.

2.4.2. Solution of Continuous Microstrip in three dimensions.

Microstrip is a thin metal strip mounted on a dielectric substrate which has a metallised ground plane,[26] and is now becoming essential for achieving future communication objectives.

Fig. (2.9.) shows a typical microstrip configuration, where the strip is continuous in the z direction and situated on a dielectric substrate of relative permittivity ϵ_r the system being bounded by a perfectly conducting enclosure, with magnetic walls placed at either end of the cavity, and a magnetic wall of symmetry adjacent to the longitudinal edge of the strip. This is necessary since the methods discussed are only applicable to the solution of boundary value problems.

If the structure is totally homogeneous such that $\epsilon_r = 1$ then a pure transverse electromagnetic (TEM) wave can be supported by the multiconductor system. Within such a system, the variation of the electric potential ϕ is governed by the solution of Laplaces equation

$$\nabla^2 \phi = 0 \qquad (2.22)$$

over the volume, subject to the boundary conditions

$\phi = 0$ on the enclosure wall

$\phi = V_0$ on the strip

$\frac{\partial \phi}{\partial n} = 0$ on magnetic walls

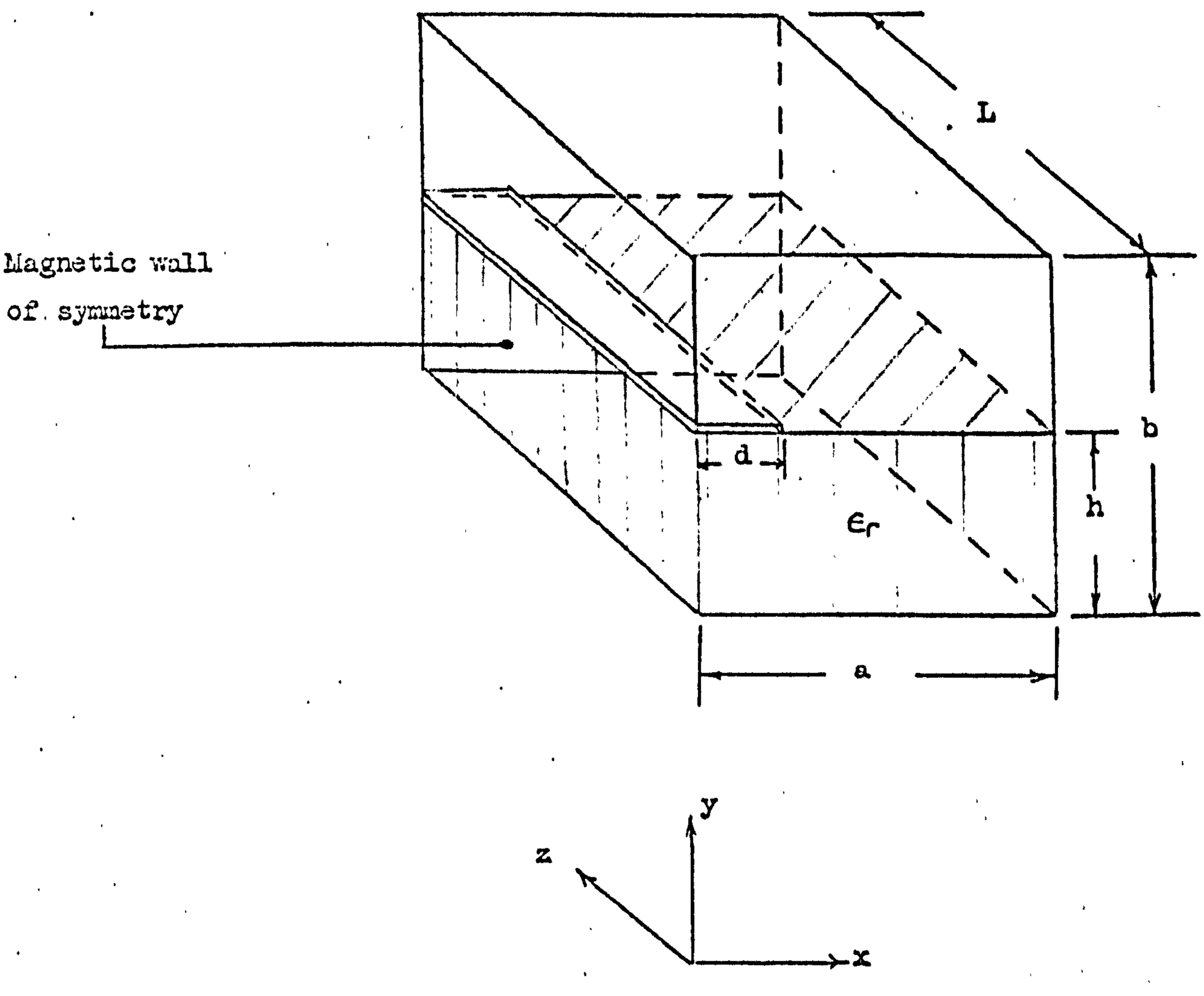

Fig. (2.9.) Typical microstrip structure.

By considering the stored electrostatic energy in the field between the two conductors, a variational expression in C, the capacitance of the system (ref.23, p.148), is given by

$$\frac{C}{\epsilon_o} = \frac{1}{V_o^2}\int_V (\nabla\phi)^2\, dV \qquad (2.23)$$

which will be stationary for a field ϕ satisfying equation (2.22) together with the associated boundary conditions.

The domain of fig.(2.9) is subdivided into unit cubic elements and thus minimization of the functional C over one such element yields,

$$\frac{V_o^2}{\epsilon_o}\frac{\partial \underline{C}}{\partial \underline{\Phi}^e} = \underline{\underline{S}}^e\,\underline{\Phi}^e \qquad (2.24)$$

where $\underline{S}^e$, $\underline{\Phi}^e$ are defined as in section (2.4.1), thus

$$V_o^2\,\frac{\underline{C}}{\epsilon_o}\bigg|_{el} = \int_{el.} \sum_{r=i,j,k..}^{P} \sum_{q=i,j,k...}^{P} \left\{ \frac{\partial \underline{N}_r}{\partial x}\frac{\partial \underline{N}_q}{\partial x} + \frac{\partial \underline{N}_r}{\partial y}\frac{\partial \underline{N}_q}{\partial y} + \frac{\partial \underline{N}_r}{\partial z}\frac{\partial \underline{N}_q}{\partial z} \right\} \phi_r\,\phi_q\, dV$$

$$= \underline{\Phi}^{eT}\,\underline{\underline{S}}^e\,\underline{\Phi}^e.$$

and if there are R elements describing the volume V

$$V_o^2\,\frac{\underline{\underline{C}}}{\epsilon_o} = \sum_{e=1}^{R} \underline{\Phi}^{eT}\,\underline{\underline{S}}^e\,\underline{\Phi}^e \qquad (2.25)$$

Hence a set of linear equations in ϕ; the potentials at each node within the region, are constructed by the application of equation (2.24) at each of the nodes, and is of the form

$$\underline{\underline{A}}\,\underline{\Phi} = \underline{0} \qquad (2.26)$$

which is solved yielding the potentials ϕ; which in turn are then substituted into equation (2.25) to produce the capacitance of the structure.

The configuration of fig. (2.9) was analysed using this procedure with the following parameters.

(i) $a/d = 4$; $a/b = 1.6$; $b = 10$ units.

(ii) $a/d = 5$; $a/b = 2.5$; $b = 8$ units.

with the inner conductor situated at $h=b/2$, and of negligible thickness.

Successive over relaxation was employed to solve equation (2.26) and the capacitance calculated from equation (2.25). The impedance, Z, of such a structure is related to the capacitance by

$$Z = \sqrt{\frac{L'}{C'}} = \sqrt{\frac{\mu_o \epsilon_o}{C'}} = \frac{1}{cC'}$$

where C', L' are the capacitance and inductance per unit length respectively and these are listed in Table (2.10), together with the analytically derived impedances obtained from Collin (ref.23,p.132), also noting the observations made by Hayt[27], namely that for a fixed separation of the ground planes, if

$$\frac{a}{b} > 1.25 ; \qquad \frac{a}{b} \cdot \left(1 - \frac{d}{a} \right) > 0.25$$

then the exact impedance and the approximate value obtained by assuming infinite width ground planes agree to within 0.25%.

The results in Table (2.10) for both cases possess tolerable errors, and of the same order despite increasing the ratios noted by Hayt, enabling the modes to possess a better approximation to infinite width ground planes. The errors incurred are due to the relatively large variations in the field about the strip edge,

TABLE (2.10)

Impedance of strip line with parameters as in fig. (2.9),

Parameters (see text)	Length of cavity	Capacitance (pF)	Capacitance /unit length (pF/m)	Impedance(ohms) Calculated	Impedance(ohms) Analytic (see text)	Error %
(i)	1	45.407	45.407	73.410	75.861	3.23
(i)	2	90.814	45.407			
(i)	5	227.034	45.407			
(ii)	1	52.848	52.848	63.074	65.413	3.57
(ii)	2	105.697	52.848			
(ii)	5	264.241	52.848			

and as no attempt was made to refine the mesh about this singularity and hence an improved field description, the variations could not be adequately described. This inadequacy may however be overcome by using the mesh refinement method or alternatively, in the method of finite differences, using mesh refinement and/or allowing the placement of 'special' nodes in a specified analytic region surrounding the singularity such that during the relaxation process the potentials at these nodes are determined by a truncated series of circular harmonics.[28,29].

If the configuration of fig. (2.9) is inhomogeneous ($\epsilon_r \neq 1$) a TEM wave cannot be supported by the system, unless under D.C. conditions, and thus the dispersion characteristics and propagation of higher ordered modes of microstrip transmission lines can never be properly investigated utilising the previously discussed TEM wave techniques. To date with few exceptions,[13,30,31], the analysis has been confined to a quasi-static approach to the problem,[32,33,34,35], i.e. the fundamental mode of propagation resembles a TEM mode sufficiently well to allow the approximation that the mode is TEM, providing the frequency of operation is not too high, and that the characteristics of such propagation can be obtained from the solution of Laplaces equation throughout the structure.

The finite element formulation of this inhomogeneous structure requires that the matrix $\underline{S}^e$ in equations (2.24), (2.25) be replaced by $\underline{S}^e \rightarrow \epsilon_{ri}\, \underline{S}^e$

where ϵ_{ri} is the relative permittivity in either of the two homogeneous regions completing the structure.

Cubic elements were again used to describe the configuration of fig. (2.9.), successive over relaxation applied to calculate the nodal potentials, and substitution of the potentials into the permittivity modified quadratic form of equation (2.25), yielded the total capacitance of the volume.

The impedance is now related to the capacitance by

$$Z_{\epsilon_r} = \frac{1}{c\sqrt{C'_o C'_{\epsilon_r}}} \qquad Z_o = \frac{1}{c C'_o}$$

where Z_{ϵ_r}, C'_{ϵ_r} represent the impedance and capacitance per unit length of the microstrip structure partially filled with dielectric, and Z_o, C'_o the impedance and capacitance of the same structure entirely filled with air.

The impedance for two ratios of h/d for differing lengths of the cavity are presented in Table (2.11). The analytical results for impedance are those obtained from Bryant and Weiss[36], where the graphical presentation of the parameters necessitated the inclusion of the relevant 'reading' errors.

The analytical and calculated impedances agree to within approximately 10%. This large error must then be attributed to the lack of mesh refinement about the strip edge, to the use of a perfectly conducting enclosure to approximate the open microstrip configuration on which Bryant and Weiss's results are based, and to the introduction of the air-dielectric interface. Results obtained by contracting the enclosure in the xy plane gave progressively worse solutions for the configuration's impedance as was expected, the results quoted in Table (2.11) being the optimum set after a trade-off

TABLE (2.11)

Impedance of enclosed microstrip with parameters as in fig. (2.9.)

a/b = 1.25; h/b = 0.25; b = 16 units.

$\frac{d}{h}$	ϵ_r	Length of cavity	Cer (pF)	C'_{er} (pF/m)	C'_o (pF/m)	Z_{ϵ_r} calculated (ohms)	Z_{ϵ_r} analtyic (ohms) (see text)	Reading error (%)
1.5	1.0	1	35.370					
		2	70.739	35.370	35.370	94.242	106.00	± 2%
		4	141.478					
	9.0	1	211.744					
		2	423.488	211.744	35.370	38.517	42.00	± 5%
		4	846.975					
	16.0	1	365.641					
		2	731.282	365.641	35.370	29.311	32.00	± 6%
		4	1462.563					
2.0	1.0	1	41.472					
		2	82.944	41.472	41.472	80.374	89.00	± 5%
		4	165.887					
	9.0	1	253.322					
		2	506.643	253.322	41.472	32.521	35.7	± 1%
		4	1013.287					
	16.0	1	438.233					
		2	876.466	438.233	41.472	24.726	26.8	± 1%
		4	1752.930					

between completeness and machine store available had been considered. The air-dielectric interface although causing the field to concentrate mostly in the dielectric and hence a larger variation in the field throughout the dielectric to be modelled by the finite element formulation, can have little effect on the solution since the errors incurred in the homogeneous cases ($\epsilon_r = 1$ Table (2.11)) are of the same order as those considered with the relative permittivity possessing other specified values.

2.4.3. Solution of inhomogeneous cavities.

The previous section indicated the manner in which parameters of enclosed microstrip structures may be calculated by utilising a static assumption, but as was noted the lack of dispersion characteristics and information regarding the propagation of higher ordered modes, placed severe restrictions on the use of such an assumption.

To try and reduce these problems, three dimensional finite element analysis was applied to the structure defined in fig. (2.6), regions V_1, V_2 consisting of uniform, sectionally constant, isotropic, source free dielectric media of relative permittivities $\epsilon_{r_1}, \epsilon_{r_2}$ respectively.

An attempt to express the transverse field components E_x, E_y, H_x, H_y, in terms of the axially directed components E_z and H_z as in equation (2.2) fails due to the presence of second order partial derivatives, and thus the derivation of a variational expression in a manner similar to that used by Ahmed[37] could not be found. However a set of equations to be satisfied by the scalar magnetic potential ϕ and the scalar electric potential ψ over a homogeneous subsection of fig.(2.6) are

$$\nabla^2\phi + R_i^2\phi = 0 \qquad (2.27a)$$

$$\nabla^2\psi + R_i^2\psi = 0 \qquad (2.27b)$$

where $R_i^2 = \omega^2\mu_0\epsilon_0\epsilon_{ri}$

subject to the usual boundary conditions on magnetic and electric walls.

If a plane, in the xy plane, is considered in fig.(2.6), then it is shown equation (2.10) is a variational functional in k^2, which when stationary yields the propagation characteristics of this two dimensional plane, satisfying the boundary conditions at the outer walls of the cross-section and also the interfacial boundary conditions.

It is now the contention that if all similar planes are considered so as to form the configuration of fig. (2.6.) then by allowing τ_i to become $\frac{1}{\epsilon_{ri}}$; $\int_s$ to become $\int_v$; ∇_{xy} to become ∇ in equation (2.10)

$$J(\phi,\psi) = \int_v \Big[\frac{1}{\epsilon_{ri}} |\nabla\phi|^2 + \bar{\beta}^2 |\nabla\psi|^2 + 2\underline{e}_z \frac{\bar{\beta}^2}{\epsilon_{ri}} (\nabla\psi \wedge \nabla\phi) - R^2(\bar{\beta}^2\epsilon_{ri}\psi^2 + \phi^2)\Big] dV \qquad (2.28)$$

where $R^2 = \omega^2\mu_0\epsilon_0$; $\phi = H_z$; $\psi = \frac{\omega\epsilon_0}{\beta} E_z$.

represents a variational expression in k^2.

Note that since the cavity is continuous in the z direction, the

field dependance of $e^{-j\beta z}$ in this direction is retained and thus the propagating constant β remains as a factor in the variational expression. The Euler equations of equation (2.28) over each homogeneous subsection of fig. (2.6) are

$$\nabla^2\phi + k^2\epsilon_{ri}\phi = 0$$

$$\bar{\beta}^2\nabla^2\psi + \bar{\beta}^2 k^2\epsilon_{ri}\psi = 0$$

which are satisfied because of the three dimensional scalar Helmholtz equations, equation (2.27).

Equation (2.28) will be stationary in k^2, if any first order change in the fields Φ , ψ from their true values, will produce only second order changes in k^2 i.e.

$$\Phi \rightarrow \Phi + \delta\Phi$$
$$\psi \rightarrow \psi + \delta\psi$$
$$k^2 \rightarrow k^2 + \delta(k^2)$$

then $\delta(k^2) = 0$ neglecting all second order variations. By actual substitution and manipulation, the variation $\delta(k^2)$ is zero provided $\delta\psi = 0$ on an electric wall, $\delta\Phi = 0$ on a magnetic wall and

$$\bar{\beta}^2\left\{-\left(\frac{\partial\psi}{\partial y}\right)_{V_1} + \frac{1}{\epsilon_{r1}}\frac{\partial\Phi}{\partial x}\right\} = \bar{\beta}^2\left\{-\left(\frac{\partial\psi}{\partial y}\right)_{V_2} + \frac{1}{\epsilon_{r2}}\frac{\partial\Phi}{\partial x}\right\} \qquad (2.29a)$$

$$\frac{1}{\epsilon_{r1}}\left(\frac{\partial\Phi}{\partial y}\right)_{V_1} + \frac{\bar{\beta}^2}{\epsilon_{r1}}\frac{\partial\psi}{\partial x} = \frac{1}{\epsilon_{r2}}\left(\frac{\partial\Phi}{\partial y}\right)_{V_2} + \frac{\bar{\beta}^2}{\epsilon_{r2}}\frac{\partial\psi}{\partial x} \qquad (2.29b)$$

on the interfacial boundary considering one of the planes z = constant, which imply continuity of $E_x\left(1 - \frac{\bar{\beta}^2}{\epsilon_{r1}}\right)$ and $H_x\left(1 - \frac{\bar{\beta}^2}{\epsilon_{r1}}\right)$ and are not the natural boundary conditions to be satisfied.

However, whilst realising that equation (2.28) did not represent a true and complete variational expression in k^2 for the configuration of fig. (2.6); the three dimensional formulation of the structure was accomplished via the variational functional of equation (2.28), applying the finite element techniques described in the previous sections.

Minimization of $J(\Phi,\Psi)$ over a cubic element, describing a section of fig. (2.6), with respect to the potential Φ,Ψ existing at each vertex of the element yields.

$$\frac{\partial J^e(\Phi,\Psi)}{\partial \underline{\Phi}^e} = \frac{1}{\epsilon_{ri}} \underline{S}^e \underline{\Phi}^e + \frac{\bar{\beta}^2}{\epsilon_{ri}} \underline{C}^e \underline{\Psi}^e - k^2 \underline{F}^e \underline{\Phi}^e \qquad (2.30a)$$

$$\frac{\partial J^e(\Phi,\Psi)}{\partial \underline{\Psi}^e} = \bar{\beta}^2 \underline{S}^e \underline{\Psi}^e - \frac{\bar{\beta}^2}{\epsilon_{ri}} \underline{C}^e \underline{\Phi}^e - k^2 \bar{\beta}^2 \epsilon_{ri} \underline{F}^e \underline{\Psi}^e \qquad (2.30b)$$

where $\underline{\Phi}^e$, $\underline{\Psi}^e$ are column matrices as before whose elements are the values of the scalar magnetic and electric potentials at the vertrices of the elements and $\underline{S}^e$, $\underline{F}^e$ are the element submatrices defined in Table (2.8). The element submatrix $\underline{C}^e$ is that derived from the 'coupling' term in equation (2.28) and whose elements are defined in Table (2.12), and for a typical interior node or vertex situated on the dielectric interface, surrounded by eight elements, then minimization of $J(\Phi,\Psi)$ as in equation (2.30) implies the equations, with reference to fig. (2.8).

TABLE (2.12)

Components of Matrix $\underline{C}^e$ for a cubic element, fig. (2.7.)

$$\underline{C}^e = \begin{array}{c|cccccccc|c} & i & j & k & l & m & n & o & p & \\ \hline & 0 & -2 & 0 & 2 & 0 & -1 & 0 & 1 & i \\ & 2 & 0 & -2 & 0 & 1 & 0 & -1 & 0 & j \\ & 0 & 2 & 0 & -2 & 0 & 1 & 0 & -1 & k \\ & -2 & 0 & 2 & 0 & -1 & 0 & 1 & 0 & l \\ & 0 & -1 & 0 & 1 & 0 & -2 & 0 & 2 & m \\ & 1 & 0 & -1 & 0 & 2 & 0 & -2 & 0 & n \\ & 0 & 1 & 0 & -1 & 0 & 2 & 0 & -2 & o \\ & -1 & 0 & 1 & 0 & -2 & 0 & 2 & 0 & p \end{array}$$

Common divisor of 12.

$$16(1/\epsilon_{r_1} + 1/\epsilon_{r_2})\phi_0 - (1/\epsilon_{r_1} + 1/\epsilon_{r_2})(\phi_{11}+\phi_{13} + \phi_{15} + \phi_{17})$$

$$- 2/\epsilon_{r_1}(\phi_7 + \phi_{10} + \phi_{14} + \phi_{18}) - 2/\epsilon_{r_2}(\phi_8 + \phi_9 + \phi_{12} + \phi_{16})$$

$$- 1/\epsilon_{r_1}(\phi_{19} + \phi_{22} + \phi_{23} + \phi_{26}) - 1/\epsilon_{r_2}(\phi_{20} + \phi_{21} + \phi_{24} + \phi_{25})$$

$$+ \bar{\beta}^2(1/\epsilon_{r_2} - 1/\epsilon_{r_1})(4(\psi_3 - \psi_1) - \psi_{11} - \psi_{15} + \psi_{13} + \psi_{17})$$

$$= \frac{k^2}{108}\left(32\phi_0 + 8\sum_{i=1}^{6}\phi_i + 2\sum_{i=7}^{18}\phi_i + \frac{1}{2}\sum_{i=19}^{26}\phi_i\right)$$

and

$$32\psi_0 - 2\sum_{i=7}^{18}\psi_i - \sum_{i=19}^{26}\psi_i - (1/\epsilon_{r_2} - 1/\epsilon_{r_1})(4(\phi_3 - \phi_1) - \phi_{11} - \phi_{15} + \phi_{13} + \phi_{17})$$

$$= \frac{k^2}{108}\Big(16(\epsilon_{r_1}+\epsilon_{r_2})\psi_0 + 4(\epsilon_{r_1}+\epsilon_{r_2})(\psi_1+\psi_3+\psi_5+\psi_6) + 8\epsilon_{r_1}\psi_4 + 8\epsilon_{r_2}\psi_2$$

$$+(\epsilon_{r_1}+\epsilon_{r_2})(\psi_{11}+\psi_{13}+\psi_{15}+\psi_{17}) + 2\epsilon_{r_1}(\psi_7+\psi_{10}+\psi_{14}+\psi_{18})$$

$$+ 2\epsilon_{r_2}(\psi_8+\psi_9+\psi_{12}+\psi_{16}) + 1/2\epsilon_{r_1}(\psi_{19}+\psi_{22}+\psi_{23}+\psi_{26})$$

$$+ 1/2\epsilon_{r_2}(\psi_{20}+\psi_{21}+\psi_{24}+\psi_{25})$$

Application of these over each vertex within the cavity, with due regard for a vertex being situated wholly in one region, and also for similarly derived equations according as to whether the vertex lies on a magnetic or electric wall yields the familiar eigenvalue equation

$$(\underline{A} - \lambda\underline{B})\underline{\Theta} = 0$$

Where again $\underline{A}$ is a symmetric, positive definite matrix ($\bar{\beta}^2<1$) and $\underline{B}$ is positive definite. Both matrices being sparse and banded. $\underline{\Theta}$ is the column matrix corresponding to the potentials existing at each node within the cavity.

Initially a cavity of width, height and length of 8 units was analysed, with a magnetic wall situated at $x=a/2$ and $z = c/2$, fig. (2.6.), with electric walls elsewhere, so that only a quarter of the total configuration need be modelled. A dielectric slab of relative permittivity 1.5 and of height b/2 was situated as shown, with the relative permittivity of region V_1 being unity.

Unlike the two dimensional equivalent, the present configuration does not have to be solved for several values of $\bar{\beta}^2$ since the phase constant is uniquely determined by the length of the cavity. Thus the finite element formulation introduces two unknowns namely k^2 and $\bar{\beta}^2$ which are interdependant by

$$\bar{\beta}^2 = 4\pi^2 / \left[R^2 \left(2. \text{ length of cavity} \right)^2 \right]$$

Successive over-relaxation was applied to the resulting eigenvalue equation, the initial estimates of k^2 and $\bar{\beta}^2$ were used in the first cycle of relaxations and applying the Rayleigh quotient to the field shape, an improved estimate of k^2 obtained, from which an updated value of $\bar{\beta}^2$ could be sought. This however caused k^2 to fluctuate rapidly and convergence failed. The alternative of fixing $\bar{\beta}^2$ and calculating k^2 gave convergence with the results of Table (2.13), row (a). The analytic results were obtained from dispersion curves by Marcuvitz[33], since the product

$$\frac{\lambda_o}{\lambda_g} \left(\frac{\text{width of cavity}}{\lambda_o} \right) = \frac{1}{2} \frac{\text{Width of cavity}}{\text{Length of cavity}}$$

is known.

TABLE (2.13)

Frequency of propagation ($\omega^2\mu_o\epsilon_o$) of the dominant mode in a slab loaded cavity, as in fig. (2.6.)

	$\bar{\beta}^2$	0.0	0.1	0.2	0.3	0.4	0.5	0.6	0.7	0.8	0.9
(a)	ϵ_r = 1.5										
	a,b,c = 8,8,8	0.2440	0.2439	0.2439	0.2438	0.2437	0.2437	0.2436	0.2435	0.2435	0.2434
	Error %	1.31	1.28	1.28	1.23	1.19	1.19	1.15	1.12	1.09	1.06
(b)	ϵ_r = 9.0										
	a,b,c = 8,8,8	0.05026	0.05024	0.05023	0.05021	0.05019	0.05017	0.05016	0.05014	0.05012	0.05010
	Error %	1.17	1.24	1.21	1.17	1.14	1.10	1.07	1.03	0.99	0.95
(c)	ϵ_r = 1.5										
	a,b,c = 8,6,12	0.1824	0.1823	0.1822	0.1821	0.1820	0.1819	0.1818	0.1817	0.1816	0.1815
	Error %	1.07	1.00	0.94	0.88	0.82	0.77	0.70	0.64	0.58	0.52
(d)	ϵ_r = 9.0										
	a,b,c = 8,6,12	0.05048	0.05040	0.05032	0.05024	0.05015	0.05007	0.04997	0.04988	0.04977	0.04967
	Error %	1.50	1.35	1.19	1.03	0.86	0.68	0.49	0.30	0.09	0.12

Analytical results:- (a) $\omega^2\mu_o\epsilon_o$ = 0.2408 at $\bar{\beta}$ = 0.8002. (b) $\omega^2\mu_o\epsilon_o$ = 0.04963 at $\bar{\beta}$ = 1.7628

(c) $\omega^2\mu_o\epsilon_o$ = 0.1805 at $\bar{\beta}$ = 0.6162 (d) $\omega^2\mu_o\epsilon_o$ = 0.04973 at $\bar{\beta}$ = 1.1740

For the range of $\bar{\beta}^2$ considered the value of k^2 did not vary appreciably; a minimum being expected around the analytical value of $\bar{\beta}^2$. Further cavity sizes with differing relative permittivities of the dielectric slab, were also investigated, the results again shown in Table (2.13) rows b, c, d. Examination of Table (2.13) indicates that k^2, the parameter representing the frequency of propagation, does not vary greatly with $\bar{\beta}$ and the method of analysis gives k^2 to reasonable degree of accuracy even for a value of $\bar{\beta} = 0$ Having thus calculated k^2, the corresponding value of $\bar{\beta}$ can quickly be found.

2.5. DISCUSSION AND CONCLUSIONS.

The analysis of waveguide structures in two spatial dimensions has been briefly described using two common techniques, namely the representation of the derivatives in the scalar Helmholtz equation, by the method of finite differences; and by utilising the stationary condition of a variational functional where the fields within the waveguide configuration are described by an algebraic polynomial of the co-ordinate directions over a small subregion or element of that configuration. The natural extension and feasibility of analysing a three dimensional cavity employing a simple cubic element was also investigated.

There is little difference in accuracy of solution between the methods of finite differences using a 5 point finite difference operator and finite elements using a square element (9 point operator) to describe the field variations over a rectangular region and likewise for the respective 3 point operators employed for those structures possessing only one spatial variation of the field. However the finite element method is recognised to be the more powerful mainly due to the symmetry of the matrix operators and thus many criteria are satisfied which permits the use of algorithms specifically designed for the solution of such matrix eigenvalue problems; and the weighting process of nodal potentials in the construction of matrix $\underline{B}$.

The subdivision of a region into a regular mesh has so far been discussed, but there are certain distinct advantages to be gained from the use of a graded or irregular mesh, to model awkward boundary

shapes or notably when considering a part of the region possessing a large field variation and thus a fine mesh is advisable to describe this variation whilst a relatively coarser mesh may be used elsewhere. The fact that 'elements' may possess any orientation to the co-ordinate axes and hence application of a graded mesh scheme or the modelling of complicated boundaries presents little difficulty, whereas the less favourable approach to the problem using a finite difference formulation would incorporate interpolation or other techniques (ref. 1, p.365) thus intensifying the already present lack of symmetry.

Variational methods have been used in conjunction with finite difference approximations (refs: 5; 1, p.329; 38) and the derivation of the relevant operator is then assured to be symmetrical. However, these operators are derived from exactly the same assumptions as those used in the finite element technique, and the two methods are then identical.

The eigenvalues and eigenvectors of the matrix eigenvalue problems were calculated using indirect and direct methods for the conditions of symmetric and at least positive semidefinite matrices, and in both cases were shown to provide the same accuracy. The direct method whilst solving for higher ordered eigenvalues than the fundamental suffered from the restriction that the whole or at least half of both matrices had to be stored, or if the band structure of the matrices utilised the number of elements required to be stored depended on the order and band width of the matrices, both of which depend on the number of nodes describing the region of interest. Consequently mesh grading or refinement schemes not only increase the order of the

matrix but also the band width and the course of refining or grading must be curtailed before the matrices become prohibitively large. The indirect method of successive over relaxation generate the elements of the matrices when required, but this iterative procedure places far more constraints on the properties of the matrices for a guaranteed convergence to the correct solution. Convergence was apparent in all configurations examined except for the solution of LSE and LSM type modes in a slab loaded waveguide, when the phase velocity of the propagating wave was allowed to be less than that of light ($\Gamma_i < 0$) and the matrix $\underline{A}$ becomes indefinite. The criterion of the matrix off-diagonal elements being less than or equal to zero which was violated by the contribution of the coupling terms at the dielectric interface of the inhomogeneous structures did not cause the method to fail, and thus in the finite element method the choice of an element need not be restricted to those giving rise to an elemental submatrix $\underline{S}^e$ whose off-diagonal terms are non positive, as is the position with a triangular element possessing an interior angle greater than 90°.

Most texts describing the techniques of successive over-relaxation, suggest that the techniques prove most beneficial when the matrix $\underline{A}$, possesses Young's property (A) (ref. 1, p. 242) which indicates the process by which an accelerated convergence can be achieved. All the matrix operators, except that resulting from the 5 point difference operator, on the pagewise ordering of the node scheme, lacked this property, but the accelerating factor, w, suggested by Carré[39] was used throughout.

This value of w being continually updated after several iterative cycles, provided a vast increase in the rate of convergence, even though it was not the optimum value. Forsythe and Wasow (ref.1, p.376) recommend an initial accelerating factor of 1 so that the residuals R existing at each node are kept to a minimum and thus allowing the Rayleigh quotient to become settled with a 'shaped' field, the accelerating factor also causes an erratic behaviour of the residuals so that a final sweep of the complete field with w = 1 is suggested to clean up the eigenvector, these procedures were adopted.

The application of the finite element method to three dimensional structures was accomplished via a simple cubic element. Although the trivial case of describing the fields and calculating the cut-off wave number of a rectangular prismatic cavity was successfully considered, the method can be readily adapted to more complicated structures, using cubic elements, or perhaps the simplest three dimensional element, the tetrahedron.

A continuous strip line situated in a totally homogeneous region was examined,by minimising the stored electrostatic energy between two conductors, and calculating the capacitance per unit length and characteristic impedance of the structure such that the equivalent circuit may be easily derived. The propagating modes of the continuous microstrip structure are of a hybrid nature and lacking a formal three dimensional variational expression for the solution of hybrid modes, the system could only be solved by assuming a quasi-static approach, which is valid for the strip width and substrate thickness dimensions being a small fraction of the wavelength in the dielectric, and whilst

being a relatively good approximation for low frequency operation and low relative permittivies, the use of such assumptions must remain suspect for high permittivity substrates and operation at higher frequencies. The large errors incurred for the analysis of the two multi conductor systems just described were assumed to originate from the failure to describe the large field variations in the vicinity of the strip, where mesh grading would have been advisable but not used, and also to the modelling of an open microstrip structure by an enclosed structure, which however tends to be the more applicable in modern microwave circuit applications. Again the trivial case of a continuous strip was analysed, but the method can easily be extended to accomodate discontinuities of one or more such conductors, such as abrupt terminations, change in line width, gaps, etc., providing the quasi-static assumption still prevails.

The attempted solution for propagation parameters of the symmetrical dielectric loaded cavity, using an incomplete variational expression, produced surprisingly accurate results. The variational functional adopted, satisfied the three dimensional scalar Helmholtz equations, but the boundary conditions satisfied at the interface, equations (2.29), required the continuity of

$$E_x\left(1 - \bar{\beta}^2/\epsilon_{r_i}\right) \quad \text{and} \quad H_x\left(1 - \bar{\beta}^2/\epsilon_{r_i}\right)$$

which are not the natural interface continuity conditions of the system.

It must be stressed that although the method yielded reasonable solutions the lack of a formally derived variational expression placed severe restrictions on the use of this method and it was concluded that this was sufficient to arrest the pursuit of further analysis.

The above methods were based on the choice of the simplest finite difference formulations and also one of the simplest elemental shapes for the finite element formulation, i.e. 5, 7, 9 point operators. Higher ordered operators may be used for both the above techniques[3,18,19], to obtain more accurate solutions, but the disadvantage of an increased complexity in formulating the methods especially in the vicinity of the boundaries describing the structure must be inherent.

CHAPTER 3.

COMPARISON OF LINEAR INTERNODAL FUNCTIONS AND CIRCULAR INTERNODAL FUNCTIONS.

The previous chapter indicated the manner in which wave guide configurations could be analysed by the methods of finite differences and finite elements. The main difficulties that arose were confined to the complexity of the respective formulations, and the inability to correctly describe the field variation between two adjacent nodes or vertices within the region. The former difficulty, can only be resolved by the user who is well aware of the many detailed mathematical procedures necessary to provide the formulation and indeed to solve the resulting eigenvalue equation, and tends to be quite tedious. The absence of a complete internodal potential function is perhaps fundamentally trivial, but as more accurate propagation characteristics are required, the discretisation of the region has to be decreased to enable the potential function between neighbouring nodes to describe a progressively smaller fraction of the total field variation, and thus requiring the number of nodes within the region and hence machine store to be increased. The purpose of this section is to examine the possibility of using circular internodal potential functions, which will possess the advantage of an improved field description error and thus less nodes required within the region of interest, with a formulation that requires only a knowledge of basic transmission line theory.

3.1. UPPER AND LOWER BOUNDS OF THE FINITE ELEMENT AND FINITE DIFFERENCE FORMULATIONS.

Fig. (3.1) shows the one dimensional model used in the previous chapter for the analysis of a TE_{mo} type mode in a homogeneous medium. Let a magnetic wall exist at $x = 0$ and an electric wall at $x = a$ such that the scalar magnetic potential satisfies,

$$\phi = 0 \quad \text{at} \quad x = 0 \; ; \qquad \frac{\partial \phi}{\partial x} = 0 \quad \text{at} \; x = a$$

If an operator A is defined such that

$$A = 2 \cos \frac{m\pi h}{2a} = 2 \cos \frac{m\pi}{2n}$$

and

$$\begin{aligned} \phi_2 &= v \\ \phi_3 &= A\phi_2 - \phi_1 = A\phi_2 \\ &\vdots \\ \phi_{i-2} &= A\phi_{i-3} - \phi_{i-4} \\ \phi_{i-1} &= A\phi_{i-2} - \phi_{i-3} \\ \phi_i &= A\phi_{i-1} - \phi_{i-2} \\ &\vdots \end{aligned} \tag{3.1}$$

then these simple recursive relationships are satisfied by the true field variation of

$$\phi(x) = \sin \frac{m\pi x}{2a} \qquad m = 1,3,5, \ldots\ldots$$

since $$\phi_i = \sin \frac{m\pi}{2a} (i-1)h$$

and from equation (3.1)

$$\phi_i = 2 \cos \frac{m\pi h}{2a} \sin \frac{m\pi}{2a}(i-2)h - \sin \frac{m\pi}{2a} (i-3)h$$

$$= \sin \frac{m\pi}{2a} (i-1)h$$

with $$\phi_2 = \sin \frac{m\pi h}{2a}$$

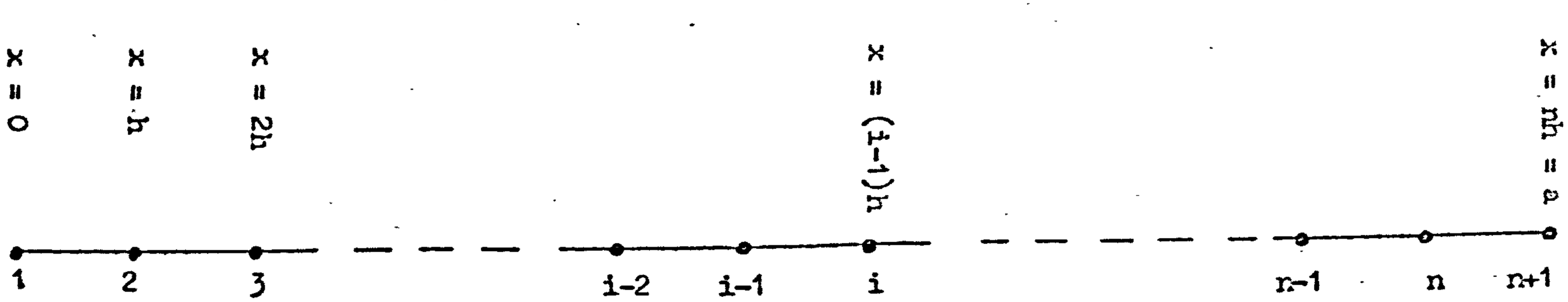

Fig. (3.1). Model used for TE_{no} mode type analysis.

The finite difference and finite element formulation of the one dimensional TE_{no} mode, relies on the repeated application of,

$$2\phi_{i-1} - \phi_i - \phi_{i-2} = k_D^2 h^2 \phi_{i-1} \qquad (3.2a)$$

or

$$2\phi_{i-1} - \phi_i - \phi_{i-2} = \frac{k_E^2 h^2}{6} (4\phi_{i-1} + \phi_i + \phi_{i-2}) \qquad (3.2b)$$

at each node of the model.

Comparing the finite difference relationship, equation (3.2a), with that of equation (3.1.),

$$k_D^2 h^2 = 2 - A = 2 - 2 \cos \frac{m\pi h}{2a}$$

and

$$\lim_{h \to 0} k_D^2 = \left(\frac{m\pi}{2a}\right)^2 \left\{ 1 - \frac{h^2}{12} \cdot \left(\frac{m\pi}{2a}\right)^2 + O(h^4) \right\} \qquad (3.3a)$$

whilst the finite element formulation yields

$$k_E^2 h^2 = 6 \frac{(2 - A)}{(4 + A)} = 6 \left\{ \frac{(1 - \cos \left(\frac{m\pi h}{2a}\right)}{(2 + \cos \left(\frac{m\pi h}{2a}\right)} \right\}$$

with

$$\lim_{h \to 0} k_E^2 = \left(\frac{m\pi}{2a}\right)^2 \left\{ 1 + \frac{h^2}{12} \left(\frac{m\pi}{2a}\right)^2 + O(h^4) \right\} \qquad (3.3b)$$

where k_D and k_E $(= w\sqrt{\mu_o \epsilon_o})$ represent the respective cut-off frequencies of the finite difference and finite element methods. Thus the cut-off wavenumbers derived from the finite difference and finite element formulations form lower and upper bounds respectively, and further

$$0 \leqslant k_D^2 h^2 \leqslant 4 \qquad \text{(finite differences)} \qquad (3.4a)$$

$$0 \leqslant k_E^2 h^2 \leqslant 12 \qquad \text{(finite elements)} \qquad (3.4b)$$

which imply that the number of modes that can be solved using either formulation is limited to the number of nodes defining the structure.

As a numerical example, consider the case n = 4, h = 1 in fig. (3.1), whereupon

$$k_D^2 = (2 - A) = 2\left(1 - \cos\frac{m\pi}{8}\right) \quad ; \quad m = 1,3,5,7.$$

$$k_E^2 = 6\,\frac{(1 - A)}{(2 + A)} = 6\left\{\frac{1 - \cos\left(\frac{m\pi}{8}\right)}{2 + \cos\left(\frac{m\pi}{8}\right)}\right\}; \quad m = 1,3,5,7.$$

These are tabulated in Table (3.1), together with the analytically exact result; $k^2a^2 = (m\pi/2)^2$. The cut-off wavenumbers corresponding to the dominant mode are those reported in Tables (2.2) and (2.5) and examination of the corresponding entries in the respective error columns indicate that these are

$$\pm \left(\frac{m\pi}{2a}\right)^2 \cdot \frac{h^2}{12} \quad 100\%$$

as forecasted by equations (3.3). The higher ordered modes, however do not follow the predicted error, but on addition of the error term in h^4, i.e.

$$+ \left(\frac{m\pi}{2a}\right)^4 \frac{h^4}{360}$$

such that the negligible residual will be of the order h^6, the errors can again by accurately predicted. One immediate advantage is that providing a reasonable choice of spatial discretization is made then the exact solutions can be obtained via equations (3.3) which are quadratic in the true cut-off wavenumber. This obviates the use of Aitkens δ^2 process (ref. 13; page 287) which relies on the ratios of successive error terms being ultimately constant, and consequently a more exact extrapolated solution can be sought.

TABLE (3.1) Theoretical results for the finite difference and finite element formulations of fig. (3.1)

m	$\left(\frac{m\pi}{2}\right)^2$	k_D^2	$k_D^2 a^2$	Error %	k_E^2	$k_E^2 a^2$	Error %
1	2.4674	0.1522	2.4359	1.29	0.1562	2.4993	1.29
3	22.2066	1.2346	19.7541	11.04	1.5545	24.8721	12.00
5	61.6851	2.7654	44.2459	28.27	5.1296	82.0727	33.05
7	120.9026	3.8478	61.5641	49.08	10.7268	171.6280	41.96

This is usually applied to three solutions k_1^2, k_2^2, k_3^2, obtained by successive mesh halving and extrapolating by

$$k^2_{extrap.} = \frac{k_1^2 k_3^2 - (k_2^2)^2}{k_1^2 - 2k_2^2 + k_3^2} ,$$

which is identical to that obtained from the application of equations (3.3).

A recent publication[11] has the same results as discussed above with extensions into two and three dimensions for the finite element formulation, and also for higher ordered polynomial elements.

The errors possessed by both the finite element and difference methods, thus cannot vanish but only minimised by a decrease in mesh discretization. The operator A is essentially a circular function, which simply adds a constant phase onto the phase of the previous nodal potential, and since it is an exact representation of the true TE_{mo} field structure, application of equations (3.1) to the model of fig. (3.1.) will provide the advantage of a complete absence of discretization errors and restrictions of the number of nodes that can be generated.

3.2. APPLICATION OF THE OPERATOR A.

Allowing fig. (3.1.) to represent the complete cross sectional model for TE_{mo} type mode propagation, such that an electric wall or perfect conductor now exists at x = 0 and x = a, then let

$$A = 2 \cos kh \quad , \quad {}_1\phi_1^+ = 1$$

where k is the angular shift (radians) per unit length across the guide, thus

$$
\begin{aligned}
{}_1\phi_2^+ &= \cos kh. \\
{}_1\phi_3^+ &= A\ {}_1\phi_2^+ - {}_1\phi_1^+ = \cos\ 2kh \\
&\vdots \\
{}_1\phi_i^+ &= A\ {}_1\phi_{i-1}^+ - {}_1\phi_{i-2}^+ = \cos\ (i-1)\ kh \\
&\vdots \\
{}_1\phi_{n+1}^+ &= A\ {}_1\phi_n^+ - {}_1\phi_{n-1}^+ = \cos\ n\ kh
\end{aligned}
\qquad (3.5)
$$

where ${}_1\phi_i^+$ is the magnetic potential existing at the i_{th} node in the 1st series of operations with A, or iterations in the direction of increasing x.

Now the system of equations (3.5) represent an electromagnetic plane wave travelling towards and incident upon a perfect conductor at x = a. The occurrence of incidence implies the introduction of a reflected wave, such that the electric field strength is reversed in phase on reflection, in order to produce a zero resultant field at the conductor, and thus for a reversal of direction of energy propagation the magnetic field strength ϕ, is reflected without a phase reversal. This reflection at the conducting boundary is accomplished by

$$
\begin{aligned}
{}_1\phi_n^- &= A\ {}_1\phi_{n+1}^- - {}_1\phi_n^- = \cos\ (n+1)\ kh. \\
&\vdots \\
{}_1\phi_i^- &= A\ {}_1\phi_{i+1}^- - {}_1\phi_{i+2}^- = \cos\ (2n-i+1)\ kh. \\
&\vdots \\
{}_1\phi_1^- &= A\ {}_1\phi_2^- - {}_1\phi_3^- = \cos\ 2nkh
\end{aligned}
$$

where ${}_1\phi_i^-$ is similar to ${}_1\phi_i^+$ but obtained from the first iteration in the direction of decreasing x.

If there are in all P such series of iterations, then the field shape across the one dimensional model can be obtained from

$$\Phi_i = \sum_{p=1}^{P} \left({}_p\phi_i^+ + {}_p\phi_i^- \right) \qquad i = 1,2,3 \ldots\ldots n+1. \qquad (3.6)$$

where ${}_p\phi_i^+ = \cos\ (2(p-1)n+i-1)kh.$

${}_p\phi_i^- = \cos\ (2pn-i+1)\ kh.$

Except for discrete values of the angular shift per unit length, k, the field across the one dimensional model of the waveguide will be zero. This can readily be observed from equation (3.6), where in the limit of P tending to infinity, the forward and backward directed waves, interfere destructively with each other, producing a null field, except in the cases when they become coherent and add constructively. In this situation, the field and the value of k, satisfy the one dimensional Helmholtz equation

$$\frac{\partial^2\Phi}{\partial x^2} + k^2\Phi = 0$$

together with the boundary conditions, at cut-off.

Thus, to obtain a cut-off solution, a suitable node within the model has to be chosen and the sum of successively reflected magnetic potentials at that node calculated for a range of k, until a maximum potential is achieved, thus ensuring the particular value of k is causing coherent addition. The choice of node is of importance and in this present representation since the field is known to be a maximum at either x = 0 or x = a, it is reasonable to take the corresponding node as a solution point.

Fig. (3.2) indicates the manner in which the output represents itself due to the multiple reflected wave for an arbitary value of k, and consists of a sequence of unit magnitude delta functions of period λ multiplied by the waveform cos (knph), thus

$$\phi(nph) = \cos(knph) \sum_{l=1}^{P} \delta(nph - l\lambda)$$

Summation of the areas of these delta functions as in equation (3.6) produces the amplitude of the field at the chosen node for the particular value of k. Ideally this will either produce a zero or infinite magnitude of potential, but practically the number of iterations will be limited to P, and the magnitude of the field, will lie somewhere between these two extremes, thus the response of the model to variations in k, for a fixed number of iterations P is given by

$$\Phi(k) = \int_{-\infty}^{\infty} \cos(knph) \sum_{l=1}^{P} (nph - l\lambda)\, d(nph)$$

and this is representative of the real part of a Fourier transform integral.

Defining

$$\Phi(k) = \frac{1}{2\pi} \int_{-\infty}^{\infty} \phi(nph) e^{-jknph}\, d(nph)$$

with the inverse transform

$$\phi(nph) = \int_{-\infty}^{\infty} \Phi(k) e^{jknph}\, dk$$

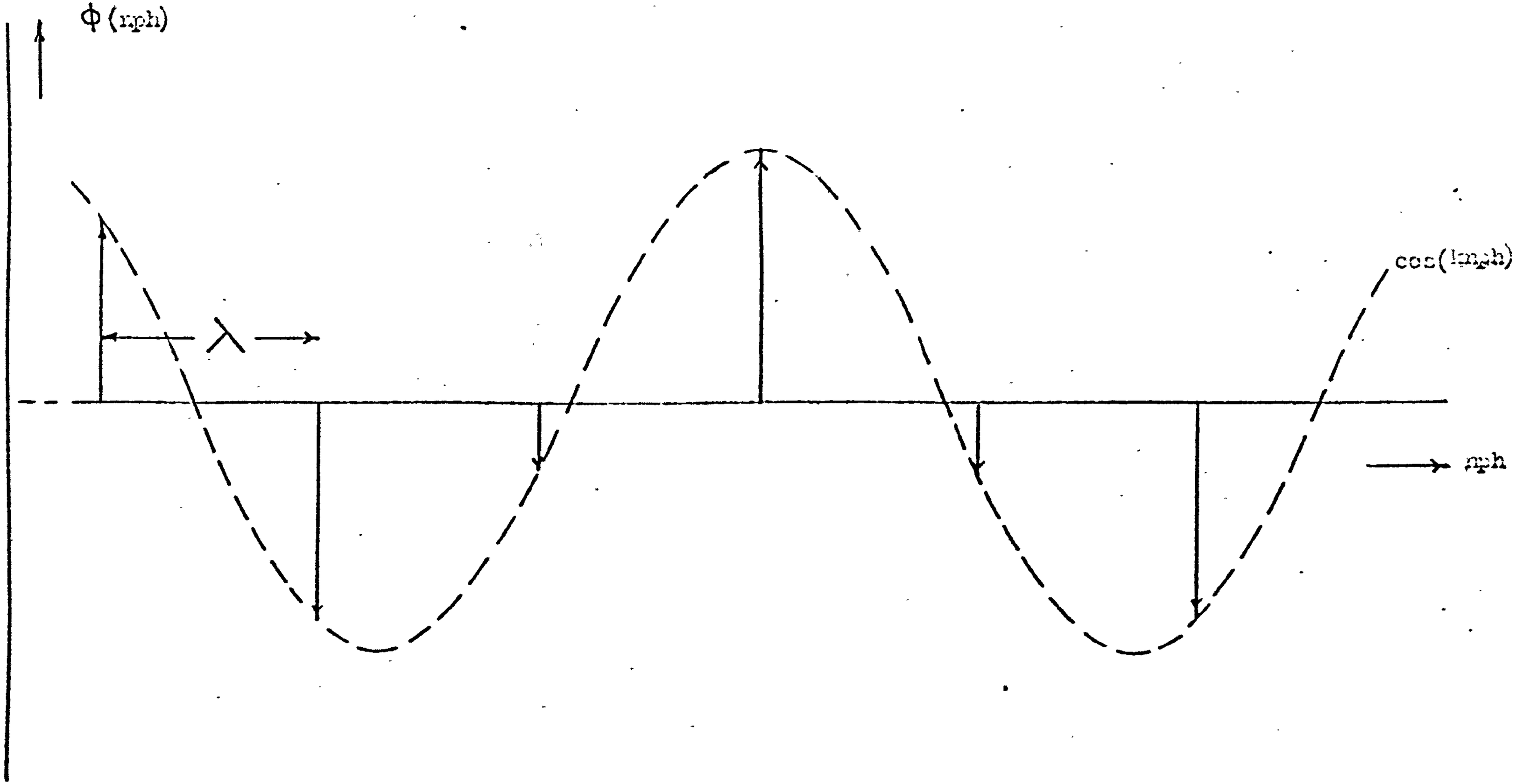

Fig. (3.2) Modal output derived from a multiple reflected wave.

such that $\Phi(k)$ is measured as Amplitude/(radians/unit length), then

$$\Phi(k) = \int_{-\infty}^{\infty} \sum_{r=-\infty}^{\infty} \delta(nph - r\lambda) \quad F(nph) e^{-jknph} \quad d(nph) \qquad (3.$$

where $F(nph) = 1 \qquad 0 \leqslant nph \leqslant P$

$= 0 \qquad 0 > nph > P$

The k-spectrum of equation (3.7) can then be obtained via the Fourier transform pair, by convolving the transform of the delta functions with that of the unit rectangular function, i.e.

$$\Phi(k) = \Phi_1(k) * \Phi_2(k) = \int_{-\infty}^{\infty} \Phi_1(k') \quad \Phi_2(k-k') \, dk'$$

where

$$\Phi_1(k) = \frac{1}{\lambda} \sum_{r=-\infty}^{\infty} \delta\left(k - \frac{2\pi r}{\lambda}\right)$$

and

$$\Phi_2(k) = \frac{P\lambda}{2\pi} \frac{\sin(kP\lambda/2)}{(kP\lambda/2)} \quad e^{-jkP\frac{1}{2}\lambda}$$

thus

$$\Phi(k) = \frac{P}{2\pi} \int_{-\infty}^{\infty} \sum_{r=-\infty}^{\infty} \delta\left(k' - \frac{2\pi r}{\lambda}\right) \quad \frac{\sin(k-k')P\lambda/2}{(k-k')P\lambda/2} \quad e^{-j(k-k')P\frac{1}{2}\lambda} \, dk' \qquad (3.8)$$

Thus the k- spectrum of $\phi(nph)$ is of a (sin x)/x nature centred about values of k corresponding to $k = 2\pi r/\lambda$; $r = -\infty \ldots 0, \ldots \infty$. As P tends to infinity, $\phi(k)$ assumes its correct form of a delta function situated at each of the previously specified values of k.

Since the choice of node was taken at either of the extremities of the waveguides cross section, $\lambda = 2a$, hence

$$k = \frac{\pi m}{a} \qquad m = 0,1,2, \ldots\ldots \infty \tag{3.9}$$

ignoring the negative values of r, which serve only to place k in its negative plane, and thus equation (3.9) represent all the cut-off wavenumbers of the propagating modes within the waveguide. Should the solution point be taken at the centre of the waveguide then the period $\lambda = a$, and thus (sin x)/x type envelopes develop about $k = 2\pi m/a$, corresponding to the cut-off wavenumbers of the even ordered modes. This is to be expected since the field is identically zero at this point for all odd ordered modes.

The approximation of the ideal k- spectrum consisting of a sequence of delta functions, by the sequence of (sin x)/x type functions, will however cause some inaccuracy due to the interference of the side lobes of the relevant function on neighbouring solutions, and thus tends to displace the true solutions as in fig. (3.3), where the true solutions of a particular structure are denoted by k_1, k_2, but side lobe interference from neighbouring (sin x)/x type solutions cause the solutions to deviate to k_1', k_2'. The influence of the side lobes however can be minimized, by taking the number of iterations sufficiently large, such that the width of the curve becomes small, and the magnitude of the side lobes negligibly small.

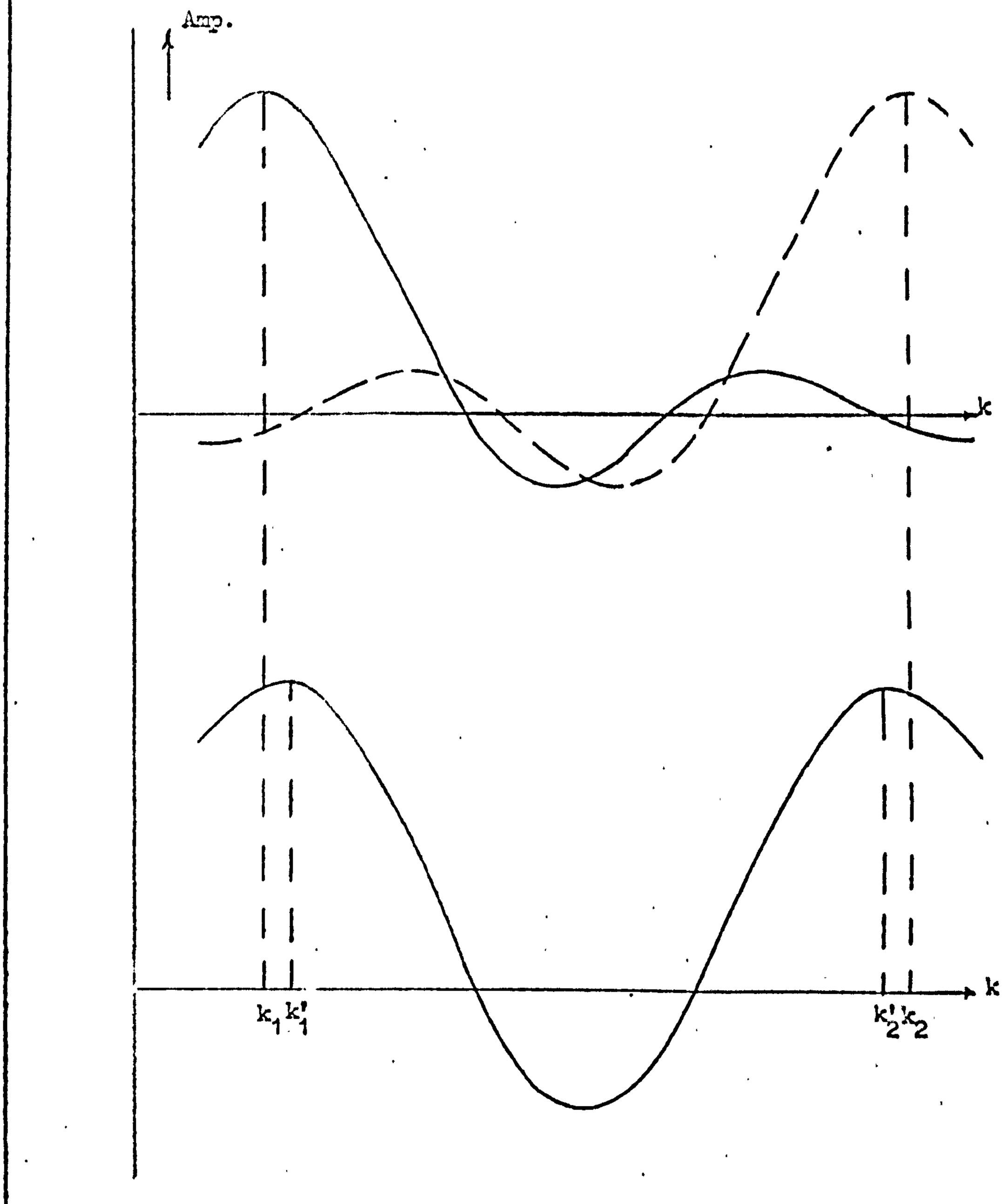

Fig. (3.3). Displacement of true solutions k_1, k_2 by interference from side lobes of neighbouring solutions.

Choosing a solution point, i, other than the two previously mentioned, would yield two sets of unit impulses, both of periodicity λ and modulated by the wave form $\cos(knph)$, but each set possessing a phase difference, defined by equation (3.6), of $(2n - 2i + 2)kh$. This has the advantage of suppressing the influence of modes possessing a zero field at that particular point, as was demonstrated by choosing the solution point as the centre of the guide, due to the reasons discussed immediately above.

If the technique of summing potentials at a solution point, due to a multiply reflected wave, is performed with the operator A in equations (3.5) and (3.6) being replaced by the appropriate finite difference and finite element operators, then since these linear functions approximate the true sinusoidally varying field, the form of the solution will be similar to that of equation (3.8). The solutions obtained from the application of the two linear operators will differ from the correct solution by amounts predicted by equations (3.3), being upper and lower bounds to the required solution, and also restricted to solving the propagating modes whose cut-off wavenumbers are limited by equation (3.4).

The three techniques were applied to fig. (3.1), with a magnetic wall at $x = 0$ and an electric wall at $x = a$, the solution point being taken at the node on the electric wall. The magnetic wall requires no special treatment except for a reversal of phase, however the periodicity of the sequence of pulses formed at the solution point now becomes

$$2nh\left(k + \frac{\pi}{2nh}\right)$$

which implies $k' \rightarrow k' + (\pi/2nh)$ in equation (3.8), and thus the solutions according to equation (3.8) will again be of a $(\sin x)/x$ nature centred about values of k, corresponding to

$$k = \frac{2\pi m}{2nh} - \frac{\pi}{2nh} = (2m - 1)\frac{\pi}{2a} \quad , \quad m = 0, \ldots\infty$$

which are the cut-off wavenumbers of the odd ordered modes propagating within the waveguide. The semiwidth of the waveguide is a = 4 corresponding to n = 4 and h = 1, and the value of v - equation (3.1) - was set to unity, an arbitary choice, for the finite difference/element descriptions. The form of the solution about the true cut-off wavenumber of the dominant mode is displayed in fig. (3.4), for P = 100 iterations, and the results tabulated in Table (3.2) for various values of P. Table (3.2) indicates that P does not have to be made relatively large for the correct solutions to emerge using the method of a circular internodal function, but P must be increased for the linear internodal function methods to yield their solutions, and must therefore be more susceptible to interference from their respective neighbouring solutions. The latter two methods, when settled, i.e. P is taken sufficiently large, possess the cut-off wavenumbers as predicted in Table (3.1). Any attempt to exceed the limitations expressed in equations (3.4) causes the respective methods to fail, when the field being constructed at a solution point tends to diverge. The use of the circular internodal function possessed no such disadvantages and yielded exact solutions of the system for any mode, an example being the calculation of the cut-off wavenumber, k^2, of the $TE_{25,0}$ mode which yielded the exact result of 96.3829 (rad./unit length)^2.

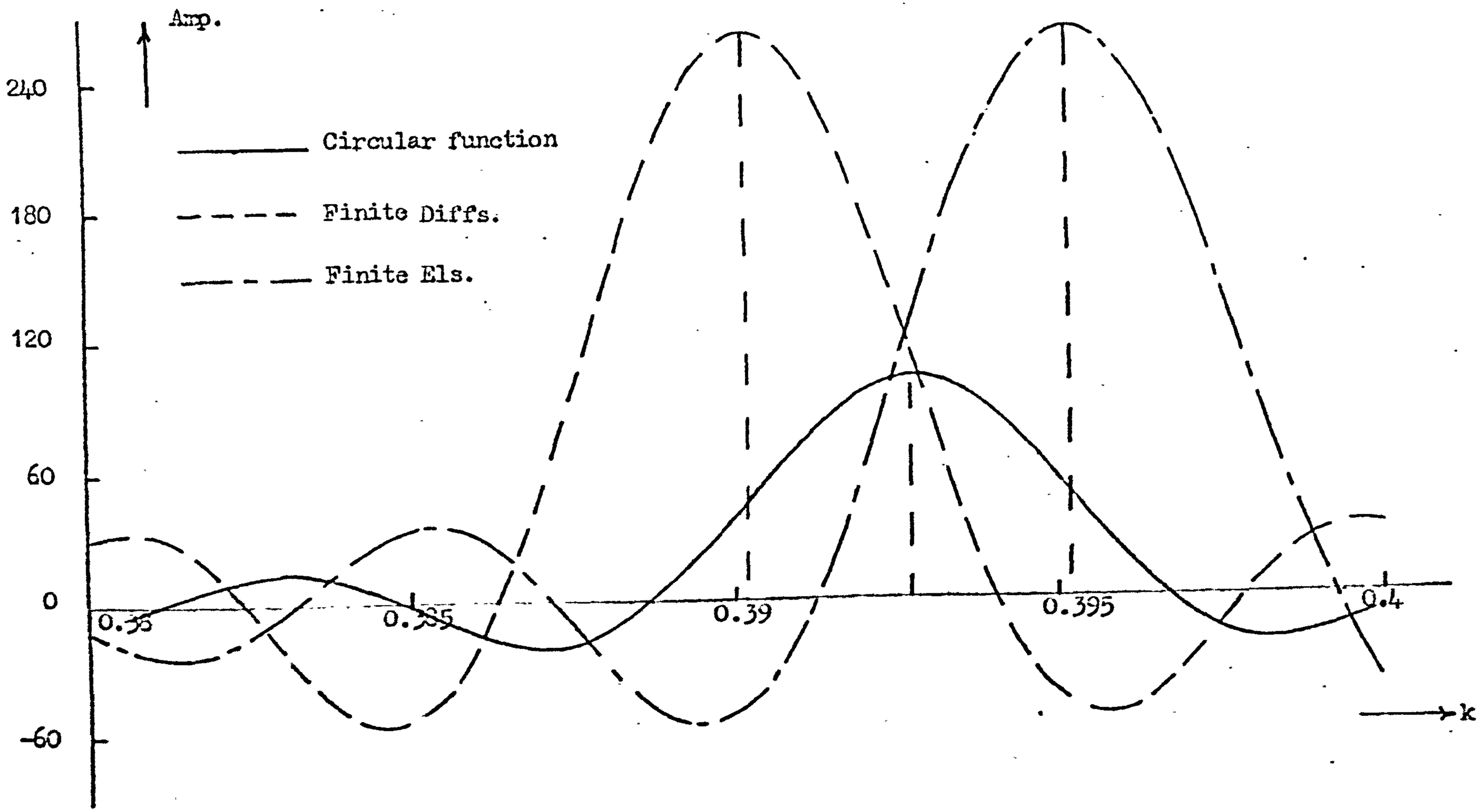

Fig. (3.4). Solution for TE_{10} mode defined by fig. (3.1).

TABLE (3.2) Cut-off wavenumbers (k^2) of TE_{mo} modes propagating within a waveguide of width 8 units.

P	Mode no. m	$\left(\frac{m\pi}{8}\right)^2$	k^2 Circ. fn.	Error %	k_D^2 F. Diff.	Error %	k_E^2 F. El.	Error %
10	1	0.1542	0.1542	-	0.1514	1.81	0.1525	1.10
	3	1.3879	1.3879	-	1.2343	11.07	1.5539	11.96
	5	3.8553	3.8553	-	2.7657	28.26	5.1307	33.08
	7	7.5564	7.5564	-	3.8487	49.07	10.7335	42.05
50	1	0.1542	0.1542	-	0.1522	1.29	0.1562	1.29
	3	1.3879	1.3879	-	1.2346	11.04	1.5545	12.00
	5	3.8553	3.8553	-	2.7653	28.27	5.1296	33.05
	7	7.5564	7.5564	-	3.8478	49.08	10.7268	41.96
100	1	0.1542	0.1542	-	0.1522	1.29	0.1562	1.29
	3	1.3879	1.3879	-	1.2346	11.04	1.5545	12.00
	5	3.8553	3.8553	-	2.7653	28.27	5.1296	33.05
	7	7.5564	7.5564	-	3.8478	49.08	10.7268	41.96

The passage of the multiply-reflected waves represented by equations (3.5) and (3.6) across the waveguide can easily be seen to be equivalent to the passage of TEM wave down a single coaxial transmission line with the appropriate short circuited or open circuited terminations. The model of fig. (3.1) then represents such a transmission line subdivided into finite elemental sections, each of which becomes a distributed constants network, possessing a series impedance $Z = R + jwL$ per unit length and a shunt admittance $Y = G + jwC$ per unit length. For the case under discussion i.e. propagation in a lossless medium, $R = G = 0$, and the elemental transmission line sections are thus illustrated by fig. (3.5), where L is the inductance per unit length and C the capacitance per unit length of such a section.

Over such a section, basic transmission line theory states

$$-\frac{\partial V}{\partial x} = L\frac{\partial}{\partial t}(I^+ - I^-) \quad ; \quad -\frac{\partial}{\partial x}(I^+ - I^-) = C\frac{\partial V}{\partial t}$$

yielding

$$\frac{\partial^2 V}{\partial x^2} = LC\frac{\partial^2 V}{\partial t^2} \qquad (3.10)$$

whilst Maxwells field equations for a TE_{mo} mode, at cut-off become

$$-\frac{\partial H_z}{\partial x} = \epsilon_o\frac{\partial E_y}{\partial t} \quad ; \quad \frac{\partial E_y}{\partial x} = -\mu_o\frac{\partial H_z}{\partial t}$$

which yield

$$\frac{\partial^2 H_z}{\partial x^2} = \mu_o\epsilon_o\frac{\partial^2 H_z}{\partial t^2} \qquad (3.11)$$

comparing equations (3.10) and (3.11), the identities

$$H_z \equiv V \quad ; \quad E_y \equiv (I^+ - I^-) \quad ; \quad L \equiv \epsilon_o \quad ; \quad C \equiv \mu_o$$

are formed together with

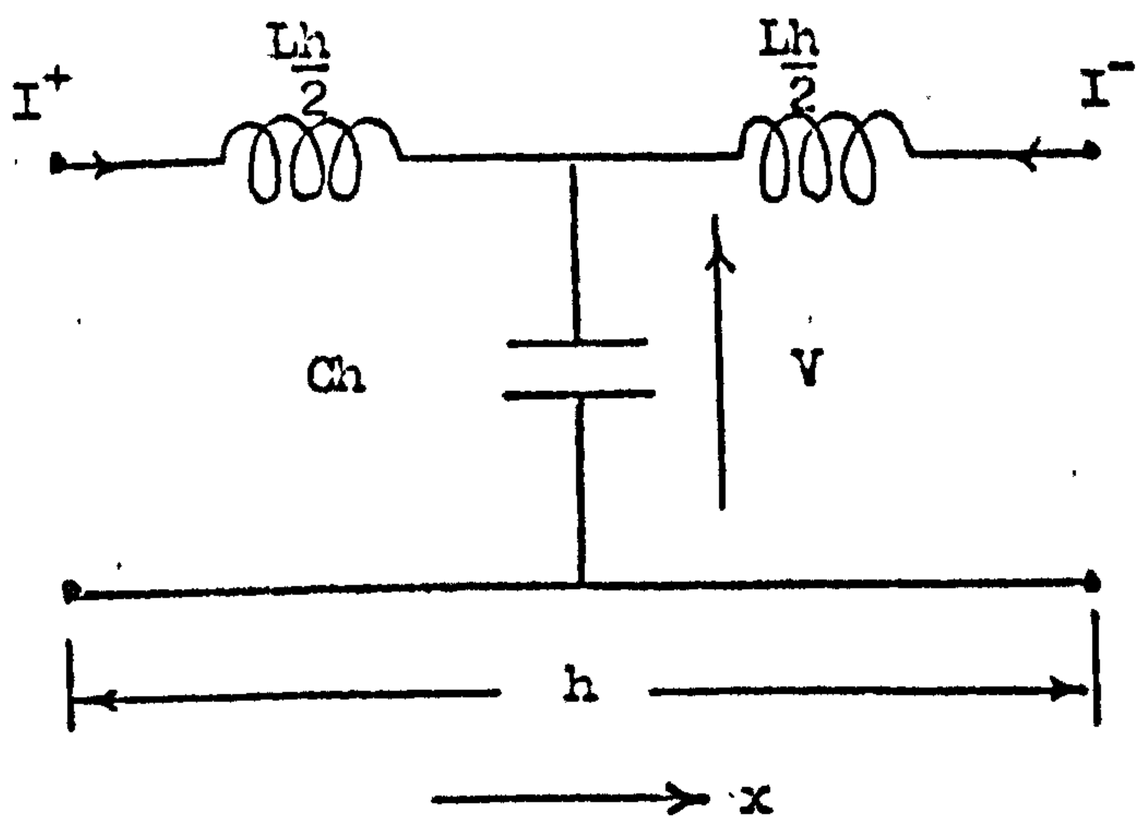

Fig. (3.5). Transmission-line element.

$$v = \text{velocity of propagation} = \frac{1}{\sqrt{LC}} = \frac{1}{\sqrt{\mu_o \epsilon_o}} = c$$

$$Z_o = \text{characteristic impedance} = \sqrt{\frac{L}{C}} = \sqrt{\frac{\epsilon_o}{\mu_o}}$$

on the transmission line.

The boundary conditions are then represented by a short circuit or open circuit terminations on the transmission line 'replacing' magnetic or electric walls in the waveguide structure, respectively.

Further, if the characteristic impedance of the transmission line is normalised, the electric field component Ey may be obtained at a solution point, i, by the operation,

$$Ey = \sum_{p=1}^{P} \left({}_p\phi_i^+ - {}_p\phi_i^- \right)$$

using the same notation as that of equation (3.6).

3.3. TWO DIMENSIONAL APPLICATIONS.

The concept of two dimensional propagation may be envisaged by considering the transmission line of the previous discussion to be loaded at the nodes, with open circuited stubs of physical length $l\lambda/2$ (l is an arbitary constant) and of identical characteristic impedance to that of the transmission line, as in fig. (3.6). This is equivalent to the arbitary placing of electric walls across the direction where the field variations of the TE_{mo} modes are zero, and consequently has no effect on the required solution. The stubs, however introduce point discontinuities in the elemental sections of the transmission line, with reflection and transmission coefficients R and T respectively, in both directions, for the propagating voltage or current waveform.

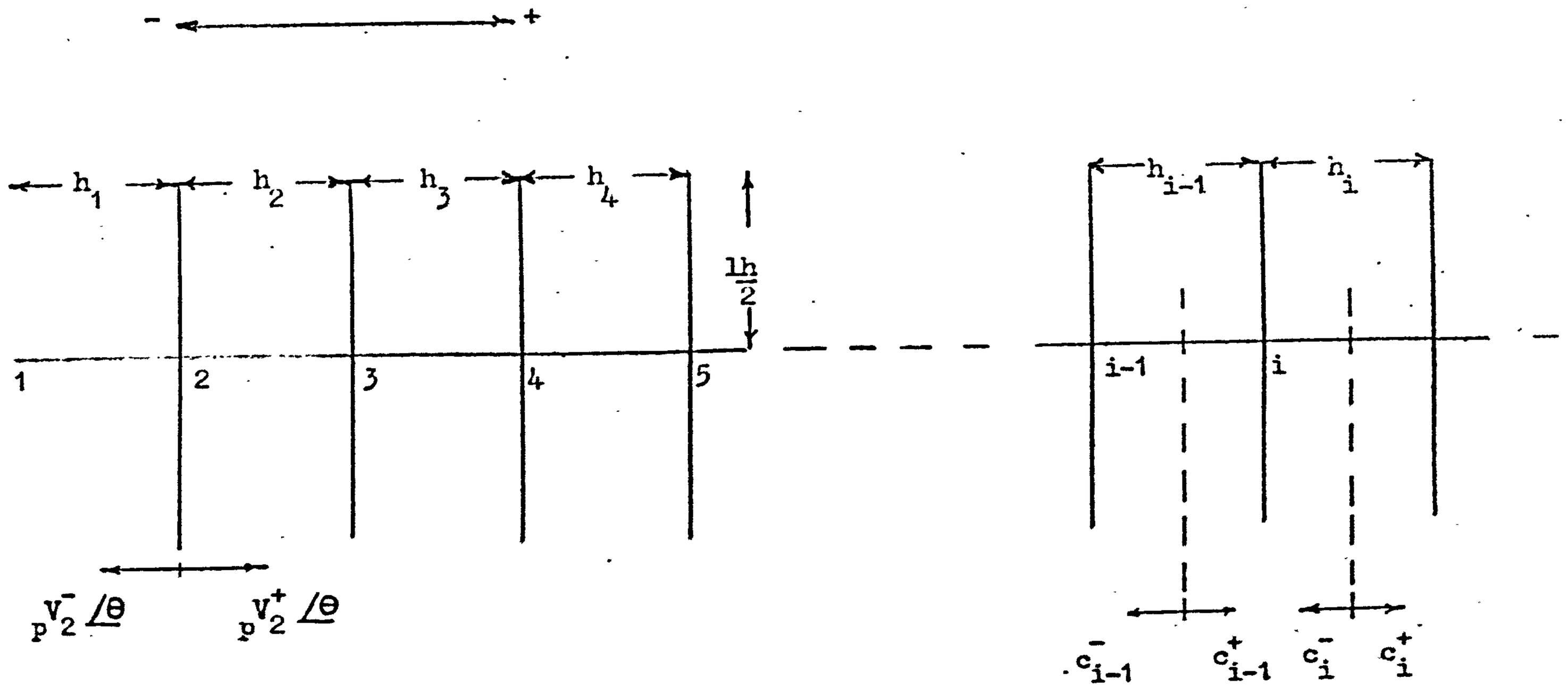

Fig. (3.6). Transmission line loaded with open circuited stubs.

To examine the mechanism of propagation, consider the stub loaded transmission line of fig. (3.6) with a short circuited termination at node 1 , and suppose that the line is excited at node 3 by a sinusoidal voltage of amplitude V, and that the frequency chosen makes the electrical length of the elemental sections between nodes, equal to $\theta_i = kh_i$, $i = 1,2 \ldots n+1$. The method of obtaining the multiple-reflected wave then reduces to one of accounting for all the reflections and transmissions that occur at each of the nodal discontinuities in the order in which they are performed in space, and summing such forward and backward propagating waves at each node.

Thus for excitation at node 3, the first order reflections occur at nodes 2 and 4 and denoting ${}_pV_i^+ \angle\theta$ as the amplitude and phase of the wave proceeding in the positive direction from node i for the p_{th} order reflections, then

$$ {}_1V_2^- \angle\theta = TV \angle\theta_2 \quad ; \quad {}_1V_2^+ \angle\theta = RV \angle\theta_2 $$

$$ {}_1V_4^- \angle\theta = RV \angle\theta_3 \quad ; \quad {}_1V_4^+ \angle\theta = TV \angle\theta_3 $$

The second order reflections are then given by,

$$ {}_2V_2^- \angle\theta = -R_1V_1^- \underline{\angle\theta+2\theta_1} = -RTV \underline{\angle\theta_2+2\theta_1} $$

$$ {}_2V_2^+ \angle\theta = -T_1V_1^- \underline{\angle\theta+2\theta_1} = -T^2V \underline{\angle\theta_2+2\theta_1} $$

$$ {}_2V_3^- \angle\theta = R_1V_2^+ \underline{\angle\theta+\theta_2} + T_1V_4^- \underline{\angle\theta+\theta_3} $$

$$ = R^2V \underline{\angle 2\theta_1} + TRV \underline{\angle 2\theta_3} $$

$$ {}_2V_3^+ \angle\theta = T_1V_2^+ \angle\theta+\theta_2 + R_1V_4^- \angle\theta+\theta_3 $$

$$ = TRV \angle 2\theta_2 + R^2V \angle 2\theta_3 $$

$$ {}_2V_5^- \angle\theta = R_1V_4^+ \angle\theta+\theta_4 = RTV \angle\theta_3+\theta_4 $$

$$ {}_2V_5^+ \angle\theta = T_1V_4^+ \angle\theta+\theta_4 = T^2V \angle\theta_3+\theta_4 $$

and so on for the higher order reflections and transmissions.

Summation of these forward and backwardly-propagating waves at each node of an elemental section after each order of reflection has been considered, tends to form the complete steady-state forward and backwardly propagating waves and hence the description of the propagating wave that would be achieved in practice.

To examine the effect of the stubs on an otherwise smooth transmission line, the stubs are allowed to be placed periodically along the transmission line. This does not necessarily mean that the method has lost some of its generality, since the previous chapter and discussions, indicate that analysis is easier if performed over a regular mesh, with slight deviations in mesh arm length to accommodate awkwardly shaped boundaries. In a similar manner, this system is included in the present model such that the transmission line of fig.(3.6) now possesses periodically loaded open circuited stubs, separated by a distance h, (electrical lengthθ = kh).

For the periodic structure of fig. (3.6), an equivalent network of an elemental section is a shunt normalized susceptance B with a lengthlh/2 of transmission line on either side. The relationships between the amplitudes of the forward- and backward-propagating waves of a typical section of transmission line, fig. (3.6), in the steady state, are related by[40],

$$\begin{bmatrix} c_{i-1}^{+} \\ c_{i-1}^{-} \end{bmatrix} = \begin{bmatrix} e^{j\frac{\theta}{2}} & 0 \\ 0 & e^{-j\frac{\theta}{2}} \end{bmatrix} \begin{bmatrix} \frac{2+jB}{2} & j\frac{B}{2} \\ -j\frac{B}{2} & \frac{4+B}{2(2+jB)} \end{bmatrix} \begin{bmatrix} e^{j\frac{\theta}{2}} & 0 \\ 0 & e^{-j\frac{\theta}{2}} \end{bmatrix} \begin{bmatrix} c_{i}^{+} \\ c_{i}^{-} \end{bmatrix} \qquad (3.12)$$

where c_{i-1}^{+} represents the amplitude of the forward propagating wave, in the steady state, at a point midway between the $(i-1)_{th}$ and i_{th} nodes, fig. (3.6).

If the waves on the periodic structure on the network possesses a propagation constant $\gamma_n = \alpha_n + j\beta_n$.

$$c_i^{+} = c_{i-1}^{+} \; e^{-\gamma_n h} \quad ; \quad c_i^{-} = c_{i-1}^{-} \; e^{-\gamma_n h} \qquad (3.13)$$

and the solutions of equations (3.12) and (3.13) yield

$$\cosh \gamma_n h = \cos\theta - \frac{B}{2}\sin\theta \qquad (3.14)$$

when

$$|\cos\theta - (B/2)\sin\theta| < 1 \; ; \; \gamma_n = j\beta_n \text{ and equation (3.14) becomes}$$

$$\cos\beta_n h = \cos\theta - \frac{B}{2}\sin\theta \qquad (3.15)$$

and when

$$\cos\theta - (B/2)\sin\theta > 1 \; ; \quad \gamma_n = \alpha_n$$

$$\cos\theta - (B/2)\sin\theta < -1 \; ; \quad \gamma_n h = j\pi + \alpha h$$

Thus there will be discrete frequency bands for which unattenuated propagation can occur (pass bands) separated by bands of frequency where the wave is attenuated (stop bands).

If discussion is restricted to the low frequency pass band, and replacing the shunt normalized susceptance B by its true form

$$B = 2\tan\frac{lkh}{2} = 2\tan\frac{l\theta}{2}$$

then equation (3.15) becomes

$$\beta_n = w\sqrt{LC(1+l)} = w\sqrt{L(C+Cl)}$$

in the limiting value of low frequency, w.

Therefore at low values of frequency, the periodically loaded line behaves as an electrically smooth line with a total shunt capacitance of (C+Cl) per unit length. The low frequency phase velocity of propagation, v_n, thus becomes

$$\frac{v_n}{c} = \frac{w\sqrt{LC}}{\beta_n} = \frac{1}{\sqrt{1+1}} \qquad (3.16)$$

Each elemental section of the transmission line may then be represented by a lumped capacitor/inductor network as in fig. (3.7). As the frequency increases the fact that the stub represents a distributed capacitance/inductance and not lumped becomes important and the phase velocity decreases according to equation (3.15). The phase velocity-frequency characteristics are presented graphically in fig. (3.8) for various values of stub length, and indicate that as the stub length is increased, i.e. more capacitance is added to the system, the usable frequency range of the periodic structure becomes severely limited. The upper limit of the lowest frequency range of propagating waves on the periodic structure is determined by the edge of the passbands, or alternativelybyconsidering the group velocity, v_g, of the wave, i.e. the velocity at which energy is transported along the transmission line. The group velocity can be expressed as,

$$v_g = \frac{dw}{d\beta} = c\frac{d\theta}{d(\beta_n h)} = c\,\frac{\sin\theta\left(1+\frac{1}{2}\cdot 1\sec^2\frac{1}{2}1\theta\right)}{2\sin\beta_n h + \cos\theta\tan\frac{1}{2}1\theta}$$

and thus shows that the group velocity becomes zero, i.e. the network itself becomes cut-off, whenever $\beta_n h = \pi$ and corresponds to

$$\theta = v_n \pi / c$$

which can be readily appreciated in fig. (3.8).

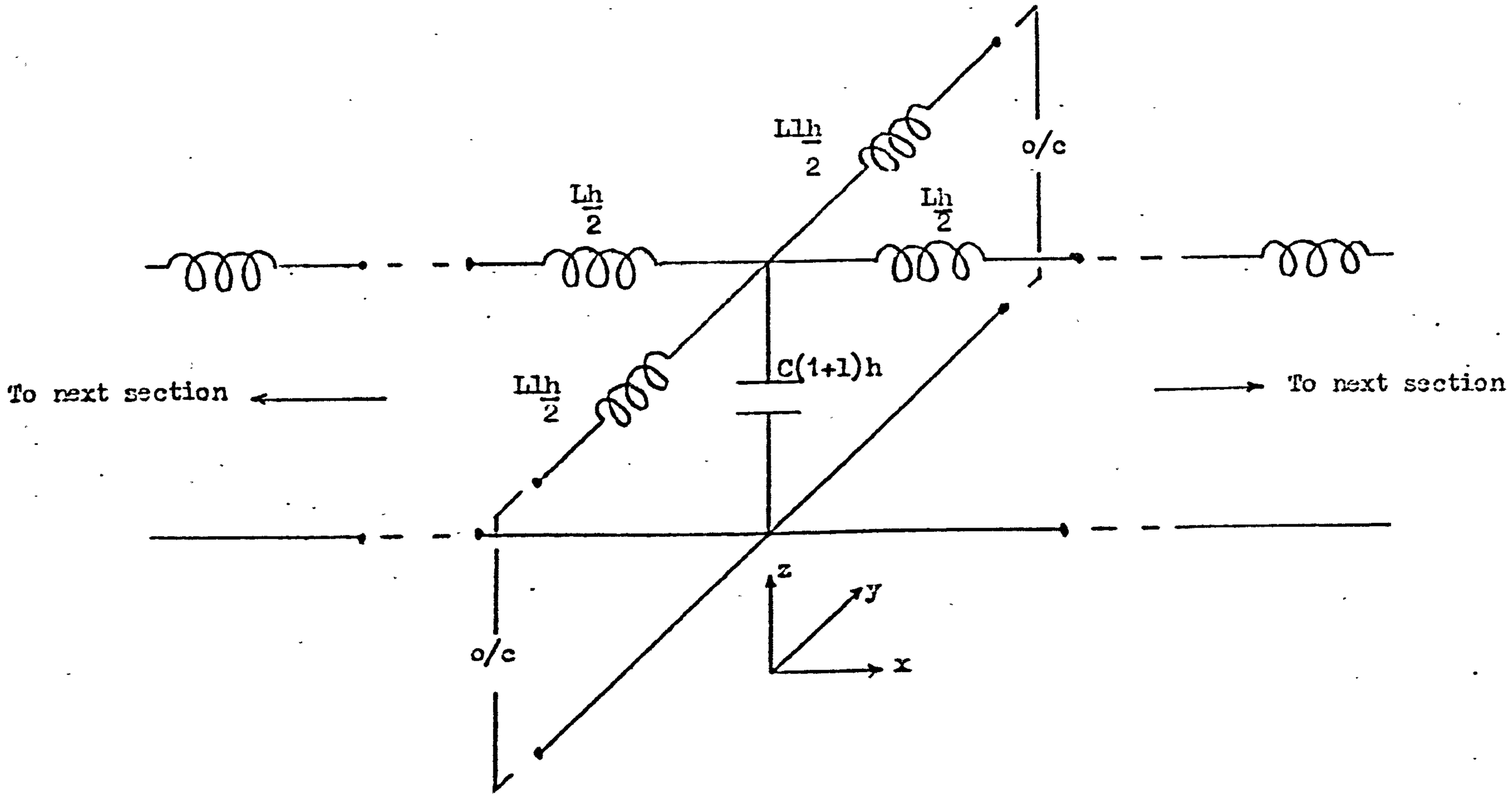

Fig. (3.7). Equivalent low frequency network, for section of open circuit stub loaded transmission line of fig. (3.6).

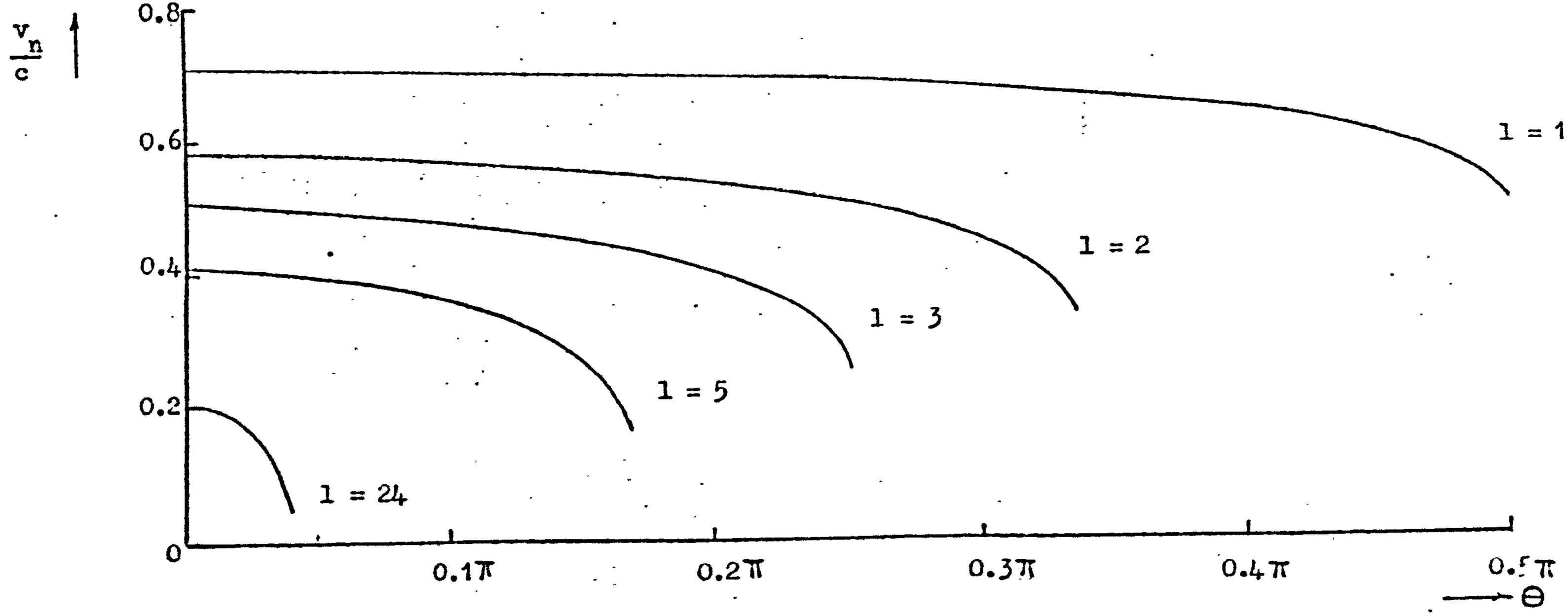

Fig. (3.8). Phase velocity characteristics for the periodic stub loaded transmission line of fig. (3.6).

The method of summing multiple reflected forward and backward propagating waves on the periodically open circuited stub loaded transmission line, so as to simulate TE_{mo} type mode analysis within a rectangular waveguide, where the voltage distribution on the network analogy represents the scalar magnetic field in the direction of propagation (equations (3.10.), (3.11)), can now be readily explained by consideration of fig. (3.9). Fig. (3.9) represents a typical nodal junction of the transmission lines formed by the intersection of the actual transmission line along which propagation occurs with the transmission lines forming the stubs, and if the characteristic impedance of the lines are normalised, a wave of amplitude V incident upon such a nodal junction along line 1 will be presented with an effective terminal impedance of 1/3 ohms. Thus a wave of amplitude V/2 will appear in lines 2,3,4, whilst a reflected wave of amplitude -V/2 will be reflected into line 1. Further, if the model represented by fig. (3.6) is placed on a two dimensional (x,y) grid such that the transmission line lies parallel to the x direction, with the stubs parallel to the y direction, shown in fig. (3.10), then if ${}_pV_1^i\ (x,y)\angle\theta$ and ${}_pV_1^r\ (x,y)\ \angle\theta$ denote the amplitude and phase of the p_{th} order wave incident on and reflected along line 1 at the node corresponding to the position (x,y)

$$ {}_{p+1}V_n^r\angle\theta \;=\; \frac{1}{2}\left[\sum_{m=1}^{4} {}_pV_m^i\angle\theta\right] \;-\; {}_pV_n^i\angle\theta \qquad (3.17) $$

for each node, and

$$ {}_{p+1}V_1^i\ (x,y_1)\ \angle\theta \;=\; {}_{p+1}V_3^r\ (x-h,\ y_1)\ \angle\theta+\theta_1 $$

$$ =\; {}_{p+1}V_3^r\ (x-h,\ y_1)\ \angle\theta+kh $$

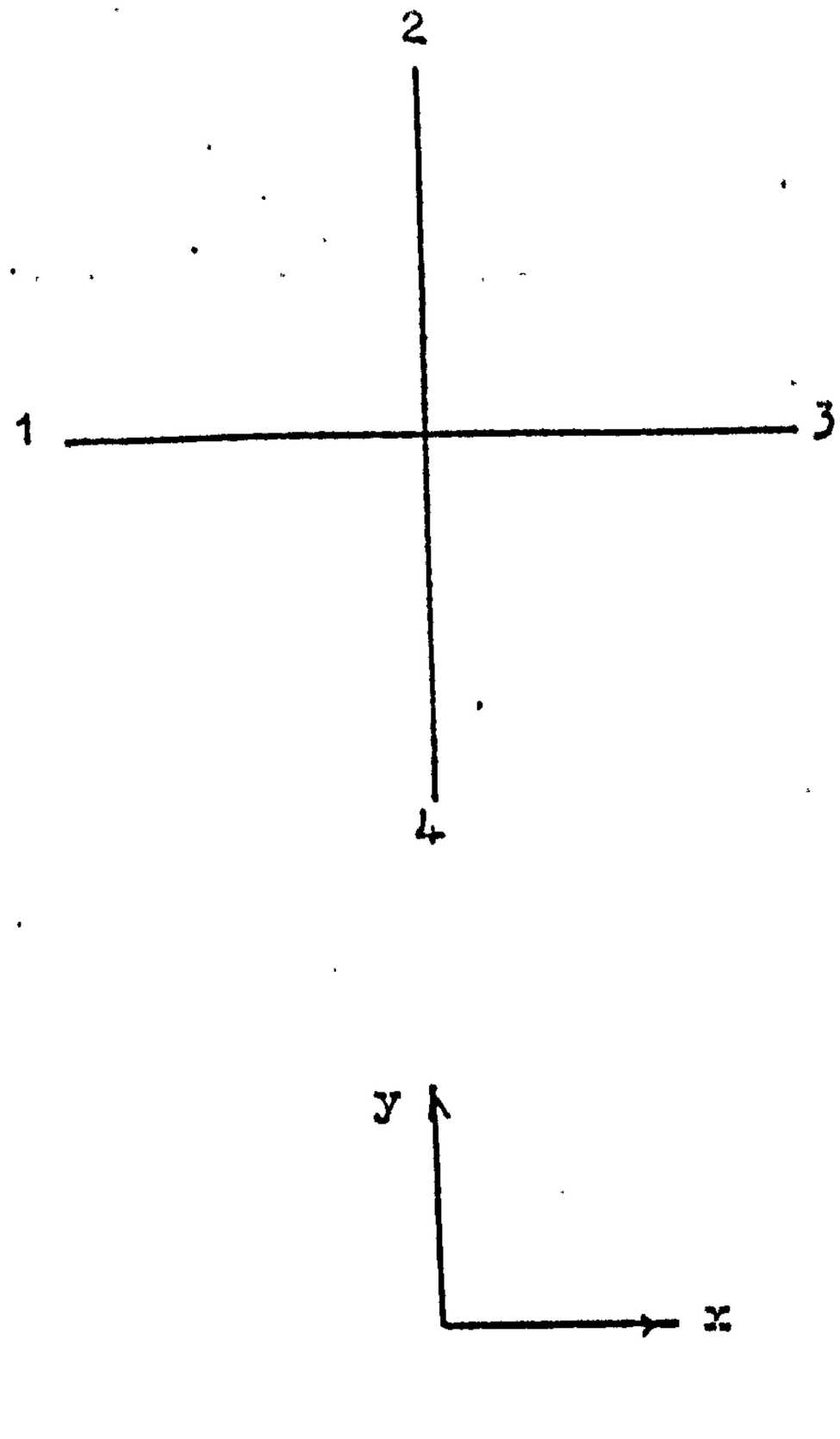

Fig. (3.9). Typical nodal junction of stub loaded transmission line.

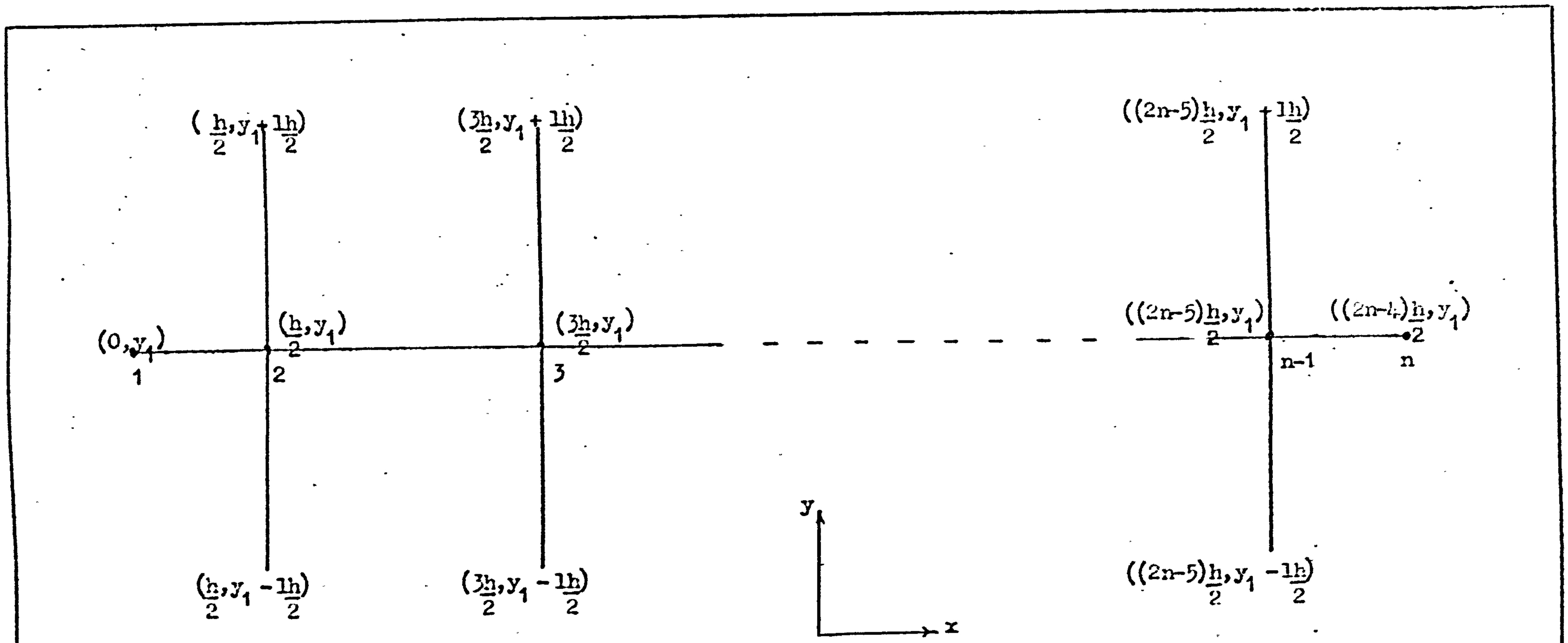

Fig. (3.10). Co-ordinate representation of fig. (3.6) with equal intermodal spacing.

$$
\begin{aligned}
{}_{p+1}V_2^i\,(x,y_1)\,\angle\theta &= {}_{p+1}V_4^r\,(x,y_1+\tfrac{1}{2}lh)\,\angle\theta+\theta_2 \\
&= {}_{p+1}V_4^r\,(x,y_1+\tfrac{1}{2}lh)\,\angle\theta+\tfrac{1}{2}lkh \qquad (3.18)\\
{}_{p+1}V_3^i\,(x,y_1)\,\angle\theta &= {}_{p+1}V_1^r\,(x+h,\,y_1)\,\angle\theta+\theta_3 \\
&= {}_{p+1}V_1^r\,(x+h,\,y_1)\,\angle\theta+kh \\
{}_{p+1}V_4^i\,(x,y_1)\,\angle\theta &= {}_{p+1}V_2^r\,(x,y_1-\tfrac{1}{2}lh)\,\angle\theta+\theta_4 \\
&= {}_{p+1}V_2^r\,(x,y_1-\tfrac{1}{2}lh)\,\angle\theta+\tfrac{1}{2}lkh
\end{aligned}
$$

For the nodes situated on the extremities of the transmission line corresponding to the boundaries of the modelled waveguide, reflection coefficients have to be introduced such that if a short circuit termination is presented to a wave travelling in the negative x direction from the node corresponding to the point $(\frac{1}{2}h,\ y_1)$ then

$$
{}_{p+1}V_1^i\,(\tfrac{1}{2}h,\,y_1)\,\angle\theta = {}_{p+1}V_3^r\,(0,y_1)\,\angle\theta+\theta_1 = {}_{p}V_1^r\,(\tfrac{1}{2}h,y_1)\,\angle\theta+kh+\pi \qquad (3.18a)
$$

and if an open circuit termination is presented to a wave travelling in the positive x direction from the node corresponding to the point $(\ (2n-5)\ \frac{1}{2}h,\ y_1)$

$$
\begin{aligned}
{}_{p+1}V_3^i\,(\ (2n-5)\ \tfrac{1}{2}h,\ y_1)\,\angle\theta &= {}_{p+1}V_1^r\,(\ (2n-4)\ \tfrac{1}{2}h,\ y_1)\,\angle\theta+\theta_3 \\
&= {}_{p}V_3^r\,(\ (2n-5)\ \tfrac{1}{2}h,y_1)\ \angle\theta+kh \qquad (3.18b)
\end{aligned}
$$

and similarly the open circuited stubs will also possess a voltage reflection coefficient of 1 such that

$$
\begin{aligned}
{}_{p+1}V_4^r \quad (x, y_1 + \tfrac{1h}{2}) \angle \theta + \tfrac{1}{2}1kh &= {}_pV_2^r \quad (x, y_1) \angle \theta + 1kh \\
{}_{p+1}V_2^r \quad (x, y_1 - \tfrac{1h}{2}) \angle \theta + \tfrac{1}{2}1kh &= {}_pV_4^r \quad (x, y_1) \angle \theta + 1kh
\end{aligned}
\qquad (3.18o)
$$

It is also to be noted that the boundaries or terminations at either extremity of the transmission line are a distance $\frac{1}{2}h$ from their immediate neighbouring stub. This is to provide consistency with the analysis performed for a periodic structure possessing sectional line elements as in fig. (3.7.).

Thus at each node the above operations are completed, and the steady state field distribution obtained by summation of the potentials existing at each node (x,y), after each order of reflections has been considered.

$$V(x,y) = \sum_{p=1}^{P} \sum_{m=1}^{l_k} {}_pV_m^r \quad (x,y) \angle \theta$$

Again truncation of the order of reflections, p, causes the spreading out of the ideal frequency response of the system of a sequence of delta functions, situated at discrete frequencies corresponding to transverse resonant conditions, into $(\sin x)/x$ natured curves centred about the same discrete frequencies.

The method was applied to the transmission line of fig. (3.10) The length of line analysed was 4h, corresponding to n = 6, with a short circuit termination (magnetic wall) at node 1 and an open circuit termination (electric wall) at node 6.

The line was excited at a source point corresponding to node 5 such that waves of unit amplitude and zero phase are launched into all four transmission lines intersecting at that node, and the amplitude of the resulting wave after P = 300 orders of reflections had been considered obtained by summation of the four incident waves after each order of reflection, also observed at node 5. This is the point where the field distribution of the TE_{mo} modes will be near its maximum. The length of stubs for which the analysis was performed were l = 1,2,3 and the results for the cut-off wave numbers k, obtained are tabulated in Table (3.3) for h = 1. Since the low frequency phase velocity of propagation along the stub loaded transmission line was shown to be $c/\sqrt{1+1}$ equation (3.16), then this is representative of allowing the wave guide of which the transmission line is the model, to be homogeneously filled with a dielectric medium of relative permittivity (1 + 1). The computed results of k have thus had to be corrected by a factor of $\sqrt{1+1}$ to permit the fact that propagation did indeed occur within an air-filled waveguide. The value of P was taken sufficiently large to minimize any truncation error, and the remaining error due to the velocity characteristics exhibited in fig. (3.8), when the frequency of excitation causes departure of the velocity of propagation from its low frequency limiting value, has been calculated and also tabulated in table (3.3). The velocity error can then be used to stipulate the error (for P large) that the computed value of k possess, which can be seen to be the case, by examination of the respective error columns in the table of results.

TABLE (3.3)

Cut-off wavelength, k, of TE_{mo} modes in a rectangular waveguide, modelled by the transmission line of fig. (3.10).

Stub length l.	Mode, m TE_{mo}	k exact $\left(\frac{m\pi}{8}\right)$	k calc.	k calc $\times\sqrt{1+1}$	Error (%)	Velocity Error %
1	1	0.3927	0.2768	0.3915	0.32	0.32
	3	1.1781	0.8077	1.1423	3.05	3.06
	5	1.9634	1.2573	1.7781	9.45	9.46
	7	2.7489	1.5356	2.1716	21.00	21.43
2	1	0.3927	0.2247	0.3892	0.88	0.86
	3	1.1781	0.6282	1.0881	7.64	7.67
	5	1.9634	0.9056	1.5685	20.14	20.24
	7	2.7489	1.0374	1.7968	34.65	36.35
3	1	0.3027	0.1936	0.3872	1.41	1.42
	3	1.1781	0.5179	1.0358	12.08	12.11
	5	1.9634	0.7040	1.4080	28.28	28.27
	7	2.7489	0.7790	1.5580	43.32	44.18

Only four modal cut-off frequencies are solvable for each of the values of l, and are due to the reasons discussed before, viz. that the stub loaded transmission line itself becomes cut-off, and the results indicate that this method of describing the fields by a circular internodal function yields an improved description of the problems than those associated with the finite difference/element techniques of table (3.2) for the same space discretization.

If a series of stub loaded transmission lines can be imagined to be placed adjacent to each other, with the appropriate stubs electrically connected as in fig. (3.11), so as to form a network of intersecting transmission lines, then if this network is excited sinusoidally at all the nodes corresponding to x = constant, with waves of unit amplitude into all four lines terminating at each of these nodes, then as the successive orders of reflection are taken, it can readily be seen that waves incident on a node, i, will reflect waves along the transmission lines in the positive and negative x directions towards nodes j and k, which are identical to those reflected from nodes j and k towards node i, following identical reactions at nodes j and k. Thus, this mechanism can be seen to represent the propagation of TE_{mo} modes within a rectangular waveguide, where variation of the field component H_z is zero in the y direction, and a plane wave traverses the network in the x direction, corresponding to the passage of TEM waves down each individual transmission line also in the x direction.

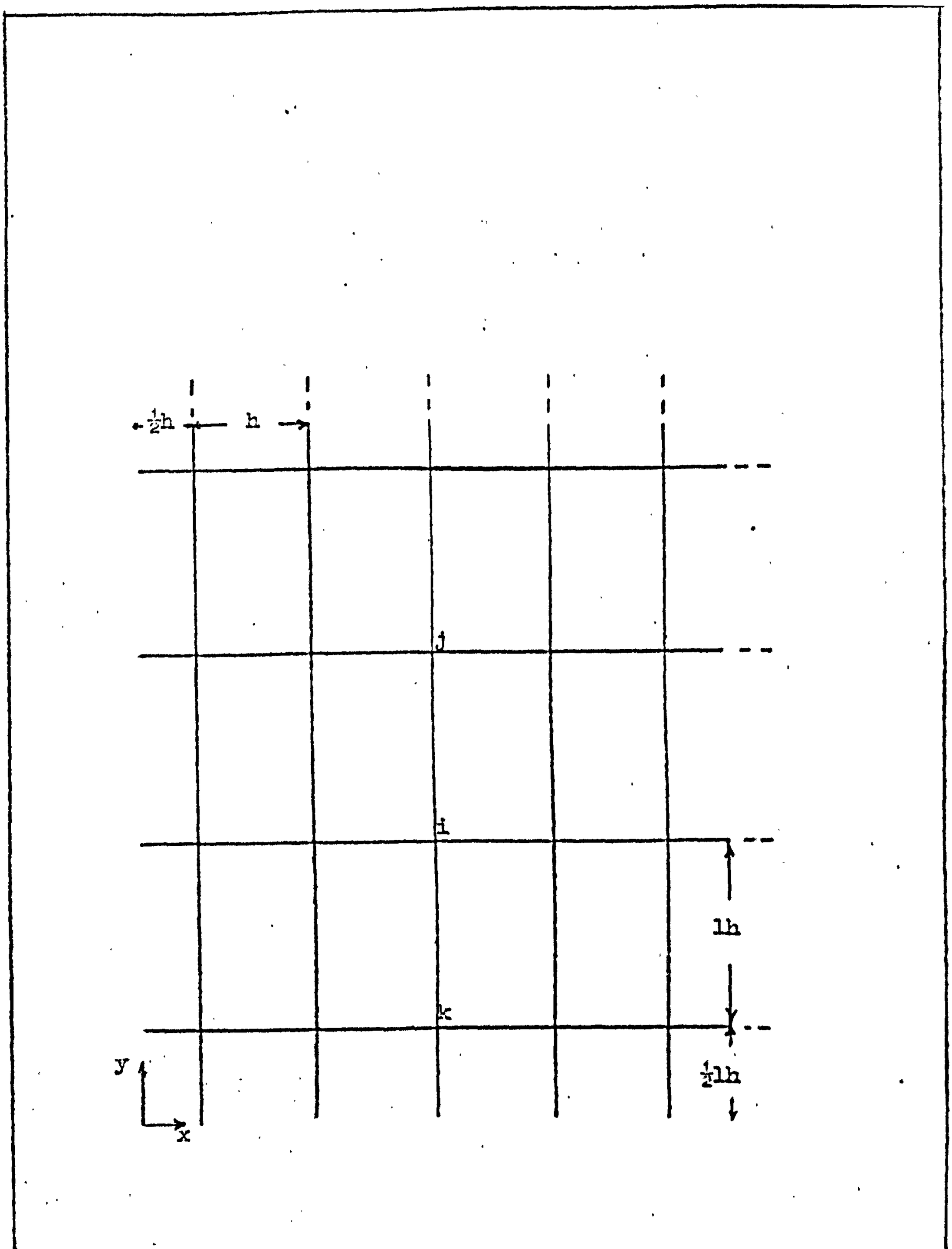

Fig. (3.11). Network of intersecting transmission lines.

The modelling of the waveguide by a network of intersecting transmission lines, has been shown to be capable of solving the cut-off frequencies of the TE_{mo} modes. However the use of such a network, since it is in effect a slow wave structure, gives the appearance that the actual wave is propagating in a medium of relative permittivity (1 + 1). To be consistent if the length of the stubs is fixed at h/2, i.e. l = 1, then the network of fig. (3.11) is regular everywhere and the optimum usable frequency range of the system is utilised, fig. (3.8.). The velocity of the waves traversing the network parallel to either of the coordinate directions is then $c/\sqrt{2}$, with due regard to the velocity errors incurred for high frequency operation, which, however, are known.

Fig. (3.12) shows a regular network of intersecting transmission lines used to simulate a square cross-sectioned waveguide. If, now, the network is simusoidally excited at nodes lying along the main 'diagonals' of the network, two waves can be considered to be travelling across the network in the direction of the diagonals i.e. 45^{o} to the direction of one of the coordinate axes. In the steady state, this can be represented by fig. (3.13), which shows the interaction between two simusoidal waves of equal amplitude, propagating in directions perpendicular to each other. Two sets of open circuited terminations $a_1\ a_2$, $b_1 b_2$; $a_1 b_1$, $a_2 b_2$ may then be placed as shown without affecting the wave pattern, and the resultant wave due to the superimposition of the two diagonal waves may be seen to be that corresponding to a TE_{11} mode propagation. Similarly the placing of magnetic walls $a_1 a_3$, $c_1 c_3$; $a_1 c_1$, $a_3 c_3$ yields TE_{22} mode propagation.

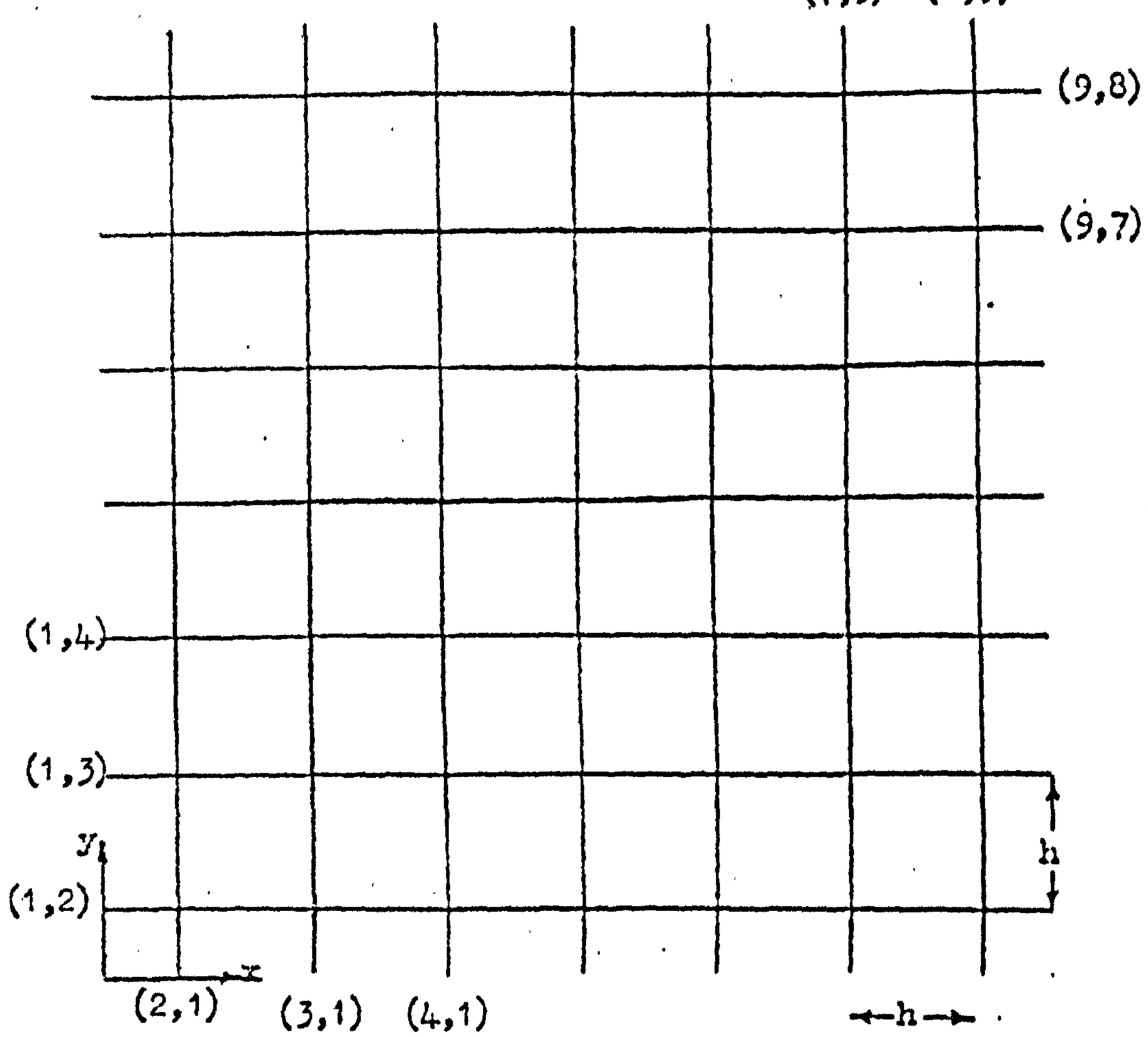

Fig. (3.12). Regular system of intersecting transmission lines used to simulate a waveguide of square cross section.

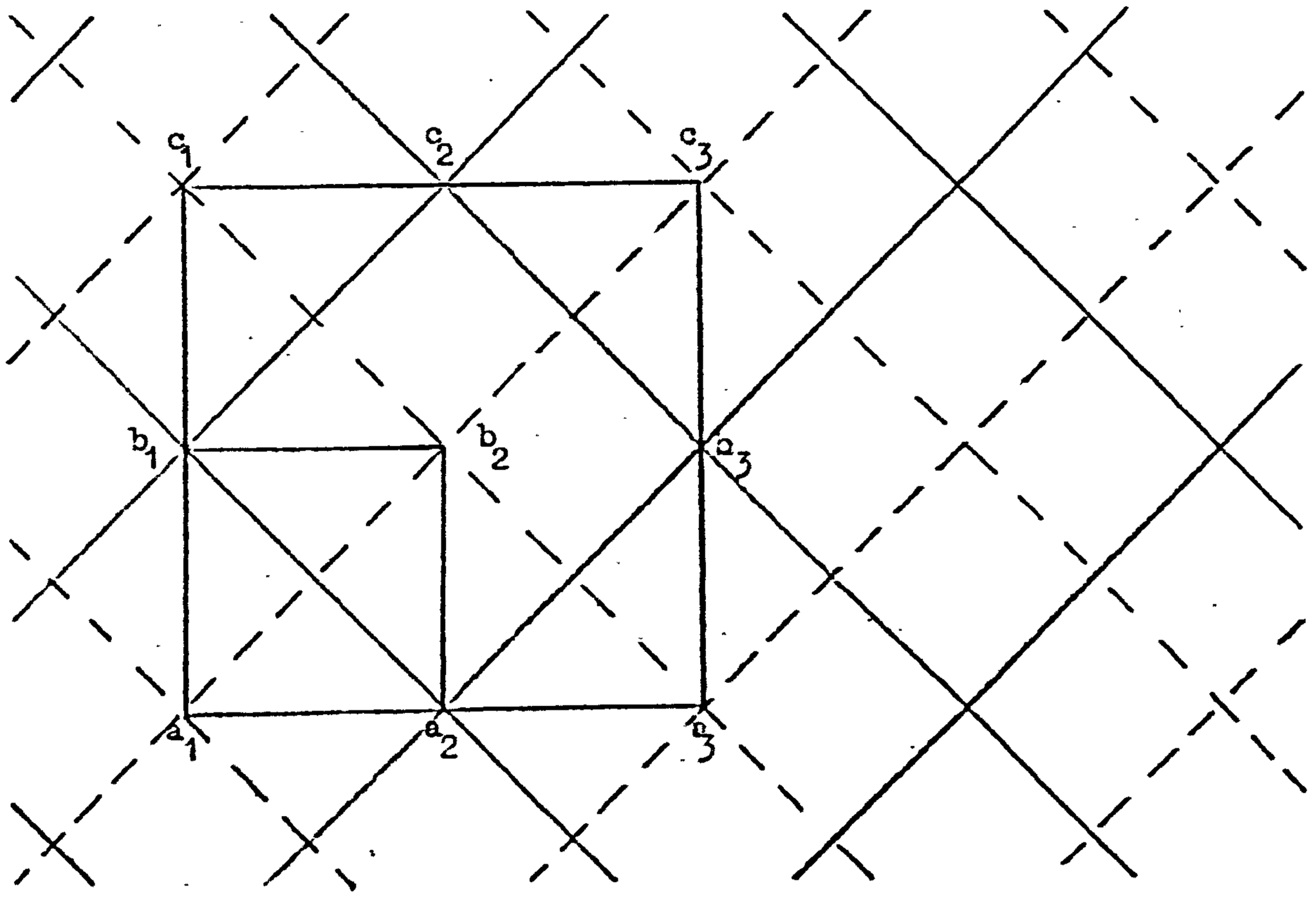

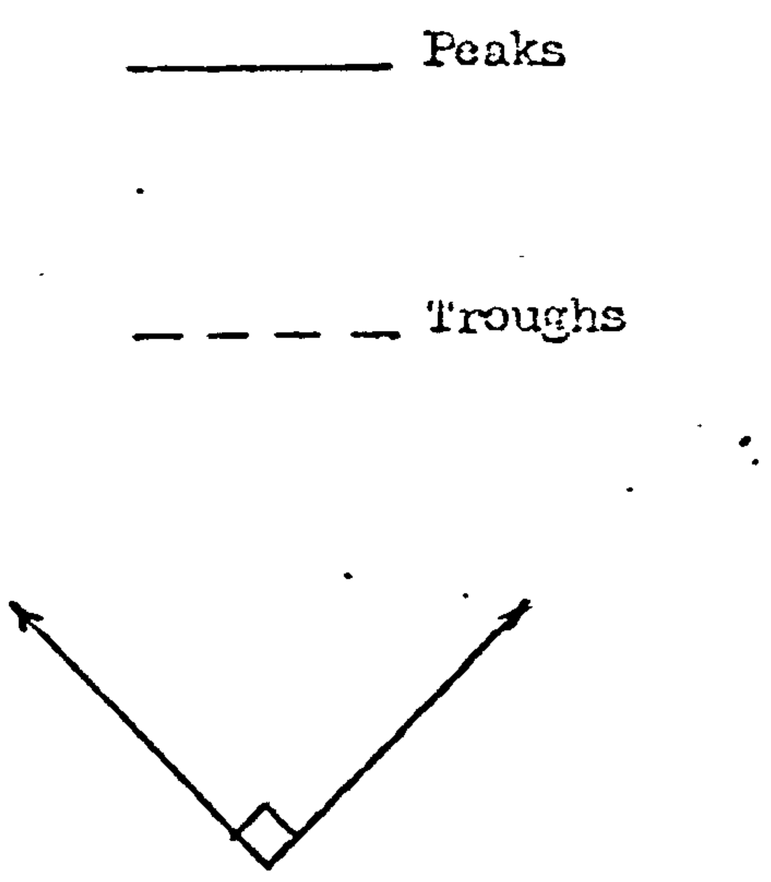

Directions of propagation.

Fig. (3.13) Interaction of two plane waves, propagating perpendicularly to each other.

Since the waves are travelling across the network in the direction of the diagonals, then the individual waves on the network travelling from node to node, when approaching any node will be presented with a matched impedance, i.e. there will be no reflection along the line of incidence, and can be seen by considering first order reflections of the system under discussion.

Under steady state conditions, the diagonal propagation of the wave over the network may be represented by equation (3.15), with B equal to zero, since there is an impedance match, thus,

$$\cos\ (\beta_n \sqrt{2}h) = \cos\theta = \cos\ \left(\frac{w}{c}\ 2h\right) \qquad (3.19)$$

since the wave although theoretically travelling a distance $\sqrt{2}\ h$ along the diagonal of a typical nodal mesh, has its component parts on the network traversing a distance 2h around the perimeter of the nodal mesh. Hence equation (3.19) implies that

$$\frac{v_n}{c} = \frac{1}{\sqrt{2}}$$

for all frequencies i.e. the network is never cut-off, but the velocity of propagation still remains at $\frac{1}{\sqrt{2}}$ that of free space, for TE_{nn} type modes. In general, however, TE_{mn} $(m \neq n)$ modes do not possess this property, but as the two extremes have been considered viz. propagation parallel and at 45° to the coordinate axes of the transmission line network, it may be recognized that if the worse possible case may arise, that of propagation parallel to one of the coordinate axes, then the velocity errors inherent in any calculation of cut-off frequency will be less than those given by equation (3.15), which becomes

$$\frac{v_n}{c} = \frac{\frac{1}{2}\theta}{\sin^{-1}\ (\sqrt{2}\ \sin\ \frac{1}{2}\theta)} \qquad (3.20)$$

for the regular mesh, and the trial frequencies of the network limited to those which restrict the internodal electrical length, θ, to be always less than $\frac{1}{2}\pi$.

The method of summing the multiple reflected waves according to equations (3.17), (3.18) was applied to a regular network, simulating a waveguide of square cross-section 7h, source and observation points were chosen so as to excite and observe the mode under analysis and the boundaries of the network being terminated in open circuits, so as to identify the electric walls of the wave guide. The results are tabulated in Table (3.4) for h = 1. The modes corresponding to diagonal propagation can be seen to experience neither velocity errors nor cut-off characteristics experienced on the network, and in a similar manner the modes that approach diagonal propagation experience progressively less velocity errors, comparing the results for the TE_{31} and TE_{23} modes. Thus for propagation in a direction between that of the diagonal and the direction of either of the coordinate axes, the cut-off frequency of the network lies between the two extremes, as do the velocity characteristics. The field patterns corresponding to modes may easily be found by summing the reflected waves at each node of the network after each order of reflection for the frequency under consideration. Fig. (3.14) shows the normalised field shape for the TE_{11} mode, the absence of the field description at the open circuited ends of the transmission line being due to equations (2.18a, b,c), which indicate that these nodes are in fact not considered during the summation of the reflected waves.

TABLE (3.4)

Cut-off wavelength, k, of TE_{mn} modes in a square cross sectional waveguide of side 7 units.

Mode (m, n) TE_{mn}	k calc.	k exact	Error %	Maximum Velocity Error %
1,0	0.4468	0.4488	0.44	0.42
1,1	0.6342	0.6347	0.08	0.87
2,0	0.8816	0.8976	1.78	1.74
2,1	0.9958	1.0035	0.77	2.26
2,2	1.2692	1.2694	0.01	3.92
3,1	1.3789	1.4192	2.84	4.78
2,3	1.6030	1.6182	0.94	7.04
3,3	1.9020	1.9041	0.1	11.68
2,4	1.9353	2.0071	3.58	12.51
4,4	2.5406	2.5388	0.07	-
5,5	3.1746	3.1735	0.03	-
6,6	3.8085	3.8082	0.01	-

(P = 500)

-1.00	-0.81	-0.44	0.00	0.44	0.81	1.00
-0.81	-0.64	-0.35	0.00	0.35	0.64	0.81
-0.44	-0.35	-0.19	0.00	0.19	0.35	0.44
0.00	0.00	0.00	0.00	0.00	0.00	0.00
0.44	0.35	0.19	0.00	-0.19	-0.35	-0.44
0.81	0.64	0.35	0.00	-0.35	-0.64	-0.81
1.00	0.81	0.44	0.00	-0.44	-0.81	-1.00

Fig. (3.14) Field configuration of the TE_{11} mode on the matrix of fig. (3.12) k = o.6342

3. 4. MAXWELL'S FIELD EQUATIONS AND THE BASIC TRANSMISSION LINE EQUATIONS.

The previous section indicated the manner by which the analysis of TE_{mn} modes may be accomplished by simulating the waveguide by a network of intersecting transmission lines, and observing certain identities between the voltages and currents on the network with the electric and magnetic field components existing within a rectangular waveguide, equations (3.10) and (3.11). Consideration of fig. (3.15), showing a typical intersection of transmission line elements of fig. (3.12), yields the following approximate relationships.

$$\frac{\partial V}{\partial y} = -L \frac{\partial}{\partial t} (I_y^+ - I_y^-)$$

$$\frac{\partial V}{\partial x} = -L \frac{\partial}{\partial t} (I_x^+ - I_x^-) \qquad (3.21)$$

$$\frac{\partial}{\partial x} (I_x^+ - I_x^-) + \frac{\partial}{\partial y} (I_y^+ - I_y^-) = -2C \frac{\partial V}{\partial t}$$

thus

$$\frac{\partial^2 V}{\partial x^2} + \frac{\partial^2 V}{\partial y^2} = 2LC \frac{\partial^2 V}{\partial t^2}$$

whilst Maxwells field equations

$$\text{curl } \underline{H} = \epsilon \frac{\partial \underline{E}}{\partial t}, \qquad \text{curl } \underline{E} = -\mu_o \frac{\partial \underline{H}}{\partial t}$$

become

$$\frac{\partial H_z}{\partial y} = \epsilon \frac{\partial E_x}{\partial t}$$

$$-\frac{\partial H_z}{\partial x} = \epsilon \frac{\partial E_y}{\partial t} \qquad (3.22)$$

$$\frac{\partial E_y}{\partial x} - \frac{\partial E_x}{\partial y} = -\mu_o \frac{\partial H_z}{\partial t}$$

i.e.

$$\frac{\partial^2 H_z}{\partial x^2} + \frac{\partial^2 H_z}{\partial y^2} = \mu_o \epsilon \frac{\partial^2 H_z}{\partial t^2}$$

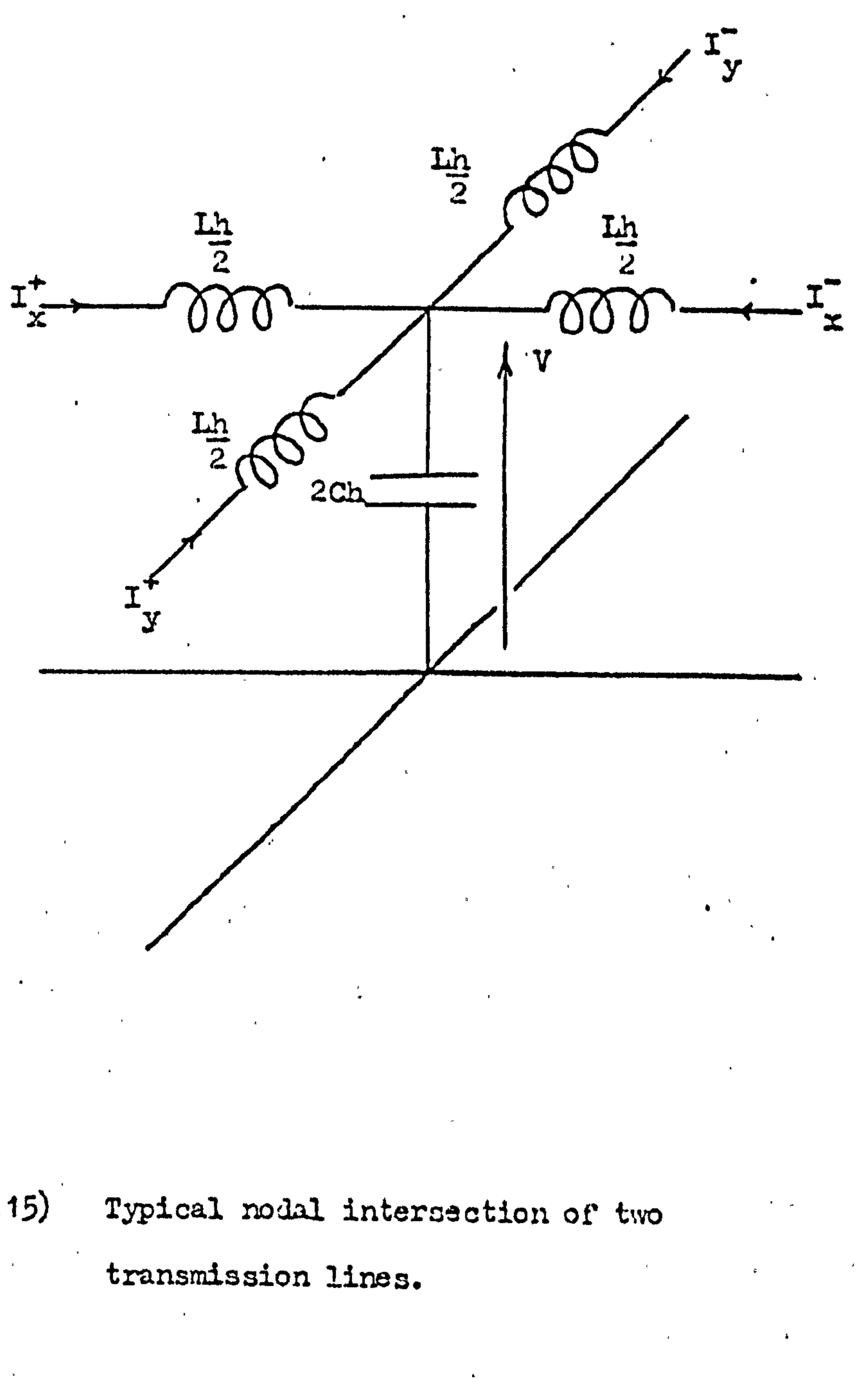

Fig. (3.15) Typical nodal intersection of two transmission lines.

and
$$\frac{\partial E_z}{\partial y} = -\mu_o \frac{\partial H_x}{\partial t}$$
$$-\frac{\partial E_z}{\partial x} = -\mu_o \frac{\partial H_y}{\partial t} \qquad (3.23)$$
$$\frac{\partial H_y}{\partial x} - \frac{\partial H_x}{\partial y} = \epsilon \frac{\partial E_z}{\partial t}$$

i.e.
$$\frac{\partial^2 E_z}{\partial x^2} + \frac{\partial^2 E_z}{\partial y^2} = \mu_o \epsilon \frac{\partial^2 E_z}{\partial t^2}$$

within a rectangular source free waveguide at cut-off. Thus Maxwell's curl equations divide into two independant sets corresponding to the propagation of TEmodes, equation (3.22) and TM modes, equation (3.23), subject to the boundary conditions that exist within the waveguide.

Comparison of equations (3.21) and (3.22) then yield the identities

$$V \equiv H_z \; ; \; E_x \equiv -(I_y^+ - I_y^-) \; ; \; E_y \equiv (I_x^+ - I_x^-)$$
$$L \equiv \epsilon \; ; \qquad 2C \equiv \mu_o$$

and the velocity of propagation $= \frac{1}{\sqrt{\mu_o \epsilon}} = \frac{1}{\sqrt{2LC}}$

Thus if each of the wave components travel over the network internodal distances at the speed of light c, they combine to form a wave travelling over the network as a whole at a velocity $c/\sqrt{2}$, and is hence confirmation of a result obtained previously. The network then represents a medium of relative permittivity twice that of free space. Further the electric walls in the waveguide must be represented by open circuits on the network, whilst the magnetic walls of symmetry must be represented by short circuits on the network.

Equations (3.21) and (3.23) yield the following identities between the voltages and currents on the network and the fields for TM mode propagation at cut-off

$$V \equiv E_z \quad ; \quad H_x \equiv -(I_y^+ - I_y^-) \quad ; \quad H_y \equiv (I_x^+ - I_x^-)$$

$$L \equiv \mu_o \quad ; \quad 2C \equiv \epsilon$$

and again the velocity of propagation $v = \frac{1}{\sqrt{\mu_o \epsilon}} = \frac{1}{\sqrt{2LC}}$

Again the network represents a medium of relative permittivity twice that of free space, but now the electric walls of the wave guide are represented by short circuits on the network and magnetic walls by open circuits.

The analysis of the previous section, dealt with the calculation of the TE_{mn} type mode cut-off frequencies for a waveguide of square cross section using the relationship that the voltage distribution on the network is representative of the scalar magnetic field, H_z, in the direction of propagation. It can now be seen from the identities derived for TE modes, that the summation of backward and forward propagating waves can be used to calculate the other field components, in particular at a node (x,y),

$$E_x(x,y) = -I_y^+(x,y) + I_y^-(x,y)$$

$$= -\sum_{p=1}^{P} {}_pV_4^i(x,y) \angle\theta + \sum_{p=1}^{P} {}_pV_2^i(x,y) \angle\theta \qquad (3.24)$$

and $$E_y(x,y) = I_x^+(x,y) - I_x^-(x,y)$$

$$= \sum_{p=1}^{P} {}_pV_1^i(x,y) \angle\theta - \sum_{p=1}^{P} {}_pV_3^i(x,y) \angle\theta \qquad (3.25)$$

using the notations of equations (3.17), providing the characteristic impedance of the line is normalised. For TE_{mo} mode types, such that the waveguide is resonated transversely in the x direction, it was stipulated that for the necessary initial excitation along a transmission line x = constant, whatever magnitude and phase of a wave reflected from any node was identical to that reflected from the immediate neighbouring node in the y direction, and hence from equation (3,24), $E_x(x,y)$ is zero, thus indicating that there is no field variation in the y direction.

Similarly for TM_{mn} type mode cut-off frequencies, the field components E_z, H_x, H_y, may be found by summing the reflected waves at discrete observation points on the network and performing the suitably adapted operations of equations (3.24) and (3.25). The method was applied to the same network as was utilised for the examination of the TE_{mn} modes, but short circuits replacing the open circuits, and the results tabulated in Table (3.5) for h = 1 together with the velocity errors which must still be inherent in these mode studies, due to the orientation of the waves over the network matrix. The cut-off wavelengths, k, reported in the table of results are identical to those in Table (3.4), as would be expected. The field configuration of the TM_{11} was also obtained and displayed in fig. (3.16), for the component E_z.

TABLE (3.5)

Cut-off wavelength, k, of TM_{mn} modes in a square cross sectional waveguide of side 7 units.

Mode (m,n) TE_{mn}	k calc.	k exact	Error %	Maximum velocity Error %
1,1	0.6344	0.6347	0.05	0.87
2,1	0.9953	1.0035	0.82	2.26
2,2	1.2683	1.2694	0.08	3.92
3,1	1.3779	1.4192	2.91	4.78
2,3	1.6032	1.6182	0.93	7.04
3,3	1.9023	1.9041	0.09	11.77
2,4	1.9351	2.0071	3.59	12.50
4,4	2.5409	2.5388	0.08	-
5,5	3.1736	3.1735	0.00	-
6,6	3.8052	3.8082	0.08	-

(P = 500)

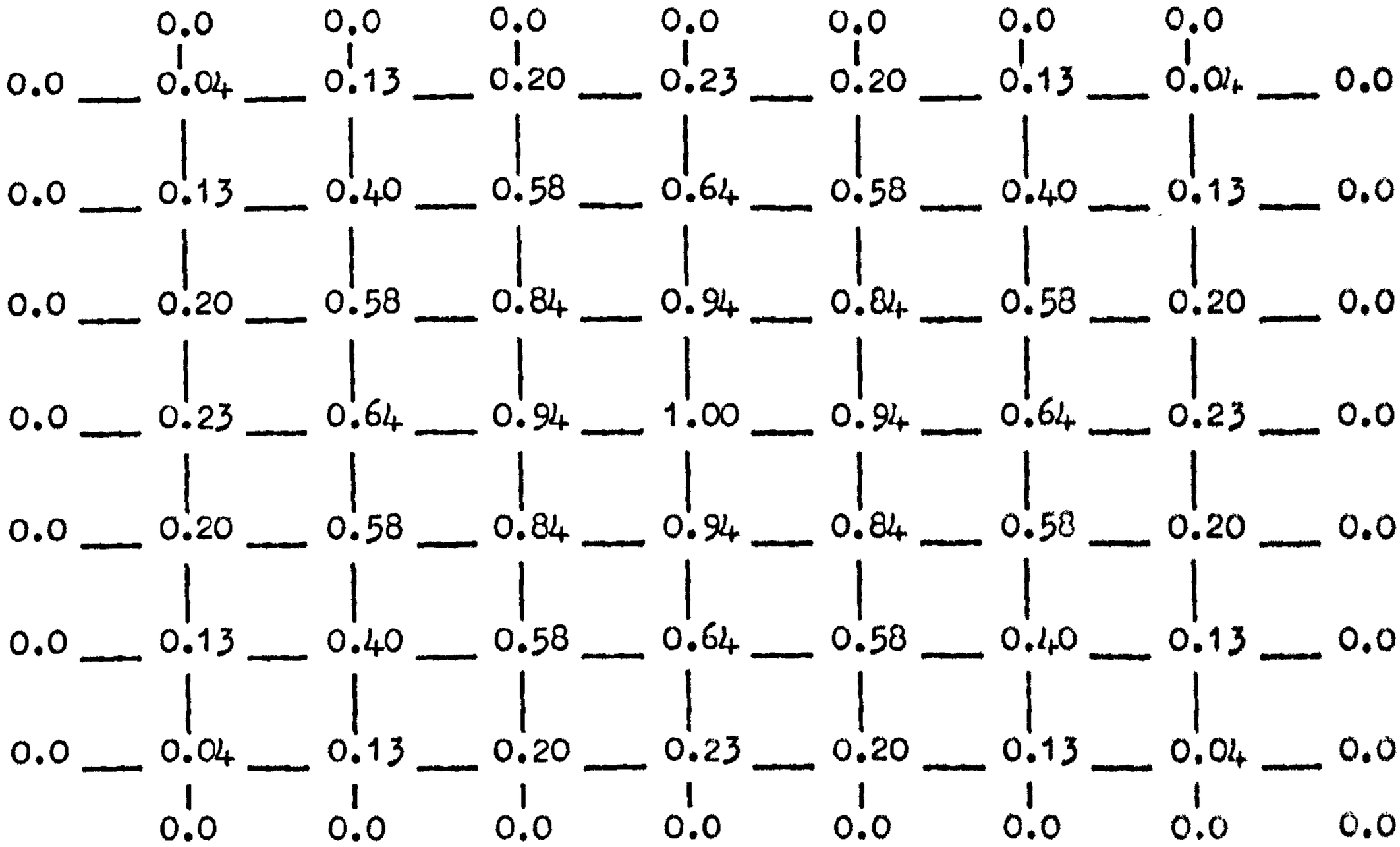

Fig. (3.16) Field configuration of the TM_{11} mode on the matrix of fig. (3.12). $k = 0.6344$.

3.5. DISCUSSION AND CONCLUSIONS.

This chapter has described a new method to solve rectangular wave guide problems, utilising the knowledge that the fields throughout any cross-sectional plane of the wave-guide vary sinusoidally in space. The finite difference/element techniques of chapter 2 base their mode of operation on describing the cross-section by a regular mesh of intersecting lines forming nodes. In their simplest form these describe the field variations between nodes as a linear function of the spatial co-ordinates and potentials existing at those nodes, and serve to approximate the known sinusoidal variation. Even extensions of the methods, permitting the use of parabolic or cubic internodal field description functions, although an improved approximation, does not complete the true field variation.

The method developed here, uses an almost identical mesh, for analysis, but the lines forming the net possess a physical interpretation, namely a set of intersecting transmission lines, which is sinusoidally excited at a node or series of nodes as would occur in practice, for a particular mode structure. The field on the matrix of transmission lines is then constructed as it would occur naturally, by considering the successive orders of multiple reflections and transmissions of waves that appear at each nodal junction of the matrix, and summing these propagating waves to obtain the shape of the field across the net of transmission lines, that is, the steady state field is built up by transient means.

The network is effectively a slow wave structure, and if regular represents propagation in a medium twice that of free space, with due regard for the direction of the waves as a whole traversing the matrix, and operations being restricted to those involving the low frequency passband characteristics of the structure. This passband serves only to standardise the method in some way, and operation of the matrix within higher frequency passbands is certainly not prohibited, providing the necessary correction factors incurred by the slow wave structure are observed. The departure of the velocity characteristics on the network from the low frequency limit of $c/\sqrt{2}$ was shown to depend on the direction of the waves over the matrix, being governed by equation (3.20) for waves propagating parallel to one of the transmission line directions and remaining at $c/\sqrt{2}$, with the matrix never becoming itself cut-off, for diagonal propagation. Propagation in any other direction must clearly possess velocity characteristics between these two extremes and is borneout by the results of tables (3.4.), (3.5.). It is worthwhile also to note that the TE_{21}, TM_{21} mode waves will possess a velocity of $c/\sqrt{2}$ and never experience cut-off in a rectangular wave guide of sides 2 : 1, since these waves also traverse the matrix at 45^{o} and can be appreciated by considering the waveguide formed by extending the open circuit wall $b_1 b_2$ of fig. (3.13) to include b_3; this result can obviously be extended to TE_{mn}, TM_{mn} modes within a rectangular wave guide of sides m :: n.

Possessing the known intermodal field variation, the method, thus must yield absolutely correct results, providing the errors presented by such a discretization of space is known. This is apparent from an examination of tables (3.3), (3.4) and (3.5) which shows that the results for the summation of the multiple reflected waves constructing the TE_{no}, TE_{nn}, TM_{nn} modes are identical to the correct solutions.

The frequency response of the network, varies according as to the observation node chosen, but is basically the same, consisting of (sin x)/x type curves centred about the frequency at which the network resonates and caused by the truncated periodic sampling of a sinusoidal waveform. The width of the main lobe and hence the side lobes depends largely on P, the number of reflections considered and greatly influences the calculated resonant frequencies, due to mutual interference. The errors associated with this truncation of order of reflections is referred to as 'truncation error' and is reported elsewhere.[41] The value of P chosen for most of the calculations, obviated the use of determining the truncation error for each result, but table (3.3) implies that some truncation error must have been present, owing to the 'crowding' of the modes, at the upper end of the frequency range, and thus a relatively large amount of mutual interference will occur. It is to be noted that the spreading out of the idealised frequency response of the network consisting of delta functions into (sin x)/x type curves is most advantageous, since it is these which aid the user in detecting the peak of the curves and hence the resonant frequency.

The attraction of this method is mainly the ease with which it may be formulated, since only basic transmission line theory is associated with the development, and detailed procedures such as the construction of a large number of algebraic simultaneous equations and the methods utilised to solve the set are not required. Since the technique relies on using a circular internodal function, to simulate the field variation across a waveguide, then the accuracy achieved using such a function must be an improvement on the solutions obtained via the finite difference/element techniques, and can be seen to be true by examination of tables (2.5) with tables (3.4), (3.5) for almost similar space discretizations.

The amount of computer store required for the method is minimal and all calculations were performed on a computer of size 12kbyte. The actual store required for the analysis of the square cross-section waveguide of fig. (3.12) was that of eight (9 x 9) matrices plus four (1 x 9) working space matrices, i.e. approximately 700 number locations. This is extremely small compared with that required in solving the set of linear equations associated with the finite difference/element methods, which for the solutions of table (2.5), h/a = 1/8, require the storage of three (28 x 28) matrices with three (1 x 28) matrices as working space, i.e. approximately 2500 number locations, and was used to describe only half the waveguide. The waveguide of fig. (3.12) would thus require 7,300 number locations to solve for the cut-off frequencies using these methods producing progressively less accurate solutions, as the frequency increased, than those of the proposed improved method.

The use of a relaxation process to solve the set of equations would require the storage of 81 numbers but only the dominant mode is then solvable.

The disadvantage of the method of utilising finite transmission line elements is the computer run time required, a typical example being 1 hour solving for each of the modes in Tables (3.4), (3.5) and is due to the repetitive vectorial addition necessary for the addition of the four waves incident at any node in the mesh, and at present no technique has become apparent by which the method may be accelerated. The transmission line element method must then appeal mainly to the user possessing a relatively small computer with a large amount of run time.

CHAPTER 4.

THE APPLICATION OF FINITE TRANSMISSION LINE ELEMENTS TO WAVEGUIDES OF A GENERALISED CROSS-SECTION.

Previous investigation indicated the feasibility of utilising a circular intermodal function over a mesh or network of transmission lines simulating a rectangular waveguide.

The steady state response of the network at a particular frequency was obtained by considering a large number of reflections that occurred due to the impedance discontinuities presented to a wave travelling along each individual transmission line at each mesh intersection, and summing the magnitude and phase of these waves at each junction so as to obtain the field description across the wave guide. This process has to be repeated for each frequency examined, and may thus be referred to as the steady state finite transmission line element method.

Such an investigation would be severely limited if the method of transmission-line elements were to be restricted only to these examples. This section is devoted to the extension of the present method whereby the propagating modes of an inhomogeneously loaded waveguide and waveguides possessing non-rectangular geometries can be found, and thus the solutions to many classes of waveguide configurations used in modern microwave applications are available. The first section of this chapter shows the manner in which the LSE and LSM modes that propagate in the dielectric slab loaded waveguide of fig. (4.1), may be solved for, whilst subsequent sections indicates how the transmission-line elements are employed in describing the propagating modes of circular and elliptical cross-sectional waveguides.

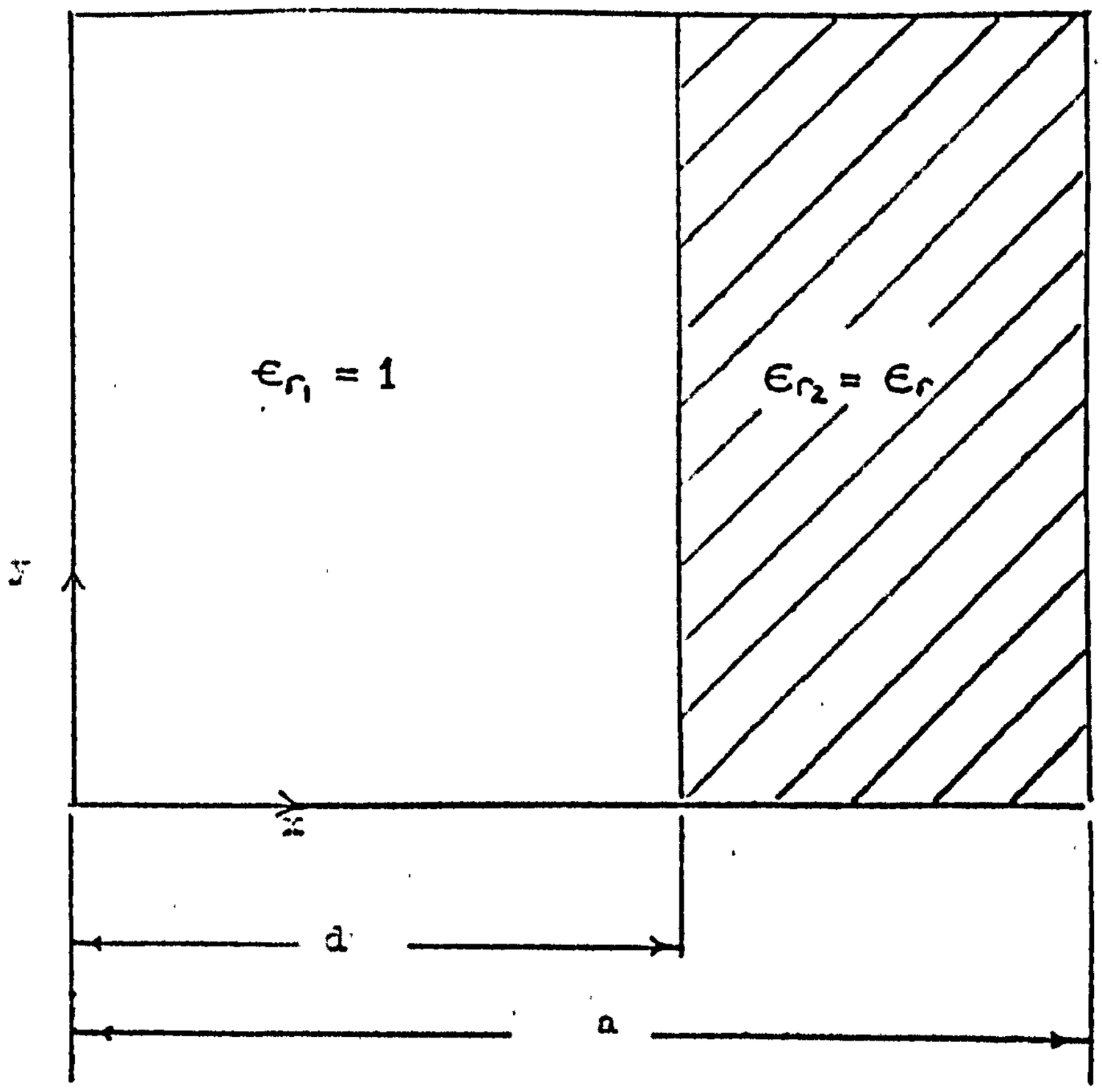

Fig. (4.1) Cross-section of a dielectric slab loaded waveguide.

4. 1. Inhomogeneously loaded waveguide.

Fig. (4.1) shows the cross-section of a dielectric slab loaded waveguide, the waveguide is assumed to be infinitely long in the z direction, with a field dependence of $e^{-j\beta z}$ in this direction, together with the time dependence of e^{jwt} understood.

The fields within such a structure may be classified as either of those possessing no component of electric field normal to the air/dielectric interface, (E_x=0), and are referred to as LSE modes, or those not possessing a component of magnetic field normal to the air/dielectric interface, (H_x= 0), and are referred to as LSM modes.

4.1.1. LSE mode structures.

The LSE mode field configurations may be obtained via a magnetic Hertzian potential[23]

$$\underline{\Pi}_h = \underline{e}_x \psi_h(x,y)\, e^{-j\beta z} \qquad (4.1)$$

such that the fields are represented by

$$\underline{E} = -j\omega\mu_o \nabla \wedge \underline{\Pi}_h \qquad (4.2)$$

$$\underline{H} = \nabla \wedge \nabla \wedge \underline{\Pi}_h \qquad (4.3)$$

and $$\nabla_{xy}^2 \psi_h + [\omega^2\mu_o\epsilon_o\epsilon_{ri} - \beta^2]\psi_h = 0$$

where $$\epsilon_{ri} = 1 \qquad 0 \leqslant x \leqslant d$$

$$= \epsilon_r \qquad d \leqslant x \leqslant a$$

and $$\psi_h = A \sin hx \cos \frac{m\pi y}{b} \qquad 0 \leqslant x \leqslant d$$

$$\psi_h = B \sin l(a-x) \cos \frac{m\pi y}{b} \qquad d \leqslant x \leqslant a$$

with $$\beta^2 = \omega^2\mu_o\epsilon_r - l^2 - \left(\frac{m\pi}{b}\right)^2 = \omega^2\mu_o\epsilon_o - h^2 - \left(\frac{m\pi}{b}\right)^2$$

$$m = 0,1,2, \ldots\ldots\ldots$$

which satisfy all boundary conditions on the waveguide's surrounding conductors, and also for matching at the interface,

$$h \tan l(a-d) = -l \tan hd$$

For the dominant mode of propagation (m = 0), equations (4.2), (4.3) imply that the only field components existing are H_x, E_y, H_z, and within each homogeneous section of the waveguide are identical to those corresponding to TE_{no} mode propagation, the dominant LSE mode is thus a quasi-TE_{no} type mode, with components H_z, E_y at the structures cut-off frequency.

This mode, as before, may be solved at cut-off in one dimension, utilising a single periodically stub loaded transmission line with the identities,

$$H_z \equiv V \; ; \; E_y \equiv (I_x^+ - I_x^-) \; ; \; L \equiv \epsilon_o \epsilon_{r_i} \; ; \; 2C \equiv \mu_o. \qquad (4.4)$$

with short circuits on the network representing magnetic walls in the waveguide and open circuits representing the electric walls.

In an inhomogeneous medium, however, the electromagnetic waves travel more slowly in the medium of higher dielectric constant, and hence the electrical length between the nodes of the model must be greater. Also because of the discontinuity in intrinsic impedance experienced by the waves at the dielectric boundary, reflection and transmission coefficients have to be formed.

On the transmission line the intrinsic impedance is given by

$$Z_o = \sqrt{\frac{L}{C}} \quad \propto \sqrt{\epsilon_{r_i}}$$

from the identities (4.4), hence, if t_{nm} and r_{nn} are the transmission and reflection coefficients for a wave travelling from medium of permittivity ϵ_n to a medium of permittivity ϵ_m, then for voltages on the matrix,

$$t_{nm} = \frac{2\sqrt{\epsilon_m}}{\sqrt{\epsilon_n} + \sqrt{\epsilon_m}} \quad ; \quad r_{nm} = \frac{\sqrt{\epsilon_m} - \sqrt{\epsilon_n}}{\sqrt{\epsilon_m} + \sqrt{\epsilon_n}} \tag{4.5}$$

and if θ_n is the electrical length between nodes in the medium of permittivity ϵ_n,

$$\theta_m = \theta_n \sqrt{\frac{\epsilon_m}{\epsilon_n}} \tag{4.6}$$

Table (4.1) shows the results for the dominant LSE mode at cut-off for the structure defined by fig. (4.2), the model of fig. (4.1) with an open circuit termination of node 1 defining an electric wall and a short circuit termination at node 10 defining a magnetic wall, thus simulating half the waveguide, with 2d = a = 8h Calculations were made for various orders of reflections in the network, and to isolate the mode under consideration, the electric field component parallel to the air/dielectric interface was excited and observed at node 9, with the equivalences of equation (4.4) being used. Permittivities of the dielectric slab examined were ϵ_r = 2.45, 9.0, 50.0, 100.0, and the maximum velocity error was 0.1% corresponding to the internodal electrical length in the dielectric region for the relative permittivity of 100. Comparison between the cut-off wave lengths obtained by finite difference/element analysis, table (2.4) with those obtained in table (4.1), indicates that the method of transmission line elements is more accurate for low values of relative permittivity but not as accurate for higher permittivities. The relatively large errors inherent in the solutions for high permittivities are due to the progressive crowding of modal cut-off wavelengths as the permittivity increases. This can be seen in Table (4.1) where the solutions tend to oscillate about the true solutions and for ϵ_r = 100 are always greater but converging to the correct solution, implying

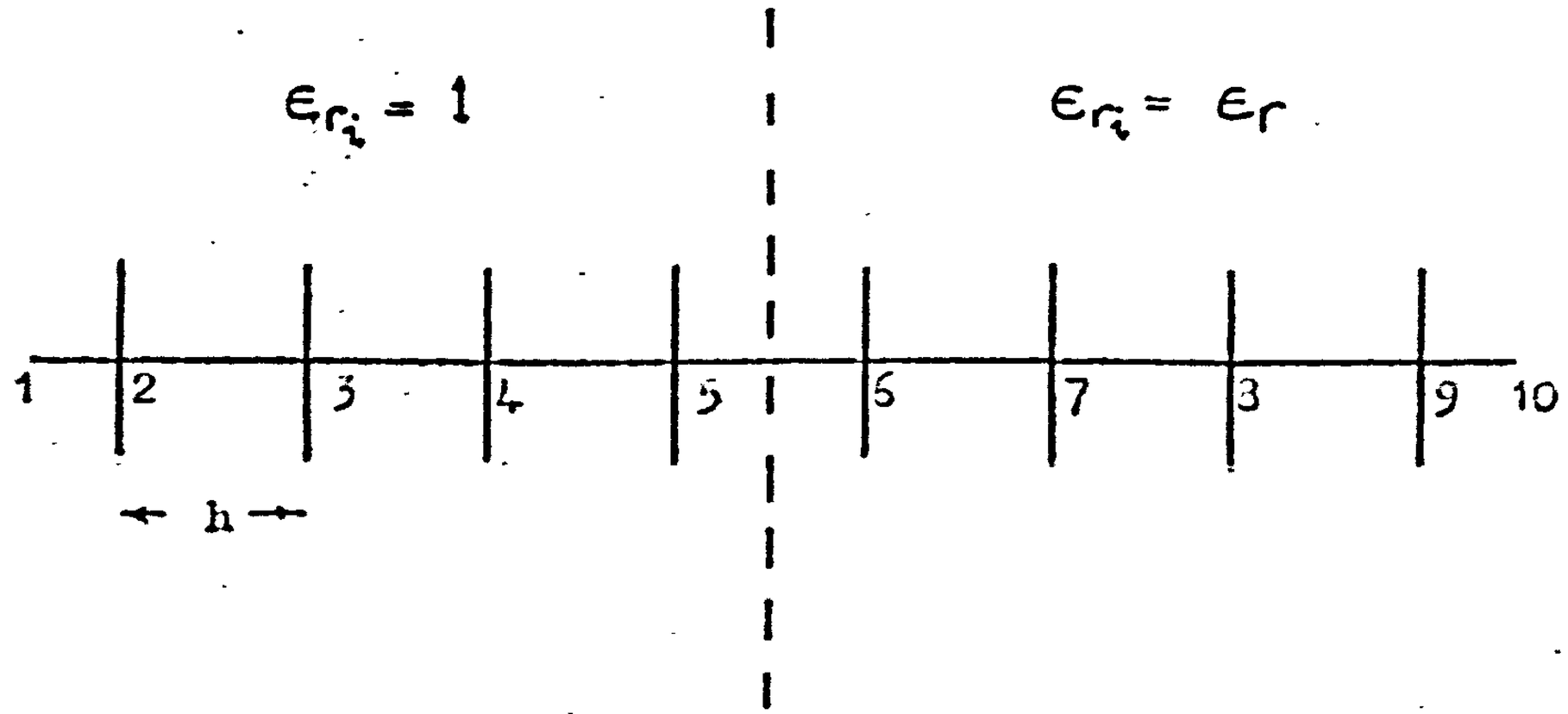

Fig. (4.2) Transmission line model used for the analysis of the dominant LSE modes of fig. (4.1).

TABLE (4.1)

Cut-off wavelengths ($a/\lambda c$) of the dominant LSE mode in a waveguide of width 2a, fig. (4.1), for various permittivities and orders of reflection.

ϵ_r	$\frac{a}{\lambda_c}$ Analytical	a/λ_c (numerical) for various orders of reflection									
		640	error %	680	error %	720	error %	760	error %	800	error %
2.45	0.3372	0.3369	0.09	0.3374	-0.06	0.3370	0.06	0.3373	-0.03	0.3370	0.06
9.0	0.1807	0.1807	0.0	0.1803	0.22	0.1810	-0.17	0.1809	-0.11	0.1806	0.05
50.0	0.07732	0.07624	1.40	0.07444	3.72	0.07642	1.16	0.07840	-1.40	0.07797	-0.84
100.0	0.05472	0.05564	-1.68	0.05535	-1.15	0.05521	-0.89	0.05506	-0.62	0.05492	-0.36

Maximum velocity error = 0.1% h/a = 1/16 (h = 1)

that the higher ordered modes are influencing the dominant mode as described in the previous chapter, and can only be overcome by increasing the order of reflections, and isolating the mode under consideration by suitable excitation and observation points. These are discussed to a greater extent in the general discussion of section(4.1.4.)

4.1.2. LSM mode structures.

The LSM mode field configurations may be derived from an electric Hertzian potential[23]

$$\underline{\Pi}_e = \underline{e}_x \psi_e(x,y)\, e^{-j\beta z} \tag{4.7}$$

and the fields $\underline{E}$, $\underline{H}$ represented by,

$$\underline{H} = j\omega\epsilon_o\epsilon_{r_1} \nabla \wedge \underline{\Pi}_e \tag{4.8}$$

$$\underline{E} = \nabla \wedge \nabla \wedge \underline{\Pi}_e \tag{4.9}$$

and $$\nabla_{xy}^2 \psi_e + (\omega^2\mu_o\epsilon_o\epsilon_{r_1} - \beta^2)\psi_e = 0$$

where $$\epsilon_{r_1} = 1 \qquad 0 \leqslant x \leqslant d$$

$$= \epsilon_r \qquad d \leqslant x \leqslant a$$

and $$\psi_e = A \cos hx \sin \frac{m\pi y}{b} \qquad 0 \leqslant x \leqslant d$$

$$= B \cos l(a-x) \sin \frac{m\pi y}{b} \qquad d \leqslant x \leqslant a$$

with $$\beta^2 = \omega^2\mu_o\epsilon_o\epsilon_{r_1} - l^2 - \left(\frac{m\pi}{b}\right)^2 = \omega^2\mu_o\epsilon_o - h^2 - \left(\frac{m\pi}{b}\right)^2$$

$$m = 1,2,3, \ldots\ldots$$

which satisfy all boundary conditions on the perfect conductors of the waveguides boundaries, and also for the dielectric interface

$$\epsilon_r h \tan hd = -l \tan l(a-d)$$

with reference to fig. (4.1).

At the structures cut-off frequency, the LSM modes possess the field components H_z, E_x, E_y, and thus the equivalences between equations (3.21) and (3.22) may be used again. These are

$$H_z \equiv V \; ; \quad E_y \equiv (I_x^+ - I_x^-) \quad ; \quad E_x \equiv -(I_y^+ - I_y^-) \; ; \qquad (4.10)$$

$$L \equiv \epsilon_o \epsilon_{ri}; \qquad 2C = \mu_o$$

Since the voltage on the network represents the field component H_z, as was the case with the LSE mode analysis, the transmission and reflection coefficients, equation (4.5), remain unchanged, as does the relationship between the electrical lengths in the two media, equation (4.6).

Table (4.2) shows the results obtained for the cut-off wavelengths for the structure defined by fig. (4.3), the model of fig. (4.1) with a wall of symmetry placed parallel to the x direction, simulating half the square cross-section waveguide of side a = 6h To isolate this mode the electric field component perpendicular tothe dielectric interface E_x is used for excitation at nodes adjacent to the short circuit wall and a similarly situated node in the dielectric chosen as the solution point for the same field component. Again four permittivities were considered ϵ_r = 2.45, 9.0, 50.0, 100, and the maximum velocity error was of the order 1.2%. Comparing the finite difference/element results in table (2.3) with those of table (4.2) indicates that the latter is more accurate for a similar space discretization. Further, these solutions are not as vulnerable to oscillations as was the case with the LSE modes, and must be due to the increased frequency separation between the dominant and higher ordered modes, hence reducing the interfering effect these modes have on each other.

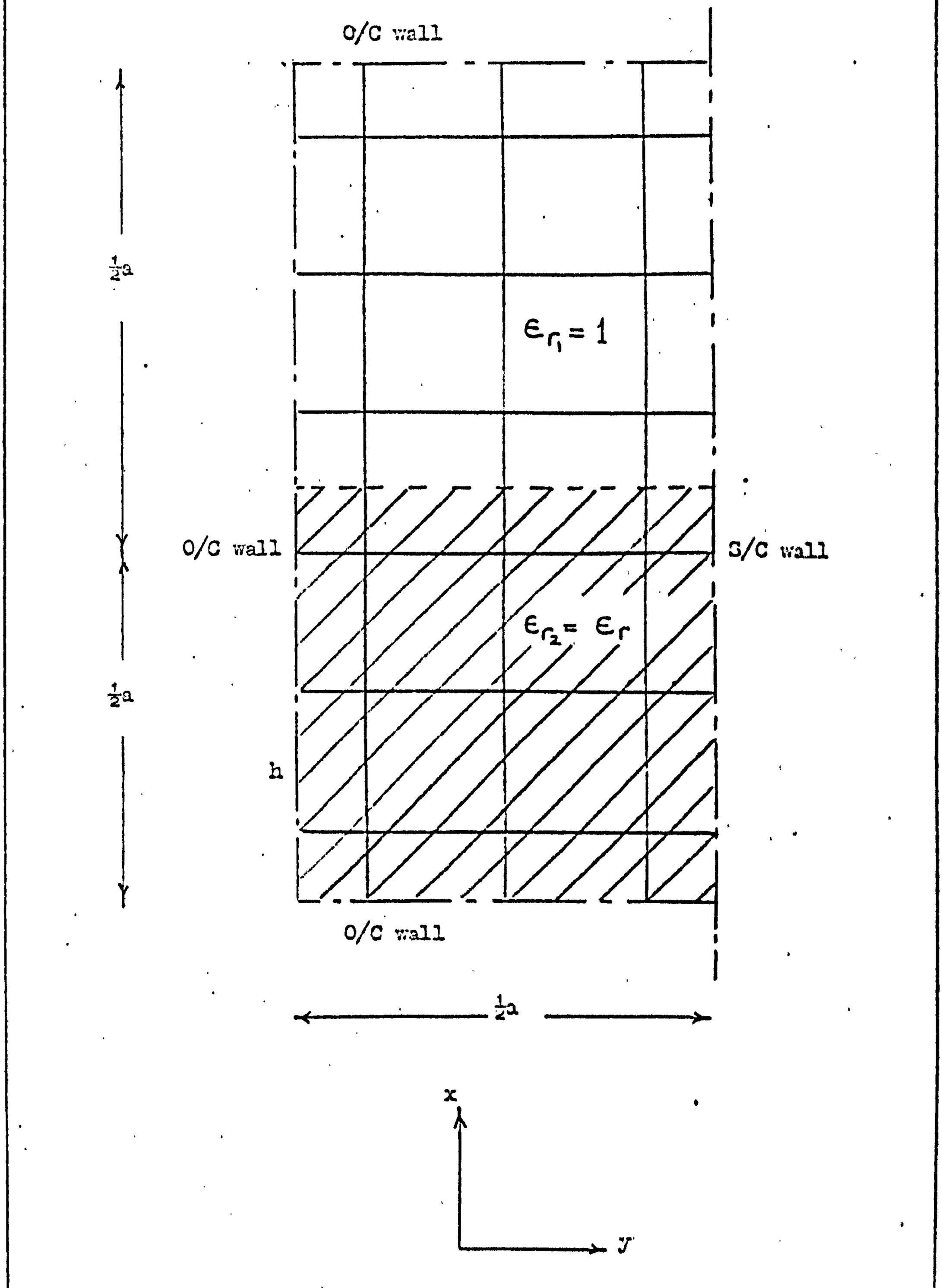

Fig. (4.3) Transmission line network used for the solution of LSM modes. Solid lines indicate transmission lines, broken lines indicate wall of waveguide.

TABLE (4.2)

Cut-off wavelength ($a/\lambda c$) of the dominant LSM mode in the structure of fig. (4.3) for various permittivities and orders of reflection.

ϵ_r	$\frac{a}{\lambda c}$ Anal:	$a/\lambda c$ (numerical) for various orders of reflection									
		80	error %	100	error %	120	error %	140	error %	150	error %
2.45	0.3858	0.3846	0.10	0.3838	0.31	0.3838	0.31	0.3838	0.31	0.3838	0.31
9.0	0.2263	0.2251	0.27	0.2259	0.15	0.2259	0.15	0.2258	0.21	0.2259	0.15
50.0	0.09930	0.09946	-0.16	0.09926	0.04	0.09919	0.10	0.09929	0.01	0.09933	0.03
100.0	0.07047	0.07054	-0.10	0.07040	0.09	0.07045	0.02	0.07045	0.02	0.07045	0.02

Maximum velocity error = 1.2% h/a = 1/6 h = 1

4.1.3. LSE mode within a rectangular cavity.

The dominant LSE mode is essentially a propagating mode possessing two spatial field variations and if the cut-off solution is required, the mode may then be solved in one dimension as in the foregoing analysis. However, the two dimensional configuration of fig. (4.1) may be utilised so as to calculate the resonant frequency of a dielectric loaded cavity supporting the LSE mode, since equations (4.2) and (4.3) imply that the field variation in the direction of the air/dielectric interface is zero. Fig. (4.4) shows the two dimensional representation where the field variation in the y direction is zero.

The transmission line equations for a network of such lines superimposed on fig. (4.4) now become

$$\begin{aligned} \frac{\partial V}{\partial x} &= -L \frac{\partial I_x}{\partial t} \\ \frac{\partial V}{\partial z} &= -L \frac{\partial I_z}{\partial t} \\ \frac{\partial I_x}{\partial x} + \frac{\partial I_z}{\partial z} &= -2C \frac{\partial V}{\partial t} \end{aligned} \qquad (4.11)$$

whilst Maxwell's field equations for the structure become

$$\begin{aligned} \frac{\partial E_y}{\partial x} &= -\mu_o \frac{\partial H_z}{\partial t} \\ \frac{\partial E_y}{\partial z} &= \mu_o \frac{\partial H_x}{\partial t} \\ \frac{\partial H_x}{\partial z} - \frac{\partial H_z}{\partial x} &= \epsilon_o \epsilon_{ri} \frac{\partial E_y}{\partial t} \end{aligned} \qquad (4.12)$$

such that the identities between the fields within the waveguide and the voltages and currents on the network are

$$E_y \equiv V \; ; \quad H_z \equiv I_x \; ; \quad H_x \equiv -I_z \; ; \quad L \equiv \mu_o ; \quad 2C \equiv \epsilon_o \epsilon_{ri} \qquad (4.13)$$

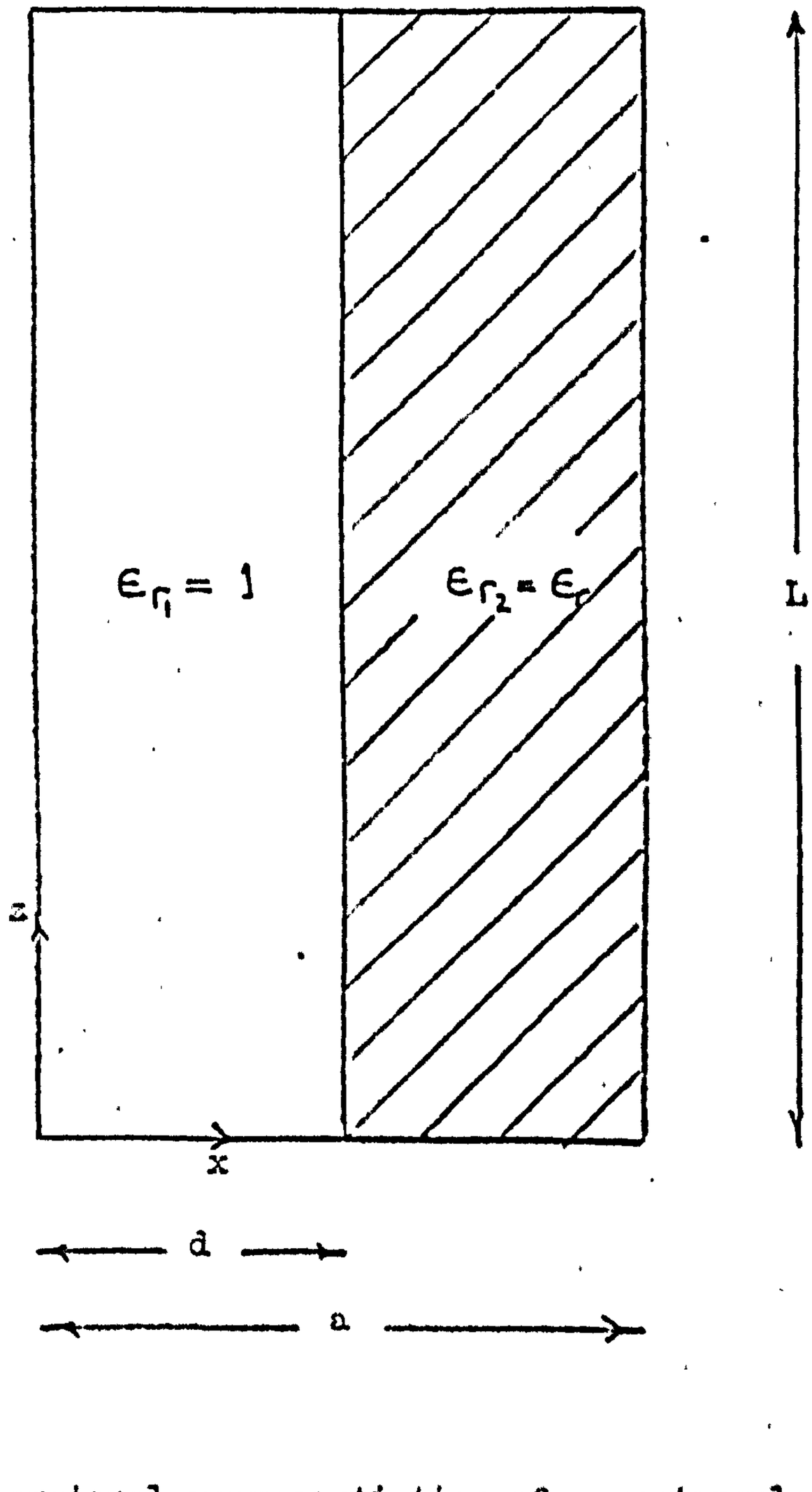

Fig. (4.4) Two dimensional representation of a rectangular dielectric loaded cavity capable of supporting the dominant LSE mode.

with short circuits on the network simulating the electric walls of the waveguide and open circuits simulating magnetic walls of symmetry.

The intrinsic impedance of a transmission line on this network is given by

$$Z_o = \sqrt{\frac{L}{C}} \propto \frac{1}{\sqrt{\epsilon_{r_1}}}$$

and thus the transmission and reflection coefficients t_{nm}, r_{nm}, now become

$$t_{nm} = \frac{\sqrt{\epsilon_n}}{\sqrt{\epsilon_m} + \sqrt{\epsilon_n}} \quad ; \quad r_{nm} = \frac{\sqrt{\epsilon_n} - \sqrt{\epsilon_m}}{\sqrt{\epsilon_n} + \sqrt{\epsilon_m}} \qquad (4.14)$$

and $\theta_m = \theta_n \sqrt{\frac{\epsilon_m}{\epsilon_n}}$ again.

An identical mesh of intersecting transmission lines to that of fig. (4.3) was used to describe the structure of fig. (4.4), with short circuits at x = 0, z = 0 and open circuits at z = L, x = a, thus simulating a quarter of the rectangular cavity possessing a centrally located dielectric slab.

Table (4.3) shows the results for the resonant frequency of this structure for several orders of reflection, the dimensions of the structure being a = 2d = 6h, L = 3h, simulating a cavity of width 12h and length 6h, with an arbitrary depth. The field component E_y was excited at the node corresponding to z = L - h/2, x = a - h/2 and the frequency response observed at this same node where the field will be a maximum at the correct solution. The results again indicate the reliability of the method, with the oscillations in the calculated solutions not being as pronounced as those for the strictly one dimensional LSE configurations due to relatively wide frequency separations between the modes.

TABLE (4.3).

Resonant frequency ($\omega\sqrt{\mu_0\epsilon_0}$) for the dominant LSE mode of the rectangular cavity of fig. (4.4) for various orders of reflections.

ϵ_r	$\omega\sqrt{\mu_0\epsilon_0}$ Analytical	$\omega\sqrt{\mu_0\epsilon_0}$ (numerical) for various orders of reflection							
		70	error %	80	error %	90	error %	100	error %
2.45	0.3913	0.3883	0.75	0.3885	0.72	0.3885	0.72	0.3893	0.50
9.0	0.2076	0.2046	1.43	0.2056	0.95	0.2070	0.27	0.2049	1.29

Maximum velocity error = 0.84% (h/a) = 1/6 (h = 1)

4.1.4. Inhomogeneous waveguides - conclusions.

This section describing the application of the steady state transmission line element method to waveguides of an inhomogeneous nature, shows the accuracy with which a circular internodal function can describe the propagating characteristics of a particular set of modes. The main disadvantage however is the lack of completeness, whereby the dispersive characteristics of the waveguide are not fully known, except for several LSE mode types. Only the cut-off wavelengths of the various structures analysed have been calculated due to the identities exhibited at cut-off between the voltages and currents on the network of transmission lines and Maxwell's field equations, which become separable into two independent sets. The manner in which the dispersive properties of such structures may be examined is not fully apparent, but the finite difference/element techniques may afford several guidelines along which this method can proceed, namely the introduction of a coupling matrix, where two meshes are analysed simultaneously, one possessing the field components H_z, E_x, E_y, equation (3.22) and the other possessing E_z, H_x, H_y, equation (3.23). Certain transfers or coupling may then occur between the two transmission-line meshes, according to the necessary boundary conditions and Maxwells field equations, where the operator j $(=\sqrt{-1})$ necessary for such transfers and which conveniently does not appear in the finite difference/element techniques, may be replaced by the operator $\pi/2$ in this present method. Alternatively, by developing a three dimensional mesh of transmission lines, the dispersive characteristics of inhomogeneous waveguides may be obtained by varying the length of the cavity, and would also prove an invaluable asset in itself to the method as it stands. Clearly these developments afford further interesting research.

The errors inherent in the method applied to these inhomogeneous waveguides are of major interest notably the oscillations of the computed solutions about the true solutions for varying orders of reflections and every technique was adopted so as to minimise them. The errors may be divided into the three classes; method of excitation and observation of the particular fields, truncation error and velocity error.

The excitation and observation techniques proved to be crucial in solving for the individual structures, since at cut-off, the wave lengths of the dominant LSE and LSM modes are in close proximity. Should the same field component be excited and observed (e.g. H_z) in either case then both the LSE and LSM modes could be present and the separation between the cut-off wavelengths too fine to isolate each for a relatively low number of iterations. Consequently the E_y field component was excited and observed as described in section(4.1.1.) in the one dimensional model for the one dimensionally varying LSE modes, whilst the E_x field component was excited and observed as described in section(4.1.2.) for the two dimensional model necessary to examine the two dimensionally varying LSM mode. However, searching for the E_x field component in the LSM mode configuration has the effect of suppressing the LSE modes, but the predicament, presented by the excitation of the E_y field component in the LSE case, which does not necessarily imply the suppression of the LSM type modes that may propagate within such a structure, still arises. The 'down the wave guide' problem involving the two dimensionally varying dominant LSE mode, indicates how the dispersive characteristics may be obtained for this mode. Again the E_y field component was solved for, but here the

LSM modes are suppressed due to a solution being sought in two dimensions down the waveguide, whereas the LSM case would require a three dimensional treatment for similar analysis.

The oscillations in the computed solutions for the LSE modes can be seen to be more pronounced than those for the LSM modes and may be attributed to the truncation of the number of reflections. This truncation error is further influenced by four factors.

(i) The modal cut-off wavelength separation caused by the configurations dimensions, i.e. an increase in the number of nodes modelling the waveguide causes the frequency separation between modes to decrease and thus an increase in the number of reflections is required so as to define the mode being sought.

(ii) Coupled with (i) is the crowding of the modal cut-off wavelengths as the relative permittivity increases. This is to be observed particularly in the LSE modes where for high permittivities the cut-off wavelengths experience a progressive crowding and thus the higher ordered modes will tend to influence the dominant mode, and each other, to an increasing extent due to the lobe interference of the (sin x/x) type curves noted in Chapter 3.

(iii) The possibility that the modal frequency separation of the modes that may propagate within the structure examined is greater in the LSM configurations than in the LSE configurations analysed and this is greatly influenced by the field components used for excitation and observation discussed above.

(iv) If the higher ordered reflections were taken in the order they occur in time[41], then termination of the process would cause

an abrupt truncation in time. However, this process deals with the reflections as they occur in space. This implies, that although the phase of reflections is always correct, the series of reflections to a given point in time may not be complete and the distortion of the frequency response curve caused by neglecting higher order reflections is not so easily predicted.

In Chapter 3, it was shown that the velocity for waves propagating parallel to one of the coordinate directions is defined by

$$\frac{v_n}{c'} = \frac{\frac{1}{2}\theta}{\sin^{-1}(\sqrt{2}\ \sin\frac{1}{2}\theta)} \qquad (4.15)$$

where θ is the internodal electrical length and c' represents the velocity of a wave in a dielectric medium.

Equation (4.15) shows that the network acts as a slow wave structure and that as the frequency rises the velocity of the waves departs from $c'/\sqrt{2}$, and hence the percentage error caused by the slow wave structure as frequency rises is independant of the dielectric constant, thus again allowing the maximum velocity error to be stipulated in the relevant tables, and occurs for the electrical length between nodes situated in the dielectric medium.

It must therefore be emphasised, once more, to obtain reasonable results, the mode under consideration must be isolated and is achieved by using bounds of symmetry where possible, a relatively large number of iterations to reduce the truncation error and choosing field components for excitation and observation that are particular to the mode under consideration.

The one dimensionally varying LSE mode could naturally be solved utilising a stub-less transmission line as was used in section (3.2) with several point discontinuities along its length so as to determine the

length of line and to describe the position of the dielectric interface. The wave propagating along such a structure would no longer appear as if travelling in a medium of permittivity twice that of free space and thus would not possess any velocity error due to propagation on a slow wave structure. Transmission and reflection coefficients would again have to be introduced and the response to various orders of reflections computed. This model would suffer from the same defects as noted previously regarding excitation and observation components and truncation errors. The manufacture of the steady state response by considering the finite difference/element methods of summing multiple reflected waves (chapter 3) would not produce such an accurate solution since these techniques only consider a linear internodal function and will also suffer the same errors as those inherent in the method of transmission line elements. The results shown in tables (4.1.) and (4.2.) are in close agreement with those of the finite difference/element methods, tables (2.3) and (2.4) but tend to be more accurate for a similar spatial discretization, despite the fact that the finite difference/element solutions are those for a truly steady state solution and interference from higher ordered modes is eliminated by their particular processes of determining these solutions.

4.2. IRREGULAR MESH OF TRANSMISSION LINES.

The description of a waveguide cross-section whose boundaries do not lie on a cartesian mesh, present certain difficulties to the method of finite differences/elements. These are mainly overcome by permitting the mesh to be regular everywhere, except where small perturbations in mesh arm length at boundary adjacent nodes is necessary to complete the description of the structure. In much the same manner,

the method of steady state finite transmission line elements, will adopt this procedure to simulate circular and elliptical waveguides on such a cartesian mesh.

The concept of utilising a varying mesh may be envisaged by fig. (4.5) which describes an 'odd-length' of transmission-line, ah, attached to a regular periodic transmission-line structure, terminated at B, with an admittance Y_B. Since the variable mesh arm lengths are those describing the conducting boundary of the structure then Y_B will either represent a short circuit or open circuit.

For short circuits the admittance at A for a wave travelling A to B is given by

$$Y_A = \frac{j\,(3 \tan \frac{1}{2}\theta - \cot a\theta)}{1 - (2 \tan^2 \frac{1}{2}\theta - \tan \frac{1}{2}\theta \cot a\theta)} \qquad (4.16)$$

where $\Theta = \frac{wh}{c}$ the internodal electrical length,

whereas the admittance at A should be,

$$\frac{Y_A}{\sqrt{2}} = \frac{-j}{\tan \sqrt{2}\ \theta\,(\frac{1}{2} + b)} \qquad (4.17)$$

which represents the admittance at A for a wave travelling from A to B through a medium of relative permittivity 2 with a velocity $c/\sqrt{2}$. Equations (4.16) and (4.17) thus imply, that for a length bh of transmission line terminated in a short circuit, the effective physical length is given by

$$a = \frac{1}{\theta} \tan^{-1} \left(\frac{\sqrt{2} \tan \frac{1}{2}\theta - \tan \sqrt{2}\,\theta\,(\frac{1}{2} + b)}{\left(2\sqrt{2} \tan^2 \frac{1}{2}\theta - 3 \tan \frac{1}{2}\theta \tan \sqrt{2}\,\theta\,(\frac{1}{2} + b) - \sqrt{2}\right)} \right) \qquad (4.18)$$

which in the low frequency limit becomes

$$a = b$$

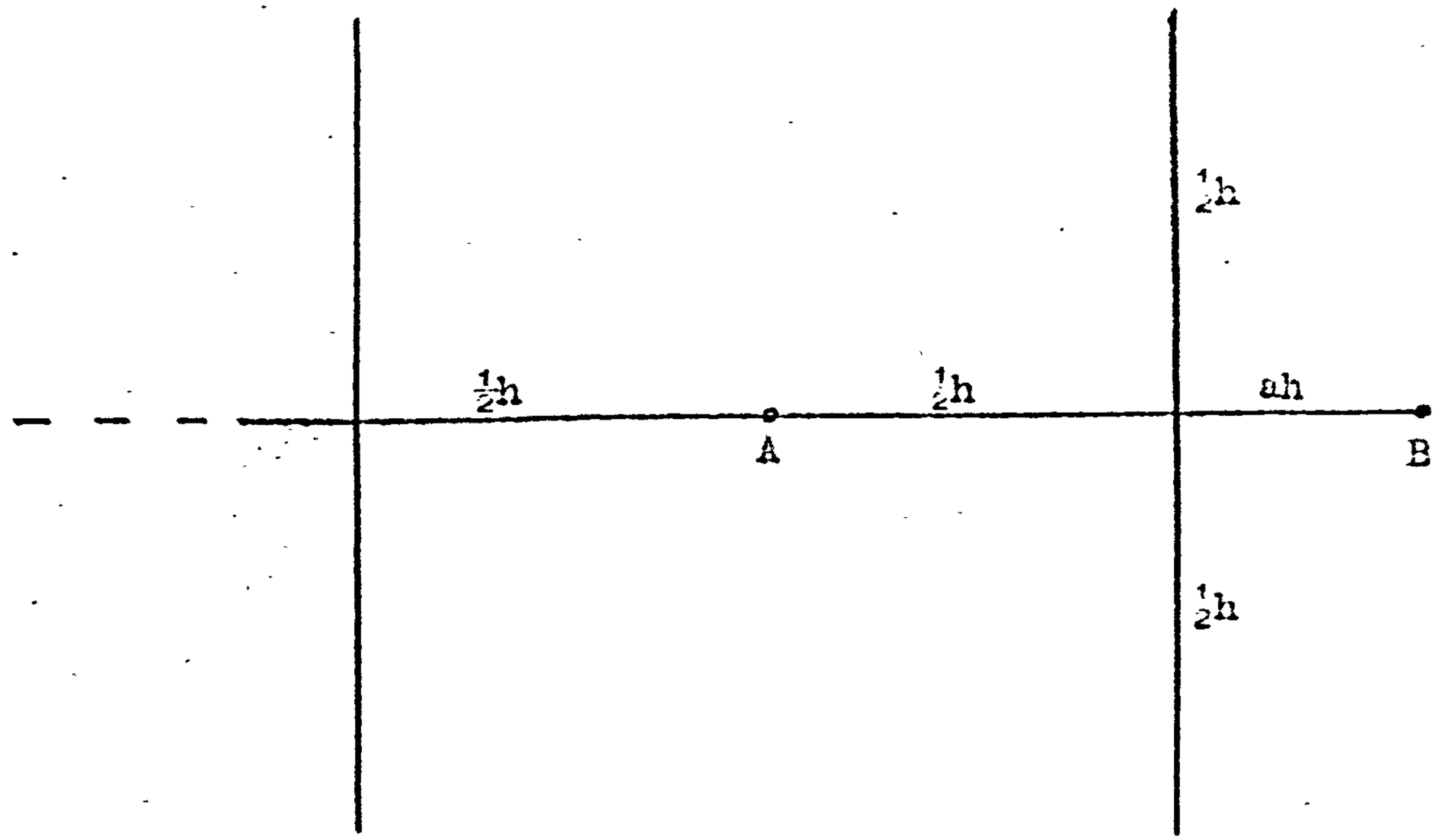

Fig. (4.5) Odd length of transmission line attached to a periodically stub loaded transmission line.

The variation of the effective length a, with electrical length θ, is recorded in fig. (4.6a), for several values of b, which indicates that a follows b with little error for $\theta < 0.6$, but for $\theta > 0.6$ the error deteriorates.

For open circuit terminations the admittance at A for a wave travelling from A to B is given by

$$Y_A = \frac{j\,(3\tan\frac{1}{2}\theta + \tan a\theta)}{1-(2\tan^2\frac{1}{2}\theta + \tan\frac{1}{2}\theta\ \tan a\theta)} \qquad (4.19)$$

whereas the admittance should be

$$\frac{Y_A}{\sqrt{2}} = j\tan\sqrt{2}\,\theta\,(\tfrac{1}{2}+b)$$

hence

$$a = \frac{1}{\theta}\tan^{-1}\left\{\frac{\sqrt{2}\tan\sqrt{2}\,\theta(\frac{1}{2}+b) - 2\sqrt{2}\tan\sqrt{2}\,\theta(\frac{1}{2}+b)\tan^2\frac{1}{2}\theta - 3\tan\frac{1}{2}\theta)}{1+\sqrt{2}\tan\sqrt{2}\ \theta(\frac{1}{2}+b)\tan\frac{1}{2}\theta}\right\} \qquad (4.20)$$

which in the low frequency limit becomes

$$a = 2b - \tfrac{1}{2}$$

The variation of the effective length a, with electrical length θ, is shown in fig. (4.6b) for several values of b, and it can be seen that b has to be corrected such that a true value of a is seen. The accuracy deteriorates far more rapidly in this case and can only be accurate for $\theta < 0.2$ without serious deviations in correct solutions.

This technique of correcting the mesh arm length, or odd length of transmission line, was applied to the calculation of the dominant TE_{10} mode in a rectangular waveguide, modelled by the transmission line of fig.(4.7), with a short circuit at B_1 (magnetic wall) and an open circuit at B_2 (electric wall), the length of the transmission line being $(6 + b_1 + b_2)h$, thus representing a waveguide of width $2(6 + b_1 + b_2)h$.

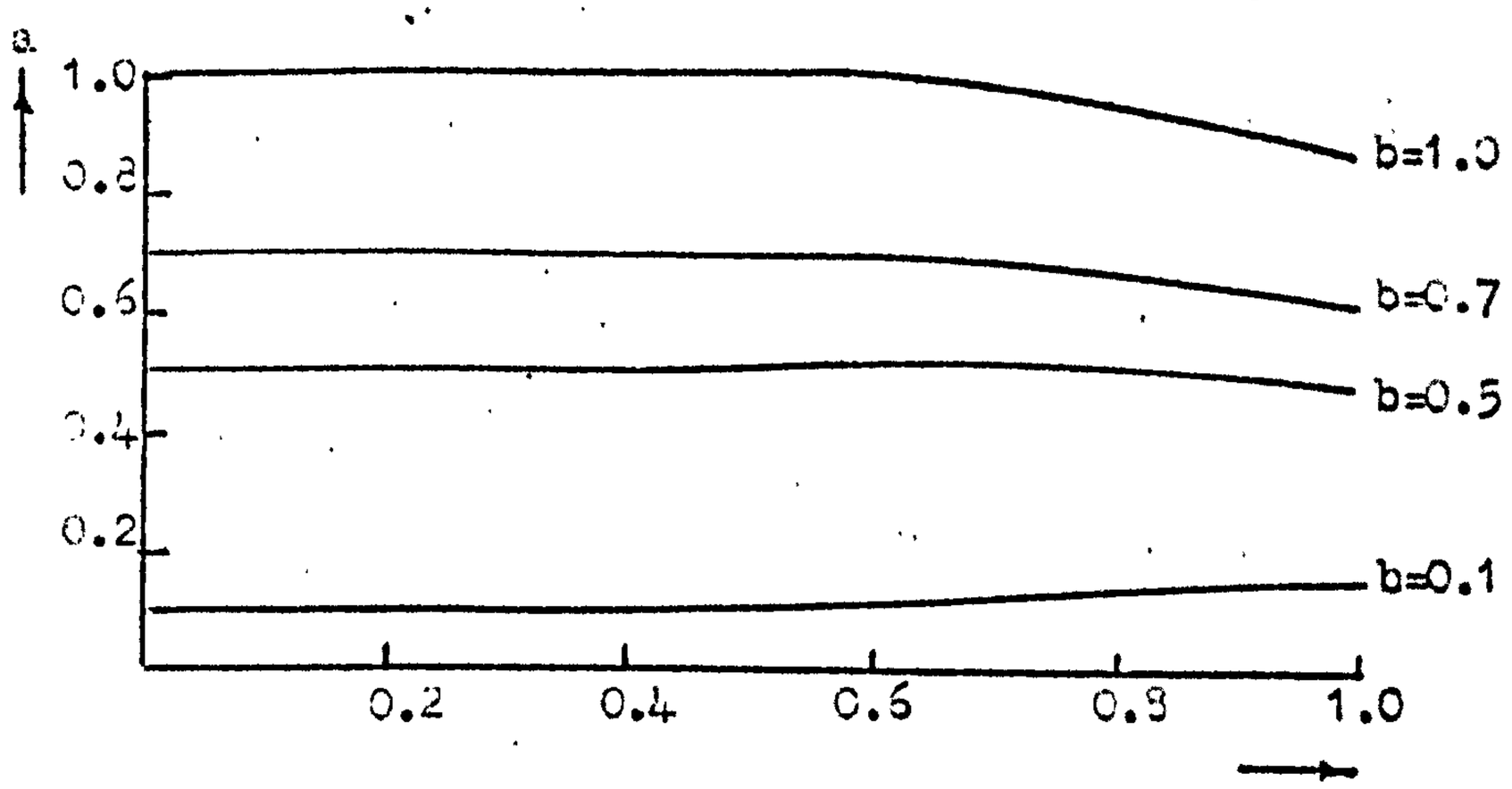

(a)

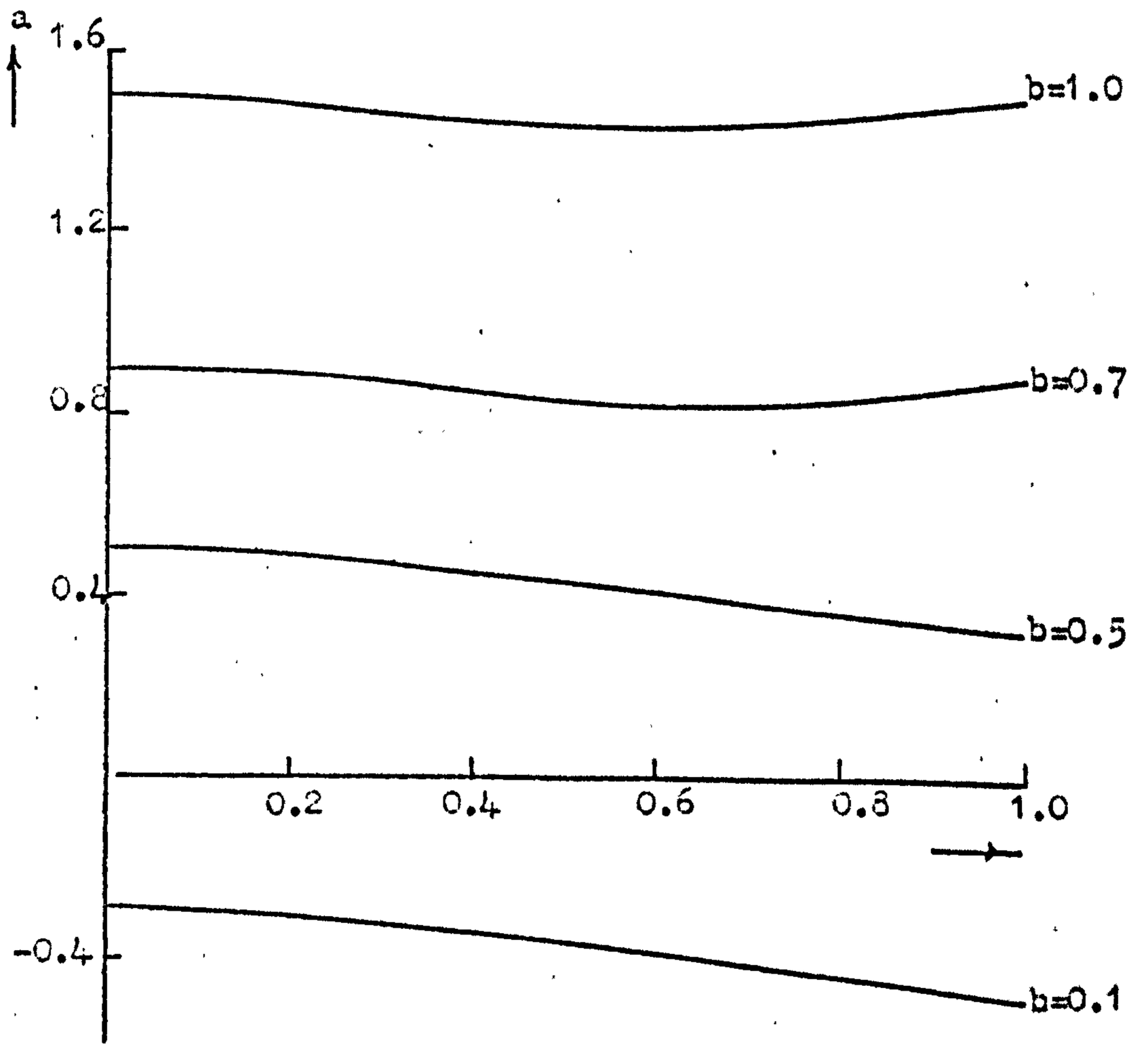

(b)

Fig. (4.6) Variation of odd lengths of transmission line with intermodal electrical length. (a) short circuits
(b) open circuits

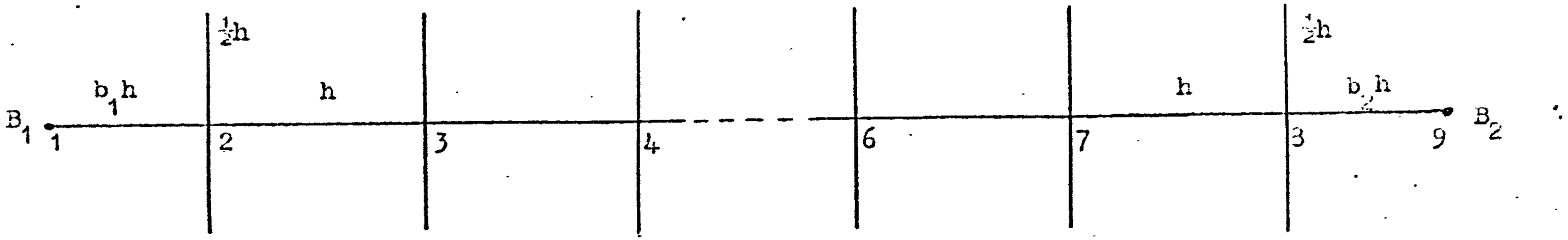

Fig. (4.7) Simulation of TE_{10} mode, with varying mesh and lengths at waveguide walls.

TABLE (4.4)

Calculation of cut-off wavelength, k_c , for varying mesh arm lengths of fig. (4.7), TE_{10} mode.

b_1	b_2	Length, L, $2(6+b_1+b_2)$	Adapted lengths a_1	Adapted lengths a_2	k_c calc.	k_c exact $= \frac{\pi}{L}$
0.5	0.5	14.0	0.5	0.5	0.2242	0.2244
0.1	0.5	13.2	0.1	0.5	0.2377	0.2380
0.7	0.5	14.4	0.7	0.5	0.2179	0.2182
1.0	0.5	15.0	1.0	0.5	0.2093	0.2094
0.5	0.1	13.2	0.5	-0.3	0.2378	0.2380
0.5	0.1	14.4	0.5	0.9	0.2179	0.2182
0.5	1.0	15.0	0.5	1.5	0.2092	0.2094

(h = 1)

Initially b_2 is held at the value of 0.5 and b_1 allowed to vary as the low frequency limit of equation (4.18), so as to examine the characteristics of a short circuit. The characteristics of the open circuit at B_2, may then be investigated by letting $b_1 = 0.5$ and b_2 vary as the low frequency limit of equation (4.20). Equations (4.18) and (4.20) thus indicate that for the simulation of a length bh of transmission line with the corresponding termination, the method of transmission line elements requires the substitution of lengths ah, in the actual procedure. The results for various values of b_1, b_2 are recorded in table (4.4) and are seen to correspond to the exact solutions, but for the velocity error, which for these frequencies is approximately 0.1%.

Increasing the length of the open circuited stubs of fig. (4.7) caused a decrease in the velocity of the wave across the matrix as was shown in chapter 3. Thus if a rectangular waveguide is simulated on a cartesian mesh of transmission lines as in fig. (4.8), such that the boundaries B_1, B_2, B_3, B_4 have associated arm lengths b_1, b_2, b_3, b_4 then for the dominant TE_{10} mode of the mesh, which represents the cross section of the waveguide of width $2(6 + b_1 + b_2)h$ and height $(4 + b_3 + b_4)h$, B_1 is a magnetic wall and B_2, B_3, B_4 are electric walls. If the lengths b_1, b_2 vary, then the previous analysis of this section enables the lengths a_1, a_2 to be substituted into the procedure so as to yield the true lengths b_1, b_2. The variation of lengths b_3, b_4, however cause the velocity of wave propagation to decrease from its nominal value of $c/\sqrt{2}$ and thus the calculated value of the cut-off wavenumber will lie between the two extremes of $c/\sqrt{2}$ and $c/\sqrt{a_3+a_4+1}$, the position depending on the number

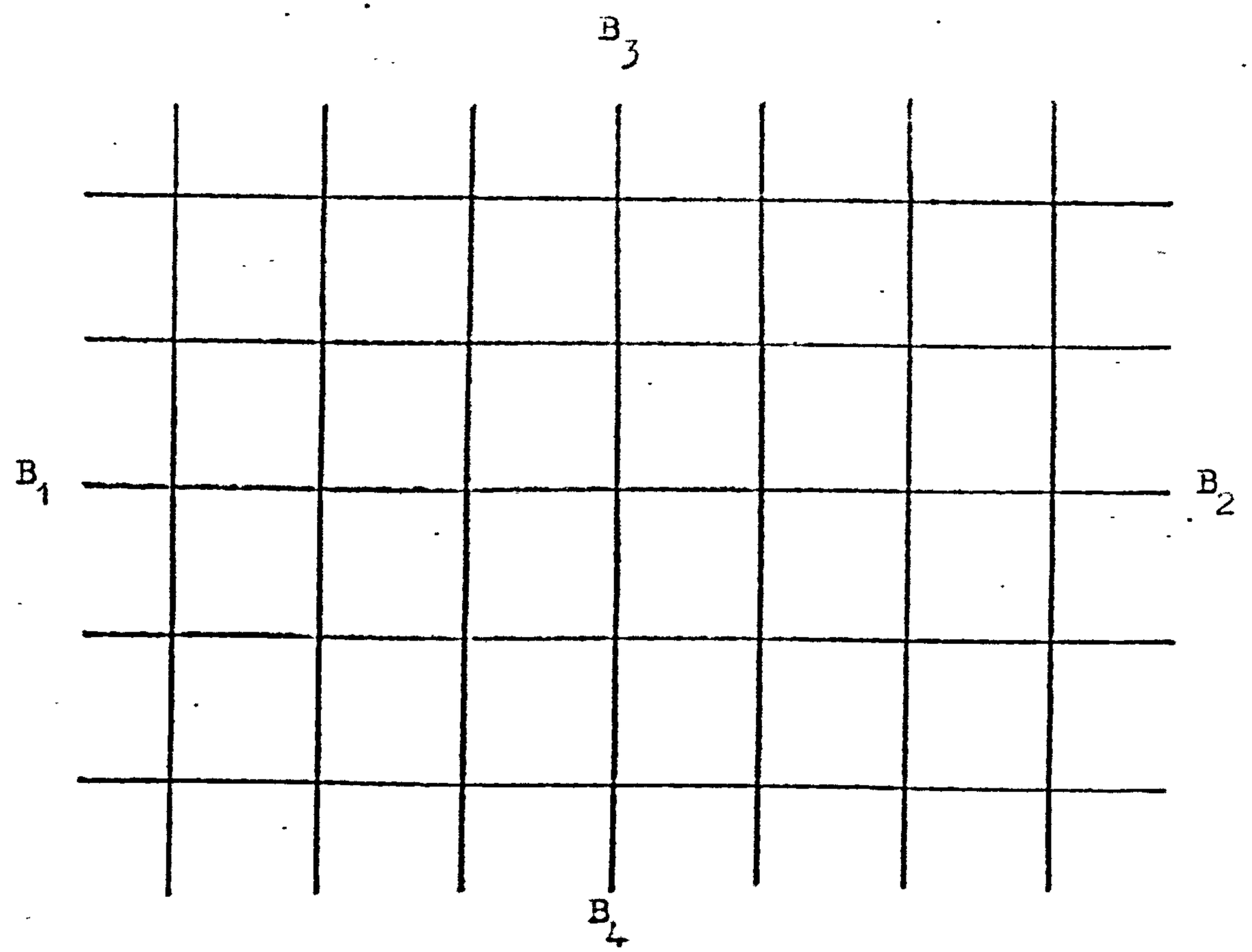

Fig. (4.8) Rectangular net of transmission lines of width $(6+b_1+b_2)$ and height $(4+b_3+b_4)$.

TABLE (4.5)

Cut-off wavelengths, k_c, for the various structures that may be represented by fig. (4.8).

b_1	b_2	b_3	b_4	Length	Width	k_c calc.	k_c exact	error %
TE_{10} mode				$2(6+b_1+b_2)$	$(4+b_3+b_4)$			
0.5	0.5	0.5	0.5	14.	5	0.2242	0.2244	0.09
1.0	0.75	0.5	0.5	15.5	5	0.2024	0.2027	0.15
0.5	0.5	0.75	0.75	14.	5.5	0.2135	0.2244	4.86
1.0	0.75	0.75	0.75	15.5	5.5	0.1936	0.2027	4.49
TE_{11} mode				$6+b_1+b_2$	$4+b_3+b_4$			
0.5	0.5	0.5	0.5	7	5	0.7712	0.7721	0.12
0.75	0.75	0.5	0.5	7.5	5	0.7149	0.7551	5.33
0.5	0.5	0.75	0.75	7	5.5	0.6992	0.7264	3.75
0.75	0.75	0.75	0.75	7.5	5.5	0.6575	0.7083	7.18
TM_{11} mode				$6+b_1+b_2$	$4+b_3+b_4$			
0.5	0.5	0.5	0.5	7	5	0.7706	0.7721	0.19
1.0	1.0	0.5	0.5	8	5	0.7388	0.7409	0.28
0.5	0.5	1.0	1.0	7	6	0.6889	0.6896	0.10
1.0	1.0	1.0	1.0	8	6	0.6583	0.6545	0.58
TE_{11} / TM_{11} modes				$2(6+b_1+b_2)$	$2(4+b_3+b_4)$			
0.5	0.5	0.5	0.5	14	10	0.3854	0.3861	0.18
0.75	1.0	0.5	0.5	15.5	10	0.3639	0.3739	2.67
0.5	0.5	1.0	0.75	14	11.5	0.3478	0.3535	1.63
0.75	1.0	1.0	0.75	15.5	11.5	0.3280	0.3402	3.59
0.5	1.0	1.0	0.5	15	11	0.3538	0.3542	0.09
0.75	0.5	0.5	0.75	14.5	10.5	0.3551	0.3694	3.87

(h = 1)

of 'regular' nodes, i.e. those surrounded by equal arm lengths, compared with that of the irregular nodes. Analysis was performed over the mesh of fig. (4.8) for the TE_{10} mode and the results tabulated in Table (4.5), solving for the cut-off wavenumber, k_c, of the structure. It can be seen that for the corrections in the odd length of transmission line in the direction that the wave travels over the network, the corrections are again valid, but for corrections to the odd lengths perpendicular to the direction of the relevant wave, the effect is to reduce the velocity of the wave from its nominal value of $c/\sqrt{2}$ and thus the medium which the network simulates is no longer isotropic.

The TE_{11} and TM_{11} modes are also solved for by allowing B_1, B_2, B_3, B_4 to become open circuits in the former case and short circuits in the latter, such that the waveguides dimensions were $(6 + b_1 + b_2)h$ wide and $(4 + b_3 + b_4)h$ deep, thus examining the effect of the short and open circuit terminations of the odd length of line on the characteristics of a diagonally or near diagonally propagating wave on the network. The results are noted again in Table (4.5) and indicate that the corrections afforded by the short circuit terminations (TM_{11} modes) present reliable and accurate solutions, whilst those for the open circuit terminations (TE_{11} modes) yield solutions which in all cases possess a greater error than the corresponding short circuit terminations.

Finally the TE_{11} and TM_{11} modes were solved on the network of fig. (4.8) with B_1, and B_4 open circuited and B_2 and B_3 short circuited, simulating a waveguide of width $2(6 + b_1 + b_2)h$ and depth $2(4 + b_3 + b_4)h$ and the solutions once again recorded in Table (4.5).

This particular analysis was performed such that the frequency at which the network was operated caused the effective odd lengths to possess an improved approximation to the low frequency limits of equations (4.18) and (4.20). The solutions although presenting less error, indicate the trends discussed previously.

The relatively large errors inherent in the structures involving open circuit terminations must therefore be attributed to the more rapid variation with frequency of the apparent electrical length of the odd length of transmission line at the boundary, which is greater for open circuit terminations than the short circuit terminations, fig. (4.6)which was noticeable even for low frequencies.

4.3. CIRCULAR AND ELLIPTICAL WAVEGUIDES.

Since most of the modes that propagate in a circular or elliptical waveguide are necessarily symmetrical about some line drawn through the cross-section, only a quadrant of each structure was analysed as in figs. (4.9) and (4.10), which show the relevant quadrants imprinted on a cartesian mesh. The odd lengths of transmission line formed by the intersection of the perimeter of the structure with the square mesh, are accounted for by altering the relevant electrical lengths between a boundary adjacent node and the actual perimeter according to the low frequency limit of equations (4.18) and (4.20). Considering the node i, in fig. (4.9), the physical length between the node and the perimeter is 0.0707h measured along either mesh direction, thus for TM type modes where the boundary is simulated by short circuits the electrical length of this odd length of transmission line is 0.0707θ. For TE mode types the boundary is simulated by open circuits and thus the low frequency electrical length of the odd length of transmission line becomes -0.3586θ from equation (4.20).

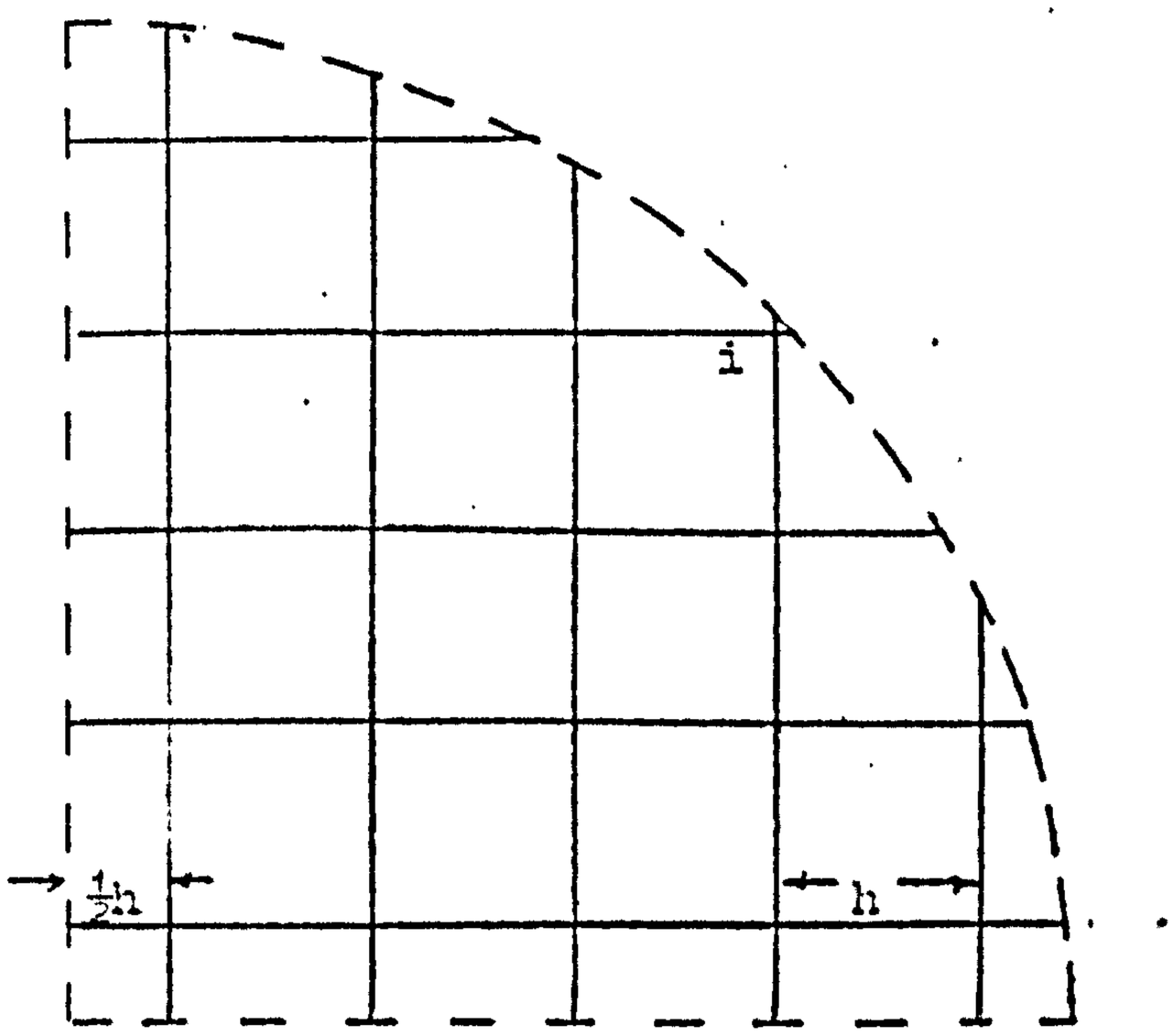

Fig. (4.9) Cartesian mesh describing quadrant of circle.

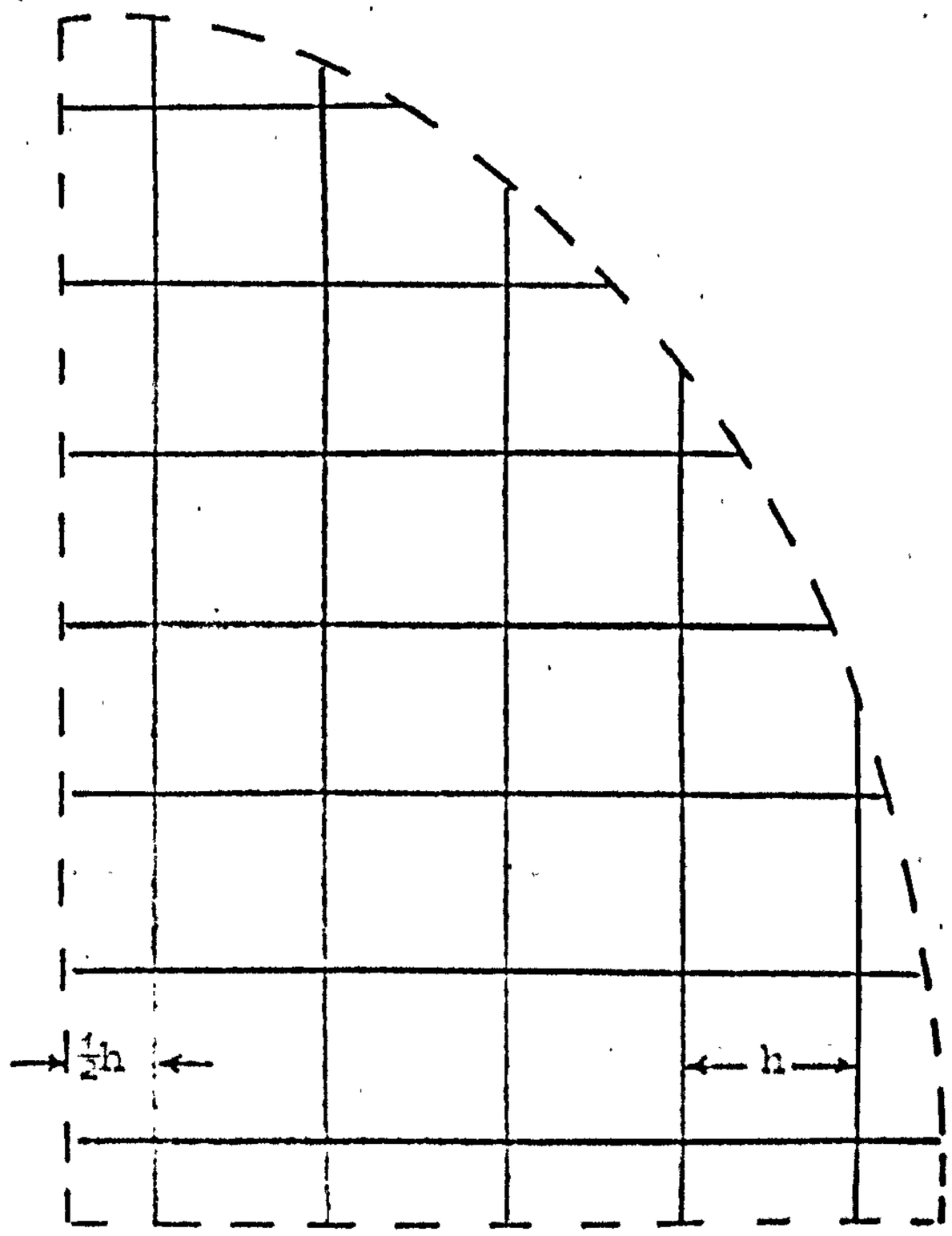

Fig. (4.10) Cartesian mesh describing quadrant of ellipse.

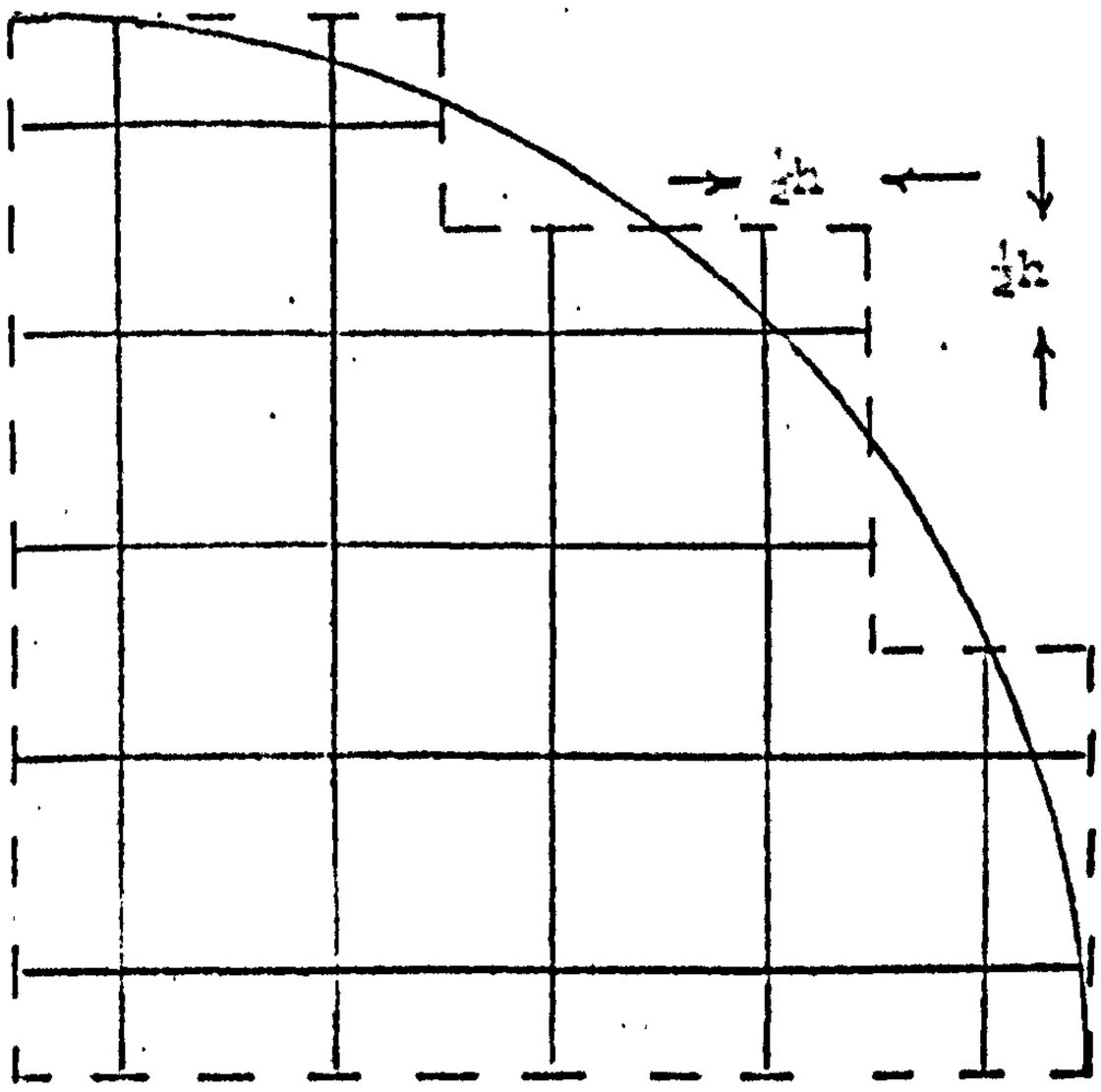

Fig. (4.11) Approximation of quadrant of circular guide by a strictly periodic network of transmission lines.

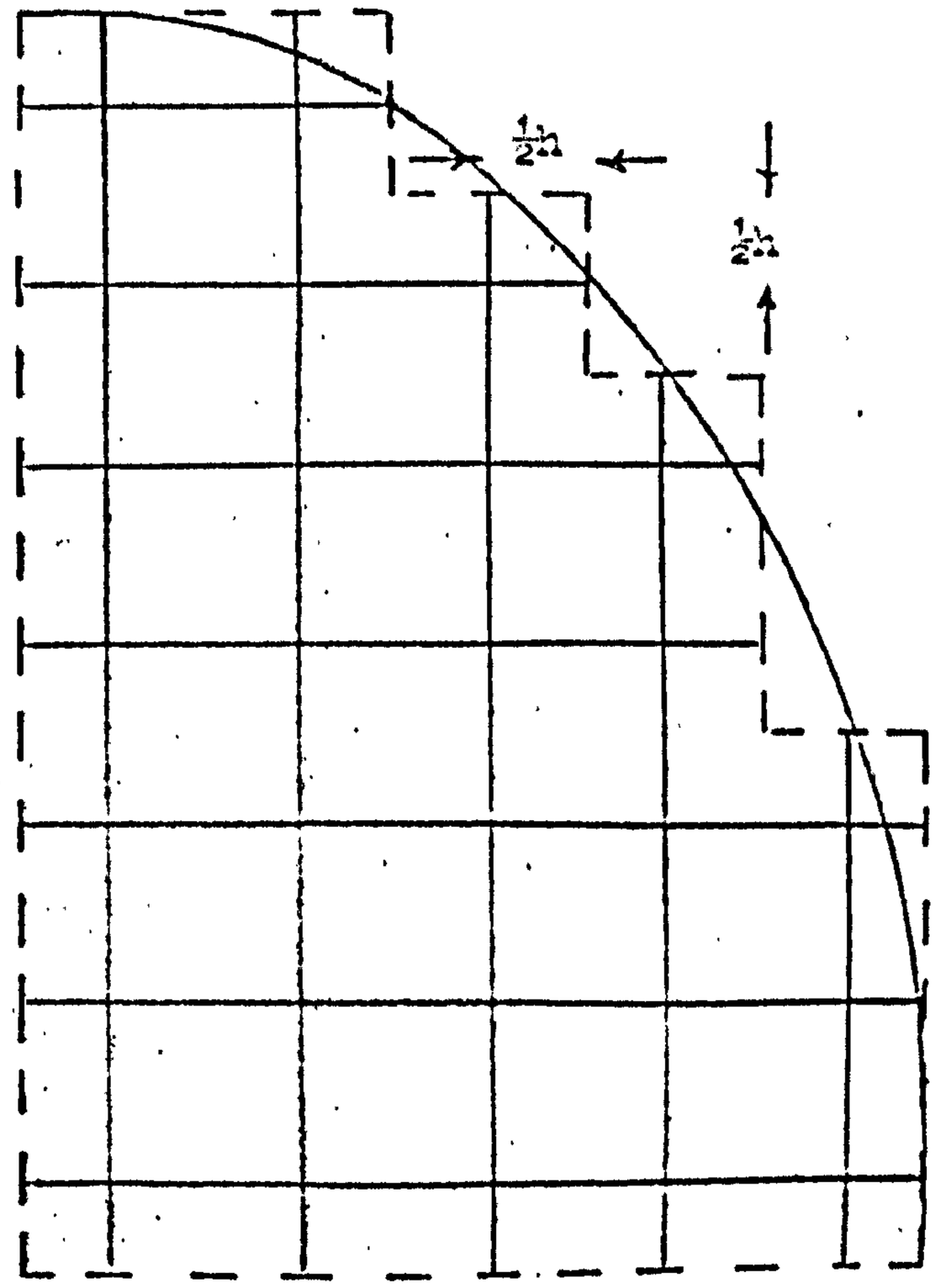

Fig. (4.12) Approximation of quadrant of elliptical guide by a strictly periodic network of transmission lines.

TABLE (4.6)

Cut-off wavelengths ($a/\lambda c$) of circular waveguide defined by figs. (4.9) and (4.11) of radius 5h.

Mode	$a/\lambda c$ anal:	$a/\lambda c$ (Uncorr: ends)	Error %	$a/\lambda c$ (Corr: ends)	Error %	Maximum velocity error %
TM_{01}	0.3828	0.3815	0.34	0.3811	0.44	0.49
TM_{11}	0.6099	0.6072	0.44	0.6048	0.83	1.28
TM_{21}	0.8174	0.8164	0.12	0.8117	0.69	2.41
TM_{02}	0.8785	0.8667	1.34	0.8699	0.98	2.84
TM_{12}	1.1166	1.0978	1.68	1.0946	1.97	4.97
TM_{22}	1.3396	1.3203	1.44	1.3193	1.52	8.06
TE_{11}	0.2930	0.2827	3.52	0.2884	1.56	0.26
TE_{21}	0.4861	0.4637	4.61	0.4765	1.97	0.8
TE_{01}	0.6099	0.5977	2.00	0.6012	1.42	1.28
TE_{12}	0.8485	0.8130	4.18	0.8406	0.93	2.63
TE_{22}	1.0673	1.0313	3.37	1.0524	1.40	4.47
TE_{02}	1.1166	1.0610	4.98	1.0845	2.87	4.97

(h = 1)

The method was applied to the quadrant of the circle in fig. (4.9) of radius 5h, with and without the corrections for the odd lengths. The model used for analysis without the odd length corrections is depicted in fig. (4.11), where the circular perimeter is approximated by a strictly periodic network. Table (4.6) shows the results for the cut-off wavelengths for several TE and TM modes after a maximum of 100 orders of reflections had been considered.

Waveguides of elliptical cross section were first investigated by Chu[42] in 1938. Several investigations followed this, notably by Kretzschmar[43]. The main difficulty of such analysis was the difficulty of numerically computing the Matthieu functions describing the electromagnetic fields within the elliptical structure, due to the slow convergence of the series representing the functions. Kretzschmar used a Bessel function product series approximation to find the 19 lowest order modes for a hollow conducting elliptical waveguide and together with Davies[44] analysed the problem using polygon approximations to the cross section which did not need reference to Matthieu functions.

The method of steady state transmission line elements was applied to a quadrant of an elliptical waveguide such as that of fig. (4.10) using to full advantage the lines of symmetry that exist within the cross section for the particular mode. An identical approach to that for the circular problem was adopted, where the odd lengths of transmission lines formed by the intersection of the perimeter of the ellipse with the rectangular mesh of transmission lines were easily calculated and directly substituted into the method for the TM mode cases, and corrected in the case for TE mode cases. The cut-off wavelengths for several modes are recorded in Table (4.7) for an ellipse of semi-

major and semi-minor axes 7h, 5h respectively, i.e. of eccentricity 0.6999. Comparison was again made between the corrected and uncorrected configurations of figs. (4.10) and (4.12). The number of reflections considered was 100 and the analytical answers supplied by Kretzschmar[43].

The results again indicate the general reliability of the method of solving waveguides of an arbitrary cross section. The comparison between the corrected and uncorrected odd length solutions for both the circular and elliptical problems show that generally the corrected length solutions are approximately twice as accurate as the uncorrected length solutions, with the TE modes possessing relatively larger errors than the TM modes, and again must be attributed to the relatively large frequency variation of the odd lengths of line to the conducting boundary of the structure. The finite difference/element solutions of the same circular configuration[4,9,22] indicate that the method employed in this section is more accurate for a similar spatial discretization, and the difference in accuracies between the two techniques become more pronounced as the higher ordered mode solutions are sought. The finite difference results for the elliptical waveguide[4] again confirm the accuracy of utilising the approximations of the finite transmission line elements.

TABLE (4.7)

Cut-off wavelengths ($a/\lambda c$) of elliptical waveguide modes defined by figs. (4.10) and (4.12) of semi major axis a, eccentricity 0.6999.

Mode	$a/\lambda c$ anal:	$a/\lambda c$ (Uncorr: ends)	Error %	$a/\lambda c$ (Corr: ends)	Error %	Maximum velocity error %
TM_{01} (even)	0.4650	0.4588	1.33	0.4646	0.08	0.37
TM_{11} (even)	0.6776	0.6745	0.45	0.6792	-0.24	0.80
TM_{11} (odd)	0.7986	0.7790	2.46	0.7919	0.84	1.12
TE_{11} (even)	0,2962	0.2861	3.41	0.2914	1.61	0.15
TE_{11} (odd)	0.4039	0.3877	4.00	0.3966	1.81	0.27
TE_{01} (even)	0.7798	0.7492	3.92	0.7629	2.17	1.06

(h = 1)

4. 3. 1. Cylindrical coordinate representation of circular waveguide.

The fact that the TM_{on}, TE_{on} circular mode field components possess a zero angular dependence, directly implies that these modes may be solved in one dimension at cut-off. However, application of the previous models used to simulate one dimensional propagation, would be insufficient since it is known that these only represent the TE_{no} modes in a rectangular guide at cut-off. Thus the model has to be adapted so as to account for the differing propagating characteristics. The cross section of a circular waveguide superimposed on a cylindrical coordinate system is shown in fig. (4.13). Following the conventional steady state finite transmission line element theory, a two dimensional mesh of open two wire transmission lines are considered in polar coordinates, as in fig. (4.13), and each node in the mesh corresponds to a junction between a pair of transmission lines. The elementary section of each line between two nodes is represented by lumped capacitances and inductances. If L and C are the inductance and capacitance per unit length respectively, as before, then the junction between a pair of lines at a mesh node can be represented by fig. (4.14). The following basic transmission line equations then apply

$$\frac{\partial I_r}{\partial r} + \frac{1}{r}\frac{\partial I_\alpha}{\partial \alpha} = -C\frac{\partial V}{\partial t}$$

$$\frac{\partial V}{\partial r} = -L\frac{\partial I_r}{\partial t} \qquad (4.21)$$

$$\frac{1}{r}\frac{\partial V}{\partial \alpha} = -L\frac{\partial I_\alpha}{\partial t}$$

whilst Maxwells field equations in cylindrical coordinates at cut-off resolve into two independent groups, viz.

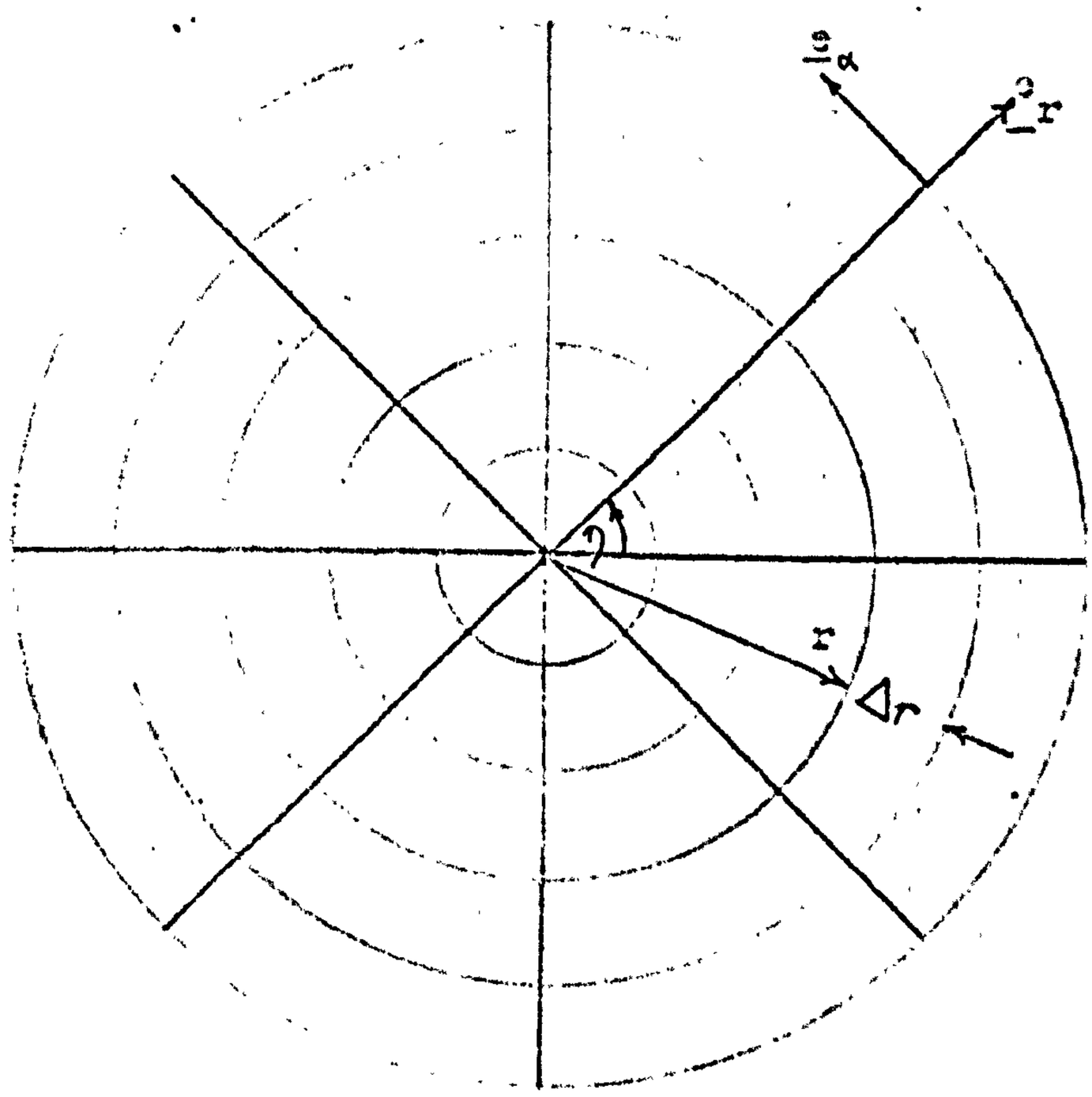

Fig. (4.13) Cross-section of circular waveguide, modelled by cylindrical mesh of transmission lines.

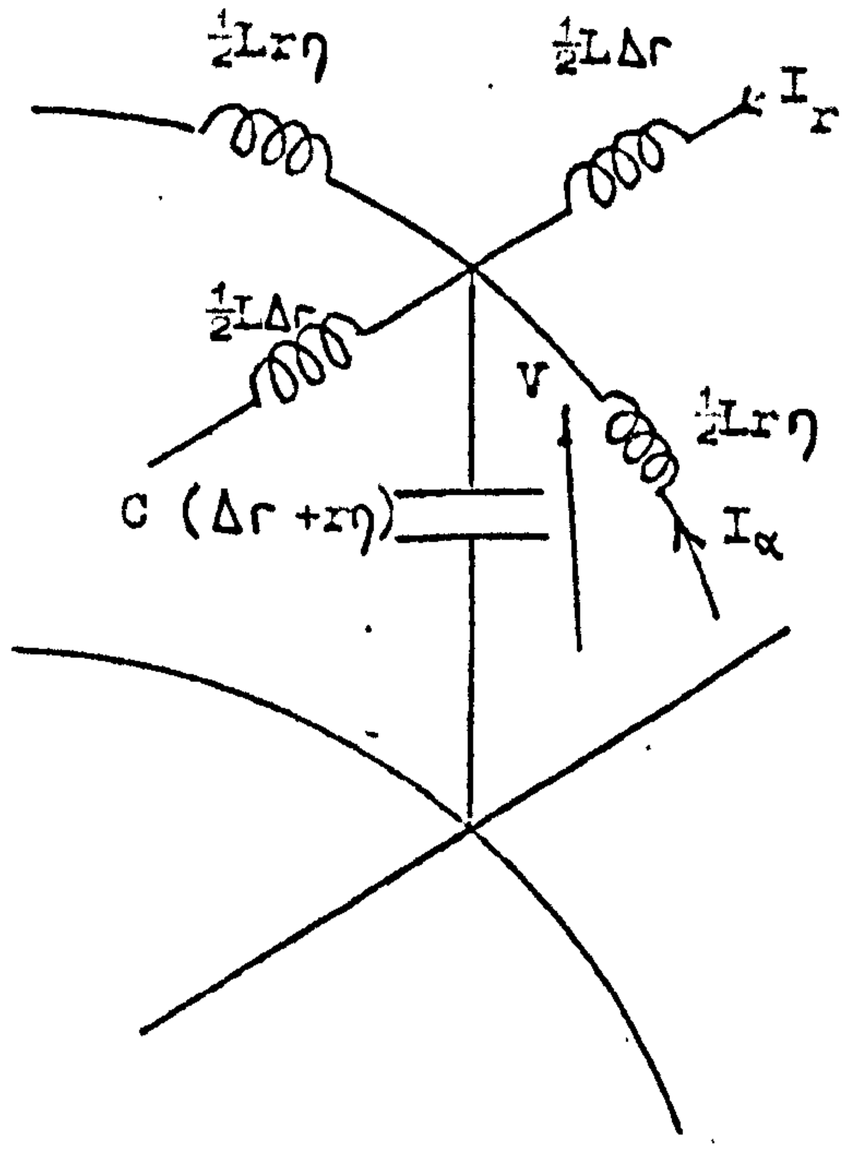

Fig. (4.14) Intersection of two transmission lines at a typical node of fig. (4.13).

Those for TM modes

$$\frac{1}{r}\frac{\partial(rH_\alpha)}{\partial r} - \frac{1}{r}\frac{\partial H_r}{\partial \alpha} = \epsilon_o \frac{\partial E_z}{\partial t}$$

$$-\frac{\partial E_z}{\partial r} = -\mu_o \frac{\partial H_\alpha}{\partial t} \qquad (4.22)$$

$$\frac{1}{r}\frac{\partial E_z}{\partial \alpha} = -\mu_o \frac{\partial H_r}{\partial t}$$

and those for TE modes

$$\frac{1}{r}\frac{\partial(rE_\alpha)}{\partial r} - \frac{1}{r}\frac{\partial E_r}{\partial \alpha} = -\mu_o \frac{\partial H_z}{\partial t}$$

$$-\frac{\partial H_z}{\partial r} = \epsilon_o \frac{\partial E_\alpha}{\partial t} \qquad (4.23)$$

$$\frac{1}{r}\frac{\partial H_z}{\partial \alpha} = \epsilon_o \frac{\partial E_r}{\partial t}$$

Thus for TM modes the identities between equations (4.21) and (4.22)

$$E_z \equiv V \;;\quad rH_\alpha \equiv -I_r \;;\quad rH_r \equiv I_\alpha \;;\quad C \equiv r\epsilon_o;\quad L \equiv \frac{\mu_o}{r}$$

specifies the cut-off frequencies of the circular waveguide. The speed at which the wave travels along each elemental section of transmission line is still $1/\sqrt{LC} = c$, but the intrinsic impedance, Z_o, of the transmission must vary as

$$Z_o = \sqrt{\frac{L}{C}} \propto \frac{1}{r} \qquad (4.24)$$

Similarly for the TE modes, the identities between equations (4.21) and (4.23) yield

$$H_z \equiv V \;;\quad rE_\alpha \equiv I_r \;;\quad rE_r \equiv -I_\alpha \;;\quad C \equiv r\mu_o;\quad L \equiv \frac{\epsilon_o}{r}$$

Again the wave travels along each elemental section at velocity c and the intrinsic impedance is also given by equation (4.24).

The model for one dimensional propagation may thus be approximated by fig. (4.15) which shows a single transmission line periodically loaded with open circuited stubs. Note that the stubs lie in the direction of the angular variation and can be of arbitrary length since the field variation in this direction is zero, but were taken as h/2 so as to allow the wave to travel over the matrix at a velocity $c/\sqrt{2}$. The transmission line however is non-uniform and consists of a series of transmission lines electrically connected (shown by the broken lines) whose intrinsic impedances Z_o, vary inversely with the distance r of the defining node, from the end A representing the centre of the guide. Since the transmission line is non-uniform reflection and transmission coefficients have to be introduced at each section of uniform transmission line. At a node i in fig. (4.15), the distance from end A of the transmission line corresponding to the radial length in the waveguide, is $(2i - 3)h/2$ and this section of line of which node i is part possesses an intrinsic impedance of $Z_{o,i} = 2/(2i - 3)h$. For voltages on the network, the transmission coefficient $t_{i-1,i}$ for a wave travelling from node $i - 1$ to node i is given by

$$t_{i-1,i} = \frac{2 Z_{o,i}}{Z_{o,i-1} + Z_{o,i}} = \frac{2i - 5}{2i - 4} \qquad (4.25)$$

whilst the reflection coefficient $r_{i,i-1}$ for a wave travelling from node i to node $i - 1$ is

$$r_{i,i-1} = \frac{Z_{o,i-1} - Z_{o,i}}{Z_{o,i-1} + Z_{o,i}} = \frac{1}{2i - 4} \qquad (4.26)$$

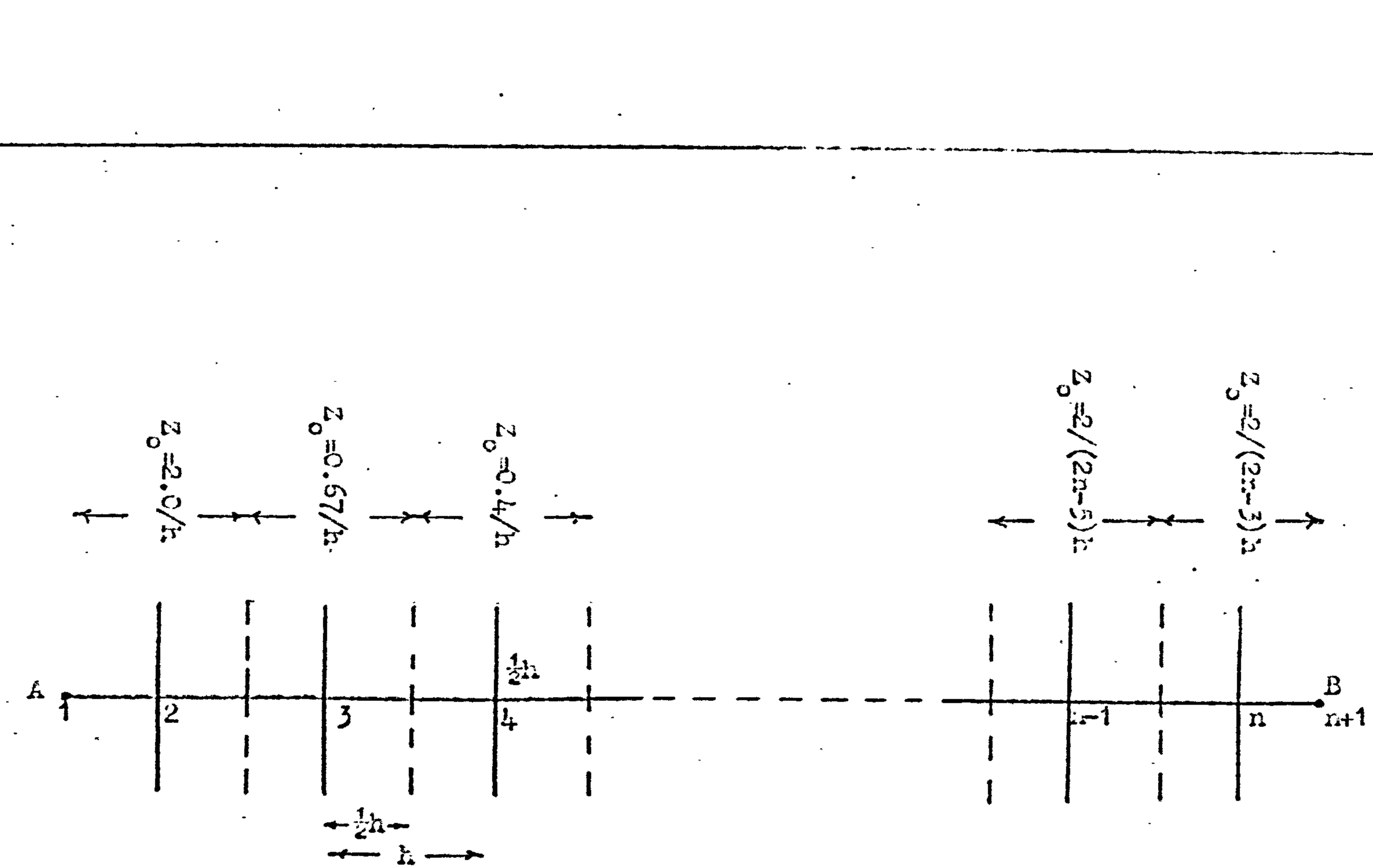

Fig. (4.15) Non-uniform stub loaded transmission line used to analyse TE'_{on}, TM'_{on} circular waveguide modes.

Similarly for waves at the junction of the transmission lines corresponding to nodes i and i + 1

$$t_{i+1,i} = \frac{2i - 1}{2i - 2} \quad ; \quad r_{i,i+1} = \frac{-1}{2i-2} \qquad (4.27)$$

Thus to analyse the configuration by the steady state transmission line element method, the passage of multiple reflected waves along the non-uniform transmission line must account for the discontinuity in intrinsic impedance between each node according to the transmission and reflection coefficients derived above.

The cut-off wave lengths for the three lowest ordered TM modes that propagate on this structure were solved for, by this method after 300 orders of reflection had been considered. The structure analysed, as in fig. (4.15) was defined by n = 20, h = 1, and A represented an open circuit and B a short circuit. The results are tabulated in Table (4.8). Also solved, were the cut-off wavelengths of the three lowest TE modes on the same model, but A and B now both becoming open circuits, these results are also recorded in Table (4.8).

Since the TE_{on}, TM_{on} circular modes are essentially modes possessing field variations in only two dimensions viz. radially and axially, the analysis described above may be extended to describe the fields and propagation parameters of these modes in a cavity of circular cross-section. The transmission lines may then form a rectangular cartesian mesh (r,z) and the basic transmission line equations become

$$\frac{\partial I_r}{\partial r} + \frac{\partial I_z}{\partial z} = -C \frac{\partial V}{\partial t}$$

$$\frac{\partial V}{\partial r} = -L \frac{\partial I_r}{\partial t} \qquad (4.28)$$

$$\frac{\partial V}{\partial z} = -L \frac{\partial I_z}{\partial t}$$

TABLE (4.8)

Cut-off wavelengths ($a/\lambda c$), for the circular TE_{on}, TM_{on} modes, modelled by the network of fig. (4.15).

Mode	$a/\lambda c$ anal:	$a/\lambda c$ numerical	Error %	Maximum velocity error %
$V \propto E_z$				
TM_{01}	0.3828	0.3817	0.28	0.03
TM_{02}	0.8785	0.8741	0.50	0.18
TM_{03}	1.3773	1.3655	0.86	0.43
$V \propto H_z$				
TE_{01}	0.6099	0.6068	0.49	0.09
TE_{02}	1.1166	1.1076	0.80	0.29
TE_{03}	1.6192	1.6011	1.11	0.61
$V \propto E_\alpha$				
TE_{01}	0.6099	0.6068	0.49	0.09
TE_{02}	1.1166	1.1087	0.71	0.29
TE_{03}	1.6192	1.6001	1.18	0.61

$n = 20, \quad h = 1 \quad$ i.e. $\quad a = 19$

whilst Maxwells field equations for TE modes with zero angular variation, $\frac{\partial}{\partial \alpha} = 0$ of field become

$$\frac{\partial H_r}{\partial z} - \frac{\partial H_z}{\partial r} = \epsilon_o \frac{\partial E_\alpha}{\partial t}$$

$$-\frac{\partial E_\alpha}{\partial z} = -\mu_o \frac{\partial H_r}{\partial t} \qquad (4.29)$$

$$\frac{1}{r}\frac{\partial (rE_\alpha)}{\partial r} = -\mu_o \frac{\partial H_z}{\partial t}$$

and the identities between the voltages and currents on the network and the field components within the cavity become

$$V \equiv rE_\alpha \; ; \quad I_r \equiv H_z \; ; \quad I_z \equiv -H_r \; ; \quad C \equiv \frac{\epsilon_o}{r} \; ; \quad L \equiv r\mu_o$$

The wave velocity of each elemental section remains at c, but the intrinsic impedance of the section must vary as

$$Z_o = \sqrt{\frac{L}{C}} \quad \propto \quad r$$

If a similar network to that of fig. (4.15), i.e. a non-uniform stub loaded transmission line, is used here with certain modifications, then the cut-off wave lengths of the TE_{on} circular modes may again be calculated. In this case however the voltage on the network becomes proportional to the electric field in the angular direction, and the intrinsic impedance of the elemental sections become proportional to the radial distance from the centre of the cavity. At a node i, therefore the intrinsic impedance $Z_{o,i}$ equals $(2i - 3)\, h/2$ and the transmission and reflection coefficients in the radial direction become

$$t_{i-1,i} = \frac{2i-3}{2i-4} \; ; \qquad r_{i,i-1} = \frac{-1}{2i-4}$$

$$t_{i+1,i} = \frac{2i-3}{2i-2} \; ; \qquad r_{i,i+1} = \frac{1}{2i-2}$$

The cut-off wave lengths of the three lowest TE_{on} circular modes were again calculated, but here both ends of the transmission line are terminated in short circuits, since this is where the electric field component (represented by the network's voltage) is zero. These results are again tabulated in Table (4.8) for the same physically sized structure as previously examined.

Although the analysis was again performed for the one dimensional TE_{on} modes, the method can obviously solve the TM_{on} modes and can be extended as already noted, into two dimensions by considering a two dimensional rectangular mesh of transmission lines so as to calculate the parameters for such modes within a cavity.

4.3.2. Circular and Elliptical waveguides - Conclusions.

This section has shown the manner in which the odd-lengths of transmission line joining a short circuit or open circuit termination to a periodic or regular network of such lines, have their electrical lengths corrected, especially for the case of open circuits. It was concluded that the short circuit terminations of odd lengths could be used successfully, but that open circuit terminations produced slight inconsistencies. This was attributed to the more rapid variation with frequency of the apparent electrical length of the odd length of transmission line at the boundary which is greater for open circuit terminations.

The results for the circular and elliptical waveguides were accurate and well within the maximum velocity errors for TM mode configurations when the odd length correction procedure was utilised, Tables (4.6), (4.7). The TE mode confidurations possess relatively

large errors, as expected, due to the open circuit terminations of the transmission lines describing the perimeter of the waveguide, and also the fact that although it was arranged for the derivatives of the field components H_z in the coordinate directions $\frac{\partial}{\partial x}$, $\frac{\partial}{\partial y}$ to be zero at the boundary it did not imply that the derivative of H_z normal to the boundary was also zero.

A slight inaccuracy that must have been present is that of using a circular internodal function to describe a Bessel function distribution (in the radial direction) in the circular waveguide and a Matthieu function distribution in the elliptical waveguide, and thus the result for these geometries, and any other non-rectangular geometry depends solely on mesh coarseness and increasing the number of nodes increases the accuracy. However the finite difference/ element methods suffer in an identical manner, but to a worse degree, since in their elementary form only utilise a linear internodal function, and hence must increase the number of nodes defining the configuration to produce the accuracy shown by this method.

The one dimensional model of the circular waveguide utilised to analyse the TE_{on}, TM_{on} modes, was shown to be represented by a transmission line consisting of sections of uniform transmission lines, each of which possessed a characteristic impedance depending on its radial distance from the end of the line representing the centre of the guide. Such a discretization provided inaccuracies for a low number of nodes defining the radius, and is caused by the relatively crude approximation of a Bessel function by a sinusoid and that the number of impedance 'shells' is not sufficient to adequately describe the variation

of characteristic impedance. The results of Table (4.8) show, however, that for 21 nodes defining the one dimensional model of fig. (4.15), the description of the problem is accurate. Comparison between the two error columns in Table (4.8) also show that as the mode order is increased, the error produced by the method tends to that of the maximum velocity error. This is due to the number of radial variations of the field, when the Bessel function becomes increasingly similar to a simusoid.

The full cylindrical co-ordinate representation of the cross section of the circular guide, fig. (4.13), could be utilised to solve for the various circular modes, but the one dimensional analysis has shown that the number of nodes has to be increased vastly to obtain a reasonable accuracy because of the necessary description of impedance variation. Further the transmission lines in the angular direction increase with radius, producing a shunt capacitance, increasing with radial distance of each elemental section of transmission line, fig. (4.14). This has the effect of reducing the velocity of the wave as it spreads out from the centre of the guide. To eliminate this effect, the electrical length between adjacent nodes in the radial direction can be arranged to decrease with radius and thus maintain the velocity of the propagating wave on the network at a nominal value. Care must also be taken at the centre of the network, where more than four transmission lines intersect and reflection and transmission coefficients have to be introduced, differing from the accustomed $-\frac{1}{2}$, $\frac{1}{2}$ used throughout the steady state transmission line element method. The development of the cylindrical co-ordinate representation of the

transmission line network was not pursued,partially because of the difficulties envisaged above, the results using a cartesian mesh were acceptable, and the representation could only be used for wave guides of circular cross-section, i.e. it becomes a one-off procedure. However, noting the previous comments, this could well become an interesting, worthwhile topic of research.

The comments made on velocity and truncation errors in section (4.1.4) also apply to the examples of this section. The truncation error is likely to resemble the transient case[41] more in these examples however, because the electrical length between nodes is the same. It is only the lengths between nodes and the boundaries of the circular or elliptical waveguides that give rise to deviations from the transient approach. It is however the purpose of such analysis in this section to compute the cut-off wavelengths of the various modes such that an increase in reflections does not cause any deviation in computed results and thus eliminating truncation error.

CHAPTER 5.

THE ANALYSIS OF NON-RECTANGULAR GEOMETRIES USING THE TRANSIENT APPROACH OF THE TRANSMISSION LINE ELEMENT METHOD.

The development of the steady state finite transmission line element from the finite difference/element methods has been shown to be extremely capable of solving several classes of waveguide problems, by considering the backward and forward reflected waves that occur on a rectangular mesh of intersecting transmission lines. Account is taken of these reflections by considering the electrical length between such intersections and assuming that the field is in effect sinusoidal in space. Vectorial addition of these individual waves at each intersection thus tends to provide the voltage or current distribution across the network simulating the fields within a waveguide.

Transient analysis of waveguide structures using transmission line network have been recently reported,[41,45,46] and although subtly different, possesses certain advantages and disadvantages over the steady state method. Basically the transient approach utilises the same network and elemental sections as in the previous chapters, but instead of being sinusoidally excited with a signal of fixed frequency, the mesh is excited at a mesh intersection or a series of intersections by a delta function impulse, and the output at an observation point observed solely in the time domain.

5. 1. THE MECHANICS OF THE TRANSIENT APPROACH.

An identical regular cartesian mesh of TEM transmission lines to that used before for the simulation of a rectangular waveguide, fig. (3.12) together with the corresponding identities between the current and voltages on the network with field components within the waveguide still exists. The mesh is excited by delta function impulses at a source point in the mesh, and the progress of the impulses followed as they propagate throughout the network. The field distribution is now represented at each node by four numbers describing the magnitude of the incident voltages along the four coordinate directions. Thus if the voltage impulses incident on a node at a time k are represented by

$$ {}_kV_1^i \;,\quad {}_kV_2^i \;,\quad {}_kV_3^i \;,\quad {}_kV_4^i $$

with reference to fig. (3.9), then at time k + 1 they become reflected pulses

$$ {}_{k+1}V_1^r,\ {}_{k+1}V_2^r \;,\quad {}_{k+1}V_3^r \;,\quad {}_{k+1}V_4^r $$

where

$$ {}_{k+1}\begin{bmatrix} V_1 \\ V_2 \\ V_3 \\ V_4 \end{bmatrix}^r = \tfrac{1}{2} \begin{bmatrix} -1 & 1 & 1 & 1 \\ 1 & -1 & 1 & 1 \\ 1 & 1 & -1 & 1 \\ 1 & 1 & 1 & -1 \end{bmatrix} {}_k\begin{bmatrix} V_1 \\ V_2 \\ V_3 \\ V_4 \end{bmatrix}^i \qquad (5.1.) $$

and also since pulses reflected from one junction become incident on neighbouring junctions.

$$
\begin{aligned}
{}_{k+1}V_1^i\,(x,y) &= {}_{k+1}V_3^r\,(x+1,\,y)\\
{}_{k+1}V_2^i\,(x,y) &= {}_{k+1}V_4^r\,(x,\,y-1)\\
{}_{k+1}V_3^i\,(x,y) &= {}_{k+1}V_1^r\,(x-1,\,y)\\
{}_{k+1}V_4^i\,(x,y) &= {}_{k+1}V_2^r\,(x,\,y+1)
\end{aligned}
\qquad (5.2)
$$

Thus the successive application of equations (5.1) and (5.2) calculates the amplitude of the individual impulses at each node in the mesh at successive intervals of time h/c, where h is the mesh pitch and c the velocity of light in free space. Note now the similarity between equations (5.1), (5.2) and (3.17) (3.18) but the elasticity of having a variable mesh pitch across the network is lost and the structure must be strictly periodic or regular so as to permit the impulse internodal transit time to remain at h/c.

A solution point is chosen within the mesh, as before, and the voltage at this node and the net current entering the node calculated as a straightforward summation i.e.

$$
\begin{aligned}
{}_kV\,(x,y) &= \sum_{j=1}^{4} {}_kV_j^r\,(x,y)\\
{}_kI_x(x,y) &= {}_kV_1^i\,(x,y) - {}_kV_3^i\,(x,y)\\
{}_kI_y(x,y) &= {}_kV_2^i\,(x,y) - {}_kV_4^i\,(x,y)
\end{aligned}
\qquad (5.3)
$$

with reference to fig. (3.9), and also providing normalised intrinsic impedances are used.

As time elapses the network becomes filled with impulses as they spread outwards from the source and are reflected from the boundaries, and the solution point 'sees' a stream of impulses.

These are stored as an output impulse function and consist of a sequence of delta function magnitudes placed in the time domain and separated by the time interval h/c, i.e. the impulse response of the network has been obtained. The output waveform corresponding to any input excitation may now be formed simply by convolving the impulse response with the shape of the input excitation.

Thus the output waveform due to a sinusoidal excitation may be obtained by convolving the output impulse function with the sinusoid and the response F(f) to such excitation may be formed simply by taking the Fourier transform of the output impulse function,

$$F(f) = \int_{-\infty}^{\infty} \delta(t - \frac{nh}{c}) e^{-jwt} \, dt.$$

$$\sum_{n=-\infty}^{\infty} \delta(t - \frac{nh}{c}) e^{-jwt}$$

since F(f) is a series of delta functions. The real and imaginary parts of the frequency spectrum then become

$$\mathrm{Re}(F(f)) = \sum_{n=1}^{N} {}_nV \cos(n\theta)$$

$$\mathrm{Im}(F(f)) = -\sum_{n=1}^{N} {}_nV \sin(n\theta) \qquad (5.4)$$

where ${}_nV$ is the amplitude of the output impulse response at time $t=nh/c$ and Nh/c is the total time for which the calculations are made and is analogous to the maximum number of reflections considered in the steady state method. The limits of summation in equation (5.4) arise because excitation is assumed to commence at time $t = 0$ and although the impulse function should ideally be taken to $t = \infty$, practically has to be truncated. θ is the internodal electrical length equal to wh/c.

Thus once the output impulse function has been obtained the response of the network to a sinusoidal excitation of any frequency may be obtained by the simple weighting and addition of these impulses by the sinusoidal waveform giving the spectral amplitude at that frequency.

For the configurations analysed in chapter 3, the theoretical response should consist of a series of delta function magnitudes in the frequency domain representing the modal cut-off frequencies of the various structures under analysis, and corresponding to the transverse resonance conditions of the one or two dimensional transmission line models utilised. However in a similar manner to that of chapter 3, truncation of the output impulse function causes these discrete modal cut-off frequencies to spread out into (sin x)/x type curves on the model.[41] Chapter 3 also indicated that the network of transmission lines was in effect a slow-wave structure exhibiting pass and stop bands. This analysis remains valid and for a regular network, which it must be in this case, to allow the internodal transit lines of the impulses to remain constant, the velocity characteristic for a wave travelling in a direction parallel to one of the transmission line directions is given by

$$\frac{v_n}{c} = \frac{\frac{1}{2}\Theta}{\sin^{-1}\left(\sqrt{2}\sin\frac{1}{2}\Theta\right)} \qquad (5.5)$$

where $\Theta = \frac{wh}{c}$ = internodal electrical length.

Thus the wave appears as if propagating in a medium of relative permittivity twice that of free space apart from an error defined by equation (5.5) which increases with frequency, the network

itself becoming cut-off when $\theta = \pi/2$. The remarks made previously regarding the propagation of waves in a diagonal direction across the matrix i.e. the velocity remains constant at $c/\sqrt{2}$ and the network does not exhibit pass/stop band characteristics, also still hold.

For the configurations examined that may be modelled by a strictly periodic network of transmission lines, where the internodal electrical length remains constant throughout the network, the steady state finite transmission line element method and the transient approach (known in the literature as the transmission line matrix method) are basically the same. However should the internodal electrical lengths differ throughout the network, then the delta function impulses will not arrive simultaneously at all of the nodes throughout the network and the method is defeated. This restricted the application of the transmission line matrix method to problems involving homogeneous waveguides and waveguides whose geometries have been made convenient for fitting on a square mesh. To describe more intricate boundary shapes two procedures were available to the user (1) to create more nodes and thus a better space discretization, but this is extremely wasteful regarding the already low computational store required, and (2) to provide a delay for pulses, i.e. to hold a pulse at a boundary for several time intervals before releasing it into the matrix again. However, this only provides for a shift of boundary of an integral number of transmission line lengths $h/2$, and again requires more store to provide the necessary impulse delays.

5. 2. TRANSIENT ANALYSIS APPLIED TO INHOMOGENEOUS WAVEGUIDES.

Inhomogeneous waveguide structures, however, have recently been analysed[47] utilising the transient approach, simply by introducing an additional open circuited stub to each node as shown in fig. (5.1) which is the model for a dielectrically slab loaded waveguide of fig. (4.1). The stubs are of length h/2 (thus preserving the impulse transit time) and of variable characteristic admittance Y_o relative to the normalised characteristic admittance of the main network of transmission lines. There are now five pulses incident on each node where the additional stub has been inserted and a revised version of equation (5.1) becomes

$$\begin{bmatrix} V_1 \\ V_2 \\ V_3 \\ V_4 \\ V_5 \end{bmatrix}^{r}_{k+1} = \frac{1}{Y_o+4} \begin{bmatrix} -(Y_o+2) & 2 & 2 & 2 & 2Y_o \\ 2 & -(Y_o+2) & 2 & 2 & 2Y_o \\ 2 & 2 & -(Y_o+2) & 2 & 2Y_o \\ 2 & 2 & 2 & -(Y_o+2) & 2Y_o \\ 2 & 2 & 2 & 2 & (Y_o-4) \end{bmatrix}_{k} \begin{bmatrix} V_1 \\ V_2 \\ V_3 \\ V_4 \\ V_5 \end{bmatrix}^{i} \qquad (5.6)$$

where V_1, V_2, V_3, V_4 represent the impulses in the original formulation and V_5 the impulse on the stub.

At low frequencies the effect of the stub is to add to each node an additional lumped shunt capacitance of CY_o h/2 where C is the total shunt capacitance per unit length of line for the main network of lines, which are of unity characteristic impedance. The total shunt capacitance at each node is therefore $2Ch(1+Y_o/4)$ and hence the low frequency velocity of waves, v_n, on the part of the network supporting the stubs becomes

$$v_n^2 = \frac{c^2}{2(1 + Y_o/4)} \qquad (5.7)$$

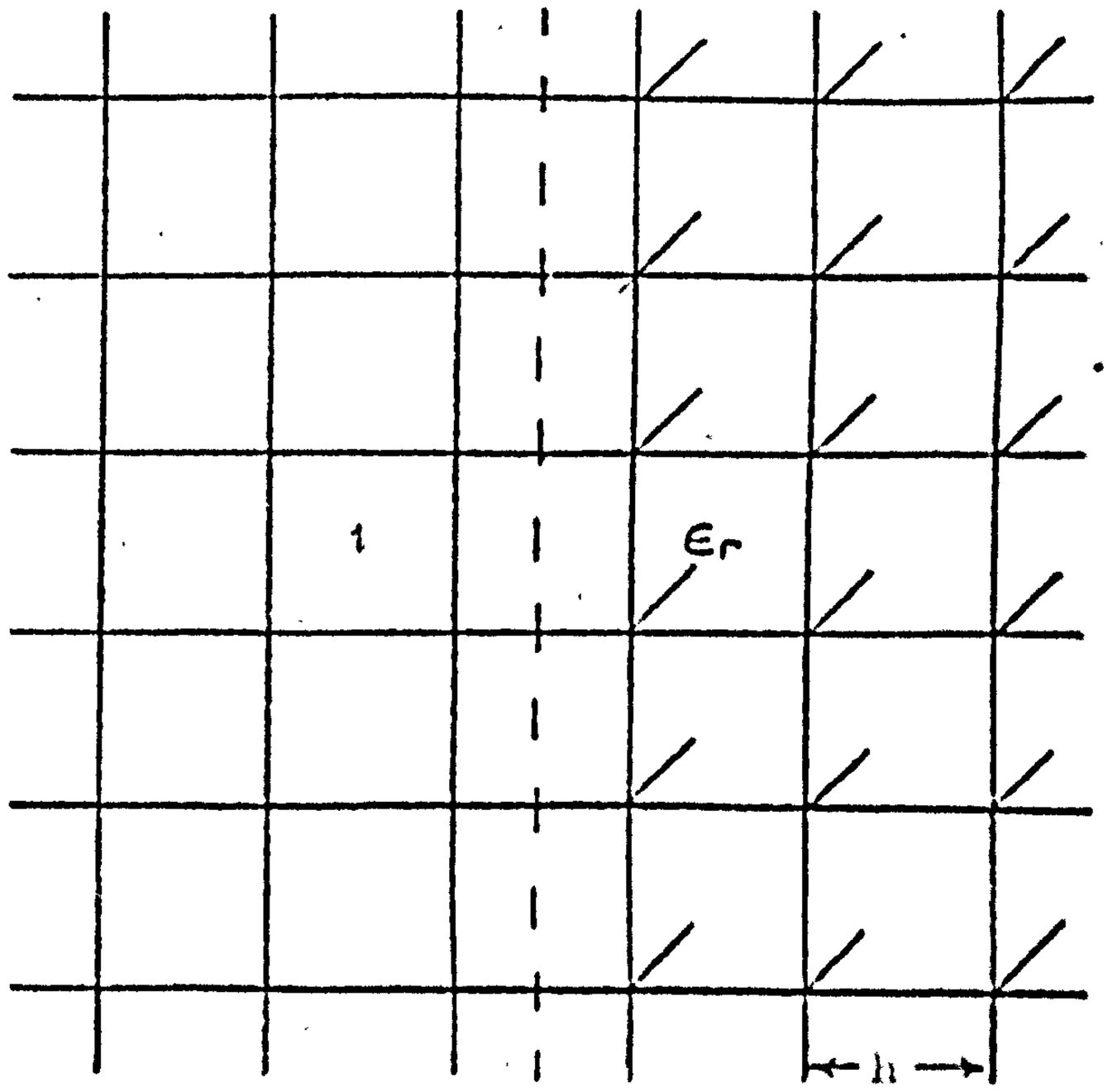

Fig. (5.1) Simulation of dielectric slab loaded rectangular waveguide by the addition of open circuited stubs.

and thus the velocity of the waves on the matrix is adjusted by altering the characteristic admittance of the stubs, Y_o.

Equation (5.7) however only determines the low frequency limit of the wave velocity. Johns[47] completes the velocity frequency characteristics for waves propagating parallel to one of the transmission line directions where

$$\frac{v_n}{c} = \frac{\theta/2}{\sin^{-1}\left\{\sqrt{2\left(1+\frac{Y_o}{4}\right)}\,\sin\frac{\theta}{2}\right\}} \tag{5.8}$$

and for waves travelling in a diagonal direction across the network

$$\frac{v_n}{c} = \frac{\theta/2}{\sin^{-1}\left\{\sqrt{1+\frac{Y_o}{4}}\,\sin\frac{\theta}{2}\right\}} \tag{5.9}$$

Equations (5.8) and (5.9) show that as the low frequency velocity is reduced by the action of the stubs so as to simulate the required dielectric permittivity, the useable frequency range also reduces. A result expected from fig. (3.8) which showed the decrease in frequency range due to an increase of capacitance in the system. It is imperative to note that although the low frequency velocity of propagation in a diagonal direction is $\sqrt{2}$ times that in the direction parallel to one transmission line direction, to travel a certain distance on the network in a diagonal direction, the waves on the individual transmission lines would have to travel $\sqrt{2}$ times that distance and hence the effective velocities in the two directions are the same.

The transient approach of the transmission line element method in solving inhomogeneous waveguide problems thus becomes highly restrictive when high dielectric permittivities are encountered due to

the small workable frequency range available, the limitations are however solely restricted to the amount of computational store that is available to the user.

The steady state transmission line element method does not possess this severe limitation since the geometry of the problem is unaltered, and as has been seen can utilize any value of permittivity.

At the dielectric boundaries, transmission and reflection coefficients have to be introduced in much the same manner as in the steady state approach, but modified according to ref: 47. Again since identities between the voltages and currents on the transmission line and Maxwells field equations within the structure examined exist only for two dimensionally varying fields, the method is limited to the calculation of cut-off characteristics or in some configurations the dispersive properties of the structure may be investigated.

5. 3. TRANSIENT ANALYSIS OF WAVEGUIDES WITH CURVED BOUNDARIES.

The transmission line matrix approach has been seen to solve waveguide problems where the transmission line network has described rectangular geometries and providing that it is a strictly periodic structure. The steady state finite transmission line element method however could remove the periodic restriction by simply correcting for the odd length of transmission line attached to the perimeter of the structure, and from chapter 4 can be seen to yield accurate solutions for the configurations under examination, namely those representing waveguides of circular and elliptical cross section.

In the transient approach, should the nodes defining the boundary lie outside the periodic nature of the network, i.e. the distance from the boundary to the boundary adjacent node is no longer h/2, the time taken for a delta function pulse to leave the boundary adjacent node, be reflected from the boundary and return to the node will differ from h/c. This presents difficulties since the impulses on the network do not possess identical internodal transit times and the output impulse function is no longer representative of the true network response. The difficulty is partially overcome by stipulating that the odd length of transmission line joining the network to the boundary be of length h/2, but that its characteristic admittance be altered to account for the difference between its true length and h/2. As in chapter 4, two cases need to be considered, the first where the boundary requires a short circuit termination of the odd length of line and secondly where the boundary requires the line to be terminated in an open circuit.

Considering a transmission line AB of length h/2 and of unity characteristic admittance as in fig. (5.2) and if B represents a short circuit termination, then the admittance at A, y_A, is given by

$$y_A = \frac{1}{j \tan (\theta\alpha/2)}$$

where $\theta = \frac{wh}{c}$ the electrical length of AB

Let A' B' be another line of length h/2 with characteristic admittance y on which waves propagate at the same velocity as on AB, fig. (5.2). If B' is also short circuited, then the characteristic admittance, y'_A, at A' is

$$y'_A = \frac{y}{j \tan (\theta/2)}$$

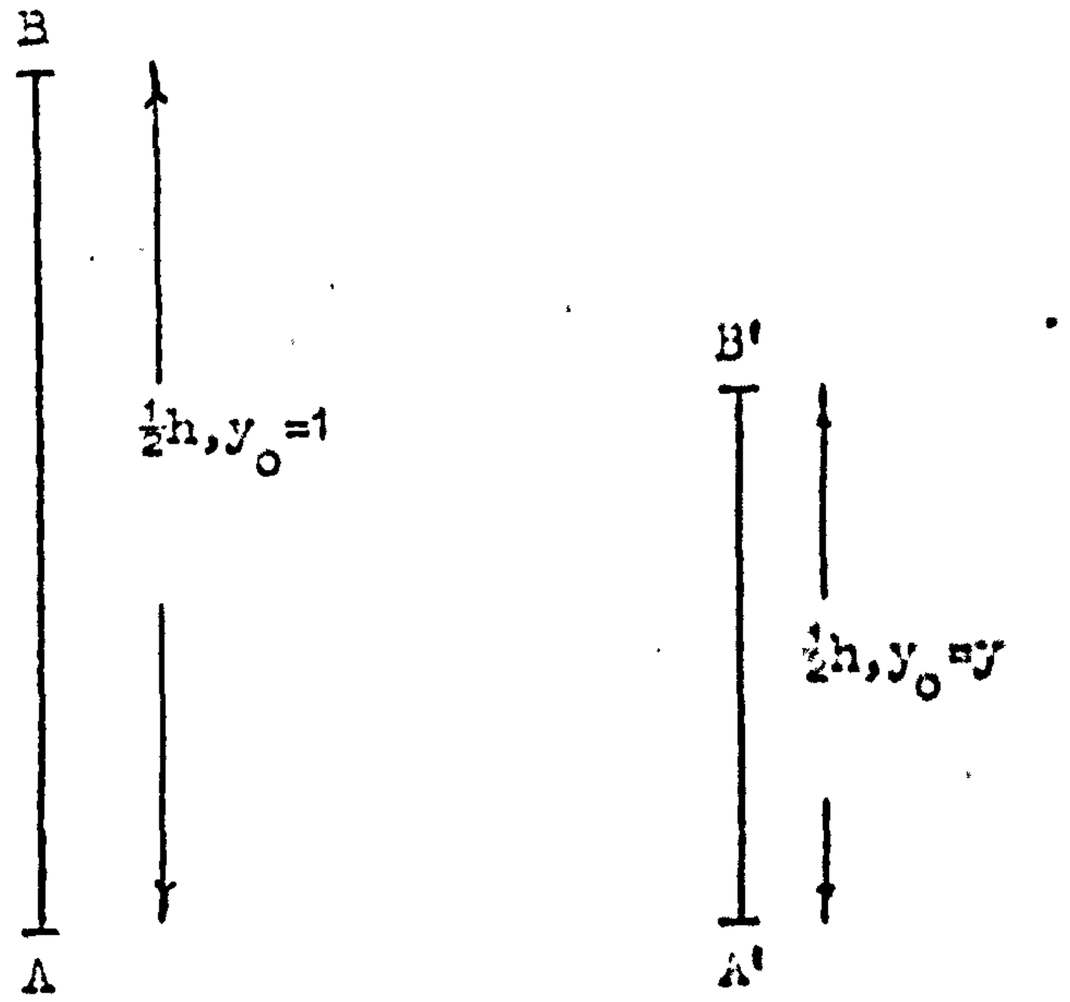

Fig. (5.2) Equivalence of transmission lines - a change in length being compensated for by a change in admittance.

Thus for $y_A = y'_A$

$$y = \frac{\tan(\theta/2)}{\tan(\theta\alpha/2)} \doteq \frac{1}{\alpha} \qquad (5.10)$$

at low frequencies.

Similarly if B and B' represent open circuit terminations

$$y_A = j \tan(\theta\alpha/2)$$

$$y'_A = jy \tan(\theta/2)$$

and

$$y = \frac{\tan(\theta\alpha/2)}{\tan(\theta/2)} \doteq \alpha \qquad (5.11)$$

for $y = y'_A$ at low frequencies.

These corrections although valid, provide only a partial correction to the odd lengths of transmission line and only allow the internodal transit times over the network to be identical. The reason for this incomplete correction may be appreciated by considering a wave propagating along a single periodically stub loaded line, with an odd length of line at one extremity being terminated in a short or open circuit. If this network was strictly periodic then as a slow wave structure, it would simulate a medium of permittivity twice that of free space. However by breaking the periodicity, by allowing the network to possess an odd length of line at the extremity then the change in characteristic admittance of this odd length enabling the structure to become strictly periodic (internodal transit times of the pulses are then identical), directly implies that there is a corresponding change in permittivity and thus the structure is no longer homogeneous.

The steady state approach to the same single stub loaded line does not suffer from this inhomogeneity since the simulated odd length of transmission line was assumed to contain the condition that the network as a whole simulated a medium of relative permittivity, 2, equation (4.17). Thus, ideally to provide a complete correction, the corrections noted in section (4.2) could have been applied so as to define an apparent length and then the corrections of this section applied to obtain a consistent impulse internodal transit time. However, inspection of fig. (4.6b) indicates that the apparent length may well be negative, which may be absorbed in the phase of the wave along such a line for the steady state method, but equation (5.11) directly implies the odd length of line possesses a negative characteristic admittance for the transient approach and the correction is thus meaningless for the pulse analysis of the network of this section.

For waves travelling in an arbitrary direction across the network, the break in periodicity presented by the odd lengths of line on the network causes the space being simulated by the slow wave structure to deviate from the nominal relative permittivity of 2 and in fact is no longer isotropic. This deviation might well be greater in the transient case than the steady state approach.

In the transient method of operating the transmission line matrix, if V_n^i is the magnitude of an incident delta function pulse on a node in the n_{th} coordinate direction, the node representing the intersection of four transmission lines of length h/2, but possessing characteristic admittances of y_i , i = 1,2,3,4, then the pulse V_n^r reflected into the n_{th} coordinate direction is given by

$$V_n^r = \sum_{m=1}^{4} T_m V_m^i - V_n^i \qquad (5.12)$$

where $T_m = \dfrac{2\, y_m}{\sum_{r=1}^{4} y_r}$ (5.13)

where y_m is the normalised admittance of the line in the m_{th} coordinate direction.

Should the four intersecting transmission lines possess unity characteristic admittance then equation (5.13) implies $T_m = \frac{1}{2}$ and equation (5.12) reduces to the familiar basis iterative scheme represented in equation (5.1).

Again recognizing that reflected pulses from one node become incident pulses on a neighbouring node according to equation (5.2) a complete iterative process may be manufactured from equations (5.12) and (5.2).

Utilising this technique, results have been obtained for both circular and elliptical waveguides, described on a cartesian mesh of intersecting transmission lines. The configurations used are those described by figs. (4.9) and (4.10) in the previous chapter. The odd lengths of transmission line joining the main network of transmission lines to the boundary of the structure being analysed are accounted for by a change in characteristic admittance of the odd length of line and stipulating that its length be h/2, according to equations (5.10) or (5.11). Considering the node i in fig. (4.9), the physical length of this odd length of line is 0.0707h measured in either coordinate direction. Thus to allow this odd length to become h/2, it must possess a characteristic

admittance of 0.1414 for short circuit terminations and 7.0721 for open circuit terminations, both admittances relative to the unity characteristic admittance of the transmission lines forming the main network. These admittances are then substituted into equation (5.13) so as to provide the relevant transmission coefficients in the iterative procedure.

Table (5.1) records the solutions for the cut-off wavelength of the quadrant of the circular waveguide, simulated by fig. (4.9), together with the solutions obtained by approximating the circular waveguide by a strictly periodic network fig. (4.11). The number of internodal transit times, or iterations was taken to be 500, and the radius was a = 5h. The number of nodes defining this structure was increased so as to provide an improved spatial discretization with a = 11h, and the solutions with and without the corrections of odd length also noted in Table (5.1), the number of iterationsbeing 1000 in this configuration to account for the increase in nodes, and thus reducing truncation error.

The elliptical waveguide of figs. (4.10) and (4.12) were also analysed, solving for the cut-off wavelength of the structure. Again an improved spatial discretization was adopted by doubling the length of the major and minor axes so as to provide the same eccentricity and results quoted for the configurations with and without line corrections. The solutions are noted in Table (5.2).

Figs. (4.11) and (4.12) both show that on the relatively coarse mesh used, the uncorrected boundaries differ considerably from the smooth curves of fig. (4.9) and (4.10). However the uncorrected boundary results in Tables (5.1) and (5.2) are reasonably accurate, and

TABLE (5.1).

Cut-off wavelengths ($a/\lambda c$) of circular waveguide with radius a. The configurations for a = 5h being modelled by figs. (4.9) and (4.11).

Mode	$a/\lambda c$ anal:	No correction applied				Corrections applied			
		a = 5h		a = 11h		a = 5h		a = 11h	
		$a/\lambda c$ num.	Error %	$a/\lambda c$ num.	Error %	$a/\lambda c$ num.	Error %	$a/\lambda c$ num.	Error %
TM_{01}	0.3828	0.3818	0.26	0.3828	0.0	0.3815	0.34	0.3826	0.05
TM_{11}	0.6099	0.6020	1.30	0.6093	0.10	0.6077	0.36	0.6091	0.13
TM_{21}	0.8174	0.8219	-0.55	0.8158	0.20	0.8159	0.18	0.8168	0.07
TM_{02}	0.8785	0.8653	1.50	0.8767	0.20	0.8679	1.21	0.8766	0.22
TM_{12}	1.1166	1.0976	1.70	1.1119	0.42	1.1099	0.60	1.1124	0.38
TM_{22}	1.3396	1.3219	1.32	1.3330	0.49	1.3280	0.87	1.3365	0.23
TE_{11}	0.2930	0.2816	3.89	0.2879	1.74	0.2834	3.28	0.2894	1.23
TE_{21}	0.4861	0.4645	4.44	0.4751	2.26	0.4741	2.47	0.4801	1.23
TE_{01}	0.6099	0.5978	1.98	0.6054	0.74	0.6024	1.23	0.6078	0.34
TE_{12}	0.8485	0.8169	3.72	0.8401	0.99	0.8332	1.80	0.8443	0.49
TE_{22}	1.0673	1.0330	3.21	1.0547	1.18	1.0603	0.66	1.0639	0.32
TE_{02}	1.1166	1.0611	4.97	1.1040	1.13	1.0887	2.50	1.1097	0.62

(k = 1) 500 iterations in circle with a = 5h. 1000 iterations in circle with a = 11h

TABLE (5.2)

Cut-off wavelengths ($a/\lambda c$) of elliptical waveguide modes of semi major axis a, eccentricity 0.6999
The configurations for a = 7h being modelled by figs. (4.10) and (4.12).

Mode	$a/\lambda c$ anal:	No corrections applied				Corrections applied			
		a = 7h		a = 14h		a = 7h		a = 14h	
		$a/\lambda c$ num.	Error %	$a/\lambda c$ num.	Error %	$a/\lambda c$ num.	Error %	$a/\lambda c$ num.	Error %
TM_{01} (even)	0.4650	0.4638	0.25	0.4667	-0.37	0.4648	0.04	0.4645	0.11
TM_{11} (even)	0.6776	0,6767	0.13	0.6762	0.21	0.6762	0.21	0.6770	0.09
TE_{11} (odd)	0.7986	0.7901	1.06	0.8020	-0.43	0.7934	0.65	0.7967	0.24
TE_{11} (even)	0,2962	0.2874	2.97	0.2890	2.43	0.2899	2.13	0.2924	1.28
TE_{11} (odd)	0.4039	0.3901	3.42	0.4008	0.76	0.3929	2.72	0.3991	1.19
TE_{01} (even)	0.7800	0.7563	3.04	0.7742	0.74	0.7634	2.13	0.7730	0.90

(h = 1)

500 iterations in ellipse with a = 7h

1000 iterations in ellipse with a = 14h

for TM mode types are of the same order, but note that in a few cases the uncorrected result has been very close to the analytical answer and in some cases the corrected result has not yielded an improved solution. The results for TE modes indicate that the corrections to the odd lengths are indeed worthwhile, the solutions for the corrected configurations generally being twice as accurate as those for the uncorrected configurations. Thus use of the correction procedure for the transmission line sections at the boundaries does produce consistent results.

The truncation error inherent in such processes is virtually eliminated in all these calculations due to the large number of iterations of the network taken. However the velocity errors exhibited by the network must still be present. This error, increasing with frequency, can be utilised so as to provide an upper bound to the correct solution. For the circular modes examined in Table (5.1) for a = 5h, the maximum velocity error is as high as 0% for the TM_{22} mode and 5% for the TE_{02} mode. The use of a finer mesh not only allows for a better description of the boundaries and fields within the structure as can be seen from the vastly improved accuracies presented by Tables (5.1) and (5.2), but also reduces the velocity error. The velocity error for the TM_{22} mode in the circular waveguide a = 11h, being 1.28% whilst the TE_{02} mode possesses a velocity error of 0.9%. Similar discussion also holds for the elliptical problems solved.

The final point to be noted from Tables (5.1) and (5.2) is that the solutions for TE modes are not as accurate for TM modes. Basically, the reason for this is the break in periodicity of the network that the odd lengths of line cause. This was noted at the beginning

of the section and reiterating briefly has the effect of simulating an anisotropic medium, where the velocity of the waves on the network do not possess their nominal value of $c/\sqrt{2}$. The steady state analysis of chapter 4 however indicated that the effect of the break in periodicity is much less serious for TM mode types than it is for TE mode types.

5.4. CONCLUSIONS.

The transient approach to the transmission line element method can be seen to provide solutions to a wide variety of wave guide problems, simply by impulsing a network of intersecting transmission lines and forming the impulsive output response which is examined for periodicities corresponding to resonant conditions. It has been shown that it is similar to the steady state approach derived and examined in chapters 3 and 4, but the flexibility of possessing a variable internodal length on the mesh is destroyed in the transient approach, since the internodal transit times of the individual impulses on the network must at all times be equal. This lack of flexibility manifests itself in many ways, particularly in those structures which possess inhomogeneities and odd lengths of transmission line to describe waveguides with arbitrary boundary shapes.

The restrictions in solving dielectric loaded waveguides stemmed from the introduction of an open circuited stub at each node simulating the dielectric, the action of which served to reduce the velocity of the wave traversing that part of the network representing the dielectric. The presence of the stub however reduced the usable frequency range of the system and thus for any arbitrary inhomogeneous system, the transient transmission line matrix method is restricted to

low values of permittivity such that the frequency range does not become overly limited. The steady state method, however does not possess such a stringent restriction since the geometry of the problem remains unaltered, and account is made for the permittivity by adjusting the internodal electrical length, implying that any value of permittivity may be investigated.

Both the steady state and transient approachs, however suffer from the inability to provide the dispersive characteristics of inhomogeneously loaded waveguides. Whereas an idea was proposed of overcoming this deficiency in the steady state method, by recognising that two transmission line meshes might be analysed simultaneously, one solving for the field components H_z, E_x, E_y and the other solving for E_z, H_x, H_y, with transfers occurring between the two described by Maxwells equations. These transfers were envisaged to be made simply by replacing the operator $j(=\sqrt{-1})$ in Maxwells equations, by operating on the phase of the relevant wave by $\pi/2$. This proposal however, is invalid in the transient approach, and recourse would have to be made to the suggestion of developing a three dimensional mesh, such that dispersive properties may be investigated.

The method is currently being adapted to provide solutions of waveguiding systems possessing wall losses[48]. This is accomplished by allowing the line terminations at the nodes defining the boundary of the waveguide to possess reflection coefficients other than those of 1 or -1 assumed for the perfectly conducting boundaries of the systems analysed here. The reflection coefficient in this case possesses both a real and imaginary part and for small losses the imaginary part may be

neglected. A strictly periodic network is utilised and the transient approach to the transmission line element method is applied with solutions obtained to a good degree of accuracy. However, should the losses become large, such that the imaginary part of the reflection coefficient can no longer be neglected, then recourse to the steady state method will have to be made, such that the corresponding phase change in the wave reflected from the boundaries may be correctly accounted for. Further research being performed also permits the introduction of lossy dielectrics, also analysed by the transient approach, simply by allowing the pulse travelling between nodes in the dielectric to suffer an appropriate decrease in magnitude, but again no account is taken for a change in phase, again for which the steady state approach could easily manage. Note that in these calculations, since the reflection coefficients are generally frequency dependent, the network has to be solved for each frequency.

It was seen that the transient approach could cater for odd lengths of line necessary to describe arbitrarily shaped waveguide cross sections. The correction applied, stipulated that the length of line was such that the periodic nature of the network remained intact, but that its characteristic admittance be altered so as to compensate for the alteration of length. This however produced slight difficulties since the change in admittance produced a discontinuity in permittivity on the parts of the network where the odd length was situated. The discussion in section (5.2) relating to inhomogeneous waveguides, indicated that for a rise in permittivity the usable

frequency range of the network became severely limited, and therefore the possibility arises, that in correcting for the odd lengths of line where the change in characteristic admittance simulates a change in medium, that the network may be operated at a frequency, such that the part of the corrected network is under cut-off conditions. The steady state approach may also suffer in the same manner for wave propagation in an arbitrary direction over the network, since both models represent an anisotropic medium, but comparison of results for the circular and elliptical waveguides examined indicate that the steady state method is generally the more reliable, and that the corrections applied provide a more consistent and improved set of solutions than if the configuration were to be approximated by a strictly periodic network.

The transient approach possesses one advantage over the steady state method, in that the network only has to be solved once to obtain an output impulse function and this is examined for periodicities corresponding to resonant conditions. The steady state method requires the response of the network to be solved for each individual frequency considered, and because of the number of trigonometrical calculations required to account for the vectorial addition of the four incident waves at each node of the network, is extremely time consuming. The amount of computational store required by the two methods is also of importance; the steady state method requiring twice as much as the transient method in order to store the phases as well as the magnitude of the waves on each individual transmission line.

It may thus be concluded that the steady state method of the transmission line element technique is the more powerful despite the much longer machine run time and increase in store required, since this method is capable of performing all the analysis demonstrated by the transient approach and as it is not as restrictive, may be utilised to provide solutions to a far wider range of configurations.

CHAPTER 6.

CONCLUSIONS.

The use of networks to solve electromagnetic field problems is not a radically new idea, but was developed in the 1940's notably by Kron[49] and others.[50,51,52] However their use was confined to an actual network analyser study, where a network of discrete components was used to simulate various waveguide configurations. Analysis was performed on this network in much the same manner as was done here, namely by exciting the network by a sinusoidal generator and examining the frequency response by sweeping through the frequency range, and obtaining the fields by measurement of the voltages and currents on the network.

The advent of digital computers caused a wane in such analysis, since the network analyzers tended to be cumbersome in size, and relatively awkward to build to manage the wide variety of boundary problems possible. Engineers thus turned to the computers to solve the field equations necessary for the solution of waveguiding systems, and developed many fine techniques, especially that of finite differences.

This thesis, however, has shown the feasibility of utilizing the ideas introduced by those concerned in network analyzer studies, with a computer simulated technique. The steady state transmission line element method however evolved from finite difference/element techniques whereby the linear spatial variation of potentials over a mesh describing the structure was replaced by a circular function variation and that the mesh was then in fact a mesh of intersecting transmission lines.

The basic alteration of the function describing the field variations, subsequently produced numerous advantages of this method over more well established techniques, notably these associated with the ease of formulation and solution of the various structures, the relatively coarse mesh and hence low computationalstore required and the solution of higher ordered propagating modes with no extra requirements made on the user. All these are of vital importance to the engineer seeking solutions to a particular microwave problem.

The first section of this work briefly reviewed the finite difference and finite element techniques and stressed the large amount of expertise needed to formulate the problem and also that required to solve the resulting system of simultaneous equations. A three dimensional cavity was solved for but the formulation used proved to be too restrictive for a general approach to be attempted. The steady state transmission line element method however was shown to be formulated through basic transmission line theory and proved to be simple in conception and manipulation and the manner in which this was evolved could provide a means by which the finite difference/element methods could be utilised so as to reduce the storage of such methods and possess much the same advantages as the present method.

The comparison of storage requirements between the two methods was quoted in Chapter 3, the transmission line element method requiring less than 1/20 of that required by finite differences/elements, for a similar spatial discretization of the structure, and yields solutions to a far better accuracy. For circular or elliptical geometries, the structure was described in a cartesian mesh and the results again show an improvement on finite differences/elements, even when considerable

trouble has been taken to approximate the boundaries by varying the shapes and sizes of the elements[9] or arms of the finite difference mesh.[55] The calculation of any field component within the structure is also an attractive feature of the method and usually relies on the addition of four numbers or the subtraction of two numbers depending on the component. The finite difference/element techniques however, since they rely solely on finding the complete steady state field description must involve some numerical integration procedure to obtain one field component from the one being solved for.

It was shown that the method could be adapted so as to compute various losses present within a waveguide, and reference (45) utilises the transient approach so as to compute impedance characterisation of various waveguide configurations including bifurcations. Perhaps an interesting point to raise, and one worthy of further work, is that of utilising an irregular mesh of transmission lines, irregular in the manner that it is periodic of a certain mesh pitch in one coordinate direction and periodic but of a different mesh pitch in the other coordinate direction, this has the effect of allowing waves propagating over the network to possess different velocities in either direction thus simulating an anisotropic medium.

The steady state (and the transient) approach to the transmission line element method however did possess several disadvantages as was noted in the solution of some inhomogeneous structures, where only the cut-off characteristics could be solved for, but use could perhaps, be made of Csendes and Silvester's Modal Approximation Technique[54] so as to compute the fields above cut-off conditions, a technique not utilised here.

The manufacture of the steady state conditions within the structures were obtained by considering multiple reflected waves traversing the network of transmission lines, simulating the waveguide. The discretization of the medium into such a mesh effected a slow wave structure representing a medium of relative permittivity 2, thus causing the wave traversing the network to possess a velocity $c/\sqrt{2}$ apart from an inherent velocity error which was dependent on the frequency of operation and provided an upper bound to the solutions obtained. Truncation of the order of reflections, caused the spreading out of the ideal response of such a simulated system into $(\sin x)/x$ type curves situated about the resonant frequencies of the structure. Thus the requirements for a low velocity error to be met implies an improved spatial discretization such that the frequency of solution is lowered, which in turn yield high truncation errors and can only be reduced by increasing the number of reflections considered. In all the investigations performed here, the number of reflections considered were chosen such that the truncation error was minimal.

Comparison of the steady state and transient approaches to the transmission line element method indicated that the former was more versatile, since it could perform identical calculations to those of the transient method, and also possessed the facility to cope with more structural configurations containing high permittivities, high losses, arbitrarily shaped boundaries and a means of solving the dispersive characteristics of dielectric loaded guides without recourse to three dimensional analysis. The disadvantage of the steady state approach, however, is the relatively long machine run time required, since the network must be solved for each frequency examined.

It is proposed that if some procedure can be found such that the computations are performed at a vastly improved rate, the steady state transmission line element method must appeal to the design engineer for accurate solutions of a wide variety of waveguide characteristics of any arbitrary shaped configuration.

Finally, although the method has been applied essentially to electromagnetic field problems, it may be adapted to form an analysis of thermal or mechanical problems[55], or even provide solutions of Schrödinger's wave equation[56]. Again it must be emphasised that the method, even though in its infancy, has been shown to possess a remarkable degree of versatility and affords not only the user with a powerful numerical technique, but also the potential researcher to develop the method and ideas raised throughout this project.

REFERENCES.

1. Forsythe, G.E., and Wasow, W.R.:
Finite Difference Methods for Partial Differential Equations.
Wiley, 1960.

2. Motz, H. :
Calculation of the Electromagnetic Field, Frequency and Circuit Parameters of High Frequency Resonator Cavities.
Proc. IEE., 1946, Vol. 93, pp 335 - 343.

3. Collins, J.H., and Daly, P. :
Calculation for Guided Electromagnetic Waves using Finite Difference Methods.
J. Electronics Control, 1963, Vol. 14, pp 361 - 380.

4. Davies, J.B., and Muilwyk, C.A.;
Numerical solution of uniform hollow waveguides with boundaries of arbitrary shape.
Proc. IEE, 1966, Vol. 113, pp 277 - 284.

5. Sinnott, D.H., Camprell, G.K., Carson, C.T., and Green, H.E.:
The Finite Difference Solution of Microwave Circuit Problems.
IEEE Trans. 1969, MTT - 17, pp 464 - 478.

6. Corr, D., Davies, J.B., and Muilwyk, C.A.:
Finite-Difference Solution of Arbitrarily Shaped Dielectric Loaded Waveguides, including Microstrip and Coaxial Structures.
Alta Frequenza, 1969, Vol. 38, pp 318 - 322.

7. Zienkiewicz, O.C., and Cheung, Y.K. :
Finite Elements in the Solution of Field Problems.
The Engineer, 1965, 221, pp 507 - 510.

8. Zienkiewicz, O.C., and Cheung, Y.K.:
The Finite Element Method in Continuous Structural Mechanics.
McGraw - Hill, 1967.

9. Silvester, P. :
Finite Element Solution of Homogeneous Waveguide Problems.
Alta Frequenza, 1969, Vol. 38, pp 313 - 317.

10. Arlett, P.L., Bahrani, A.K., and Zienkiewicz, O.C. :
Application of finite elements to the solution of Helmholtz's equation.
Proc. IEE, 1968, Vol. 115, pp 1762 - 1766.

11. Ahmed, S., and Daly, P. :
Waveguide Solutions by the Finite-element method.
Radio Electron Engr. 1969, Vol. 38, pp 217 - 223.

12. Davies, J.B. :
Review of Methods for numerical solution of the hollow - waveguide problem.
Proc. IEE, 1972, Vol. 119, pp 33 - 37.

13. Hornsby, J.S., and Gopinath, A. :
Numerical Analysis of a Dielectric-Loaded Waveguide with a Microstrip Line - Finite - Difference Methods.
IEEE Trans. 1969, MTT - 17, pp 684 - 690.

14. Fox, L. :
Numerical Solution of Ordinary and Partial Differential Equations.
Pergamon, 1962.

15. Ahmed, S., and Daly, P, :
Finite Element Methods for inhomogeneous waveguides.
Proc. IEE, 1969, Vol. 116, pp 1661 - 1664.

16. Morse, P.M., and Feshbach, H. :
Methods of Theoretical Physics.
McGraw - Hill, 1953. chapt. 3.

17. Wilson, E.L., and Nickell, R.E. :
Application of the Finite Element Method to heat conduction analysis.
Nucl. Eng. Des., 1966, Vol. 4, pp 276 - 286.

18. Silvester, P. :
High-order polynomial triangular elements for potential problems.
J. Inst. Engng. Sci., 1969, Vol. 7, pp 849 - 861.

19. Daly, P., and Helps, J.D., :
Exact Finite - element solutions to Helmholtz's equation.
Inst. J. Num. Meth. Eng. 1973, Vol.6(4), pp 529 - 542.

20. Peters, G., and Wilkinson, J.H. :
Eigenvalues of $Ax = \lambda Bx$ with band symmetric A and B.
Computer J., 1969, Vol. 12, pp 398 - 404.

21. Silvester, P. :
Biharmonic Operators for the Waveguide Problem.
IEEE Trans. 1970, MTT - 18, pp 63 - 64.

22. Beaubien, M.J., and Wexler, A. :
An Accurate Finite-Difference Method for Higher Order waveguide modes.
IEEE Trans. 1968, MTT - 16, pp 1007 - 1017.

23. Collin, R.E.:
Field Theory of Guided Waves.
McGraw - Hill, 1960, chapt. 6.

24. Marcuvitz, N, :
Waveguide Handbook.
McFraw-Hill, 1951.

25. Wilkinson, J.H., and Reinsch, C. :
Handbook for Automatic Computation (Vol.2)
Springer-Verlag, 1971.

26. IEEE Trans., 1955, MTT-3, March.

27. Hayt, W.H. :
Potential Solution of a Homogeneous Strip Line of Finite Width.
IEEE Trans., 1955, MTT-3, July, pp 16 - 18.

28. Motz, H. :
The treatment of singularities of partial differential equations by relaxation methods.
Quart. J. Appl. Math., 1947, Vol. 4, pp 371 - 377.

29. Whiting, K.B. :
A treatment for singularities in Finite-difference solutions of Laplace's equation.
IEEE Trans., 1968, MTT-16, pp 889 - 891

30. Daly, P. :
Hybrid-Mode analysis of Microstrip by Finite-Element Methods.
IEEE Trans., 1971, MTT-19 pp 19 - 25.

31. Davies, J.B., and Corr, D.G. :
Computer Analysis of the fundamental and higher order modes in single and coupled microstrip.
Elec. Letts., 1970, Vol. 6, No. 25, pp 806 - 808.

32. Silvester, P. :
TEM wave properties of microstrip transmission lines.
Proc. IEE, 1968, Vol. 115, pp 43 - 48.

33. Wheeler, H.A. :
Transmission-Line Properties of Parallel Strips separated by a Dielectric Sheet.
IEEE Trans. 1965, MTT-13, pp 172 - 184

34. Yamashita, E., and Mittra, R. :
Variational Method for the Analysis of Microstrip Lines.
IEEE Trans., 1968. MTT-16, pp 251 - 256.

35. Bryant, T.G., and Weiss, J.A. :
Parameters of Microstrip Transmission Lines and of Coupled Pairs of Microstrip Lines.
IEEE Trans., 1968, MTT-16, pp 1021 - 1027.

36. Bryant, T.G., and Weiss, J.A. :
Even and Odd Mode Characteristic Impedance for Coupled Microstrip.
The Microwave Engineers' Handbook and Buyers Guide,
Feb. 1970, pp 35 - 36.

37. Ahmed, S. :
The Finite Element Method for Waveguide Problems.
Ph.D. Thesis, University of Leeds, 1969.

38. Sinnott, D.H. :
The use of Interpolation in Improving Finite Difference Solutions of TEM Mode Structures.
IEEE Trans., 1969, MTT-17, pp 20 - 28.

39. Carré, B.A.,
The Determination of the Optimum Accelerating Factor for Successive Over-relaxation.
Computer J., 1961, Vol. 4, pp 73 - 78.

40. Collin, R.E. :
Foundations for Microwave Engineering.
McGraw - Hill, 1966, chapt. 8.

41. Johns, P.B. :
Application of the transmission-line-matrix method to homogeneous waveguides of arbitrary cross-section.
Proc. IEE, 1972, Vol. 119, pp 1086 - 1091.

42. Chu, L.J. :
Electromagnetic waves in elliptical hollow pipes of metal.
J. Appl. Phys., 1938, Vol. 9, pp 583 - 591.

43. Kretzschmar, J.G. :
Wave propagation in hollow conducting elliptical waveguides.
IEEE Trans., 1970, MTT-18, pp 547 - 554.

44. Davies, J.B., and Kretschmar, J.G. :
Analysis of hollow elliptical waveguides by polygon approximation.
Proc. IEE, 1972, Vol. 119, pp 519 - 522.

45. Johns, P.B., and Beurle, R.L. :
Numerical solution of 2 dimensional scattering problems using a transmission line matrix.
Proc. IEE, 1971, Vol. 118, pp 1203 - 1208.

46. Johns, P.B. :
The transmission-line-matrix method of waveguide analysis.
Ph.D. Thesis; to be submitted to the University of Nottingham, October 1973.

47. Johns, P.B. :
The solution of inhomogeneous waveguide problems using a transmission-line matrix.
IEEE Trans. 1974, MTT-COMP. to be published.

48. Akhtarzad, S., and Johns, P.B. :
Transmission line matrix solution of waveguides with wall losses.
Elec. letts. 1973, Vol. 9, No. 15, pp 335 - 336

49. Kron, G. :
Equivalent Circuit of the Field Equations of Maxwell - 1.
Proc. IRE, 1944, 32, pp 289 - 299.

50. Whinnery, J.R., and Ramo, S. :
A New Approach to the Solution of High Frequency Field Problems.
Proc. IRE, 1944, 32, pp 284 - 288.

51. Whinnery, J.R., Concordia, C., Ridgway, W., and Kron, G.,
Network Analyzer Studies of Electromagnetic Cavity Resonators.
Proc. IRE, 1944, 32, pp 360 - 367.

52. Spangenberg, K., Walters, G., and Schott, F. :
Electrical Network Analyzer for the Solution of Electromagnetic Field Problems.
Proc. IRE, 1949, 37, pp 724 - 729.

53. Beaubien, M.J., and Wexler, A. :
Unequal-Arm Finite Difference Operators in the Positive-Definite Successive Over-relaxation (PDSOR) algorithm.
IEEE Trans., 1970, MTT-18, pp 1132 - 1149.

54. Csendes, Z.J., and Silvester, P. :
Numerical Solution of Dielectric Loaded Waveguides: Pt.2 - Modal. Approximation Technique.
IEEE Trans., 1971, MTT-19, pp 504 - 509.

55. Vitkovitch, D. :
Field Analysis.
Van Nostrand, 1966, chapt. 7.

56. Kron, G. :
Electric Circuit Models of Partial Differential Equations.
Elec. Eng. 1948, 67, pp 672 - 684.

PRINCIPAL SYMBOLS.

$\underline{e}_x, \underline{e}_y, \underline{e}_z,$	unit base vectors of a three dimensional rectangular coordinate system.
$\underline{e}_r, \underline{e}_\alpha, \underline{e}_z,$	unit base vectors of a three dimensional cylindrical coordinate system.
$\underline{E}$	electric field vector.
$\underline{B}$	magnetic flux density vector.
$\underline{D}$	electric displacement vector.
$\underline{H}$	magnetic field strength vector.
$\underline{J}$	current density vector.
ρ	charge density.
ϵ_o, ϵ_r	absolute and relative permittivities.
μ_o, μ_r	absolute and relative permeabilities.
w	angular frequency.
α	attenuation constant.
β	phase constant.
$\gamma = \alpha + j\beta$	complex propagation constant.
∇	Laplacian operator.
∇_{xy}	Two dimensional Laplacian operator, inx and y.
c	Velocity of light in free space.
λ_o	Free space wavelength.
λ_g	Wavelength of guided wave.

APPENDIX.

Sample program for steady state finite transmission line element method.

To provide completeness, and also aid the user of the steady state transmission line element method, the following program is reproduced. This program calculates the response of a periodic network simulating the rectangular waveguide of fig. (4.8). It is reproduced in its simplest form for the purpose of clarity. Note that the storage matrices VRX, PRX, etc., may be eliminated and replaced by appropriate one dimensional matrices together with a little more logic, thus reducing the store required, and that the variable odd lengths of transmission line of chapter 4, may be written in, by manipulation of the phases when the boundary conditions are being initialized for each order of reflection considered.

```
C   SOLUTION OF RECTANGULAR WAVEGUIDE PROBLEM
C
C   (IHX,IHY): SIZE OF NETWORK
C   (IX,IY),(FX,FY): POSITION OF EXCITATION AND OBSERVATION
C   NODE RESPECTIVELY
C   NI: MAXIMUM NO. OF REFLECTIONS CONSIDERED
C   V : MAGNITUDE OF INPUT WAVE
C   THETA: FREQUENCY OF OPERATION
C   VR(X,Y),PR(X,Y) ETC.: MATRICES STORING MAGNITUDE
C   &PHASE OF NODE INCIDENT WAVES ON 4 COORDINATE DIRECTIONS
C   VRX(X,Y),PRX(X,Y) ETC.: AS ABOVE BUT PROVIDES STORAGE
C   FOR WAVES UNTIL EACH ORDER OF REFLECTION HAS BEEN
C   CONSIDERED THROUGHOUT NETWORK
C   BR,BL,BU,BD: REFLECTIONS COEFFS. AT EXTREMITIES OF
C   STRUCTURE TO ACCOUNT FOR ELEC./MAG. WALLS
C
      DIMENSION VR(9,7),VL(9,7),VD(9,7),VU(9,7),
     X   PR(9,7),PL(9,7),PD(9,7),PU(9,7),
     X   VRX(9,7),VLX(9,7),VDX(9,7),VUX(9,7),
     X   PRX(9,7),PLX(9,7),PDX(9,7),PUX(9,7)
```

```
      INTEGER X,Y,FX,FY
C
CC   DATA ACCEPTANCE
C
      CALL HEAD(IHX,IHY,IX,IY,FX,FY,NI,V,BL,BR,BU,BD)
    5 WRITE(1,200)
  200 FORMAT(30H     THETA1      THETA2       THINT,//)
      READ(1,100)THETA1,THETA2,THINT
  100 FORMAT(3F10.4)
      THETA=THETA1
C
CC  NULLIFY MATRICES
C
    6 CALL XNULL(VR,VL,VD,VU,PR,PL,PD,PU,
     X   VRX,VLX,VDX,VUX,PRX,PLX,PDX,PUX,IHX,IHY)
      TV=0.0
      TP=0.0
      IHX1=IHX-1
      IHY1=IHY-1
C
CC   INITIALIZE EXCITATION
C
      VR(IX,IY)=V
      VL(IX,IY)=V
      VD(IX,IY)=V
      VU(IX,IY)=V
      DO 4 IC=1,NI
C
CC   INITIALIZE BOUNDARY REFLECTION COEFFS.
C
      DO 1 X=2,IHX1
      PU(X,1)=PD(X,2)
      VU(X,1)=VD(X,2)*BD
      PD(X,IHY)=PU(X,IHY1)
    1 VD(X,IHY)=VU(X,IHY1)*BU
      DO 2 Y=2,IHY1
      PL(IHX,Y)=PR(IHX1,Y)
      VL(IHX,Y)=VR(IHX1,Y)*BR
      PR(1,Y)=PL(2,Y)
    2 VR(1,Y)=VL(2,Y)*BL
C
CC   SUMMATION OF INCIDENT WAVES AT SOLUTION NODE FOR
CC   EACH ORDER OF REFLECTION
C
      CALL PVX(VR(FX,FY),VU(FX,FY),VL(FX,FY),VD(FX,FY),
     X   PR(FX,FY),PU(FX,FY),PL(FX,FY),PD(FX,FY),FV,FP)
C
CC   AMPLITUDE OF WAVE AT SOLUTION NODE FOR ALL REFLECTIONS
C
      P=0.0
      CALL PVX(TV,FV,P,P,TP,FP,P,P,VXY,PXY)
      TV=VXY
      TP=PXY
C
CC   FORM AMPLITUDE & PHASE OF REFLECTED WAVES AT EACH
CC   NODE OVER NETWORK
C
```

```
      DO 3 Y =2,IHY1
      DO 3 X=2,IHX1
      P1=PD(X,Y+1)+THETA
      P2=PU(X,Y-1)+THETA
      P3=PL(X+1,Y)+THETA
      P4=PR(X-1,Y)+THETA
      V4=-VR(X-1,Y)
      CALL PVX(VD(X,Y+1),VU(X,Y-1),VL(X+1,Y),V4,
     X   P1,P2,P3,P4,VXY,PXY)
      VLX(X,Y)=0.5*VXY
      PLX(X,Y)=PXY
      P1=PR(X-1,Y)+THETA
      P2=PD(X,Y+1)+THETA
      P3=PU(X,Y-1)+THETA
      P4=PL(X+1,Y)+THETA
      V4=-VL(X+1,Y)
      CALL PVX(VR(X-1,Y),VD(X,Y+1),VU(X,Y-1),V4,
     X   P1,P2,P3,P4,VXY,PXY)
      VRX(X,Y)=0.5*VXY
      PRX(X,Y)=PXY
      P1=PR(X-1,Y)+THETA
      P2=PU(X,Y-1)+THETA
      P3=PL(X+1,Y)+THETA
      P4=PD(X,Y+1)+THETA
      V4=-VD(X,Y+1)
      CALL PVX(VR(X-1,Y),VU(X,Y-1),VL(X+1,Y),V4,
     X   P1,P2,P3,P4,VXY,PXY)
      VUX(X,Y)=0.5*VXY
      PUX(X,Y)=PXY
      P1=PR(X-1,Y)+THETA
      P2=PL(X+1,Y)+THETA
      P3=PD(X,Y+1)+THETA
      P4=PU(X,Y-1)+THETA
      V4=-VU(X,Y-1)
      CALL PVX(VR(X-1,Y),VL(X+1,Y),VD(X,Y+1),V4,
     X   P1,P2,P3,P4,VXY,PXY)
      VDX(X,Y)=0.5*VXY
      PDX(X,Y)=PXY
    3 CONTINUE
C
C     TRANSFER AMPLITUDE & PHASE OF WAVES INTO
C     WORKING MATRICES
C
      DO 4 I=1,IHX
      DO 4 J=1,IHY
      VR(I,J) = VRX(I,J)
      VL(I,J) =VLX(I,J)
      VU(I,J) = VUX(I,J)
      VD(I,J) = VDX(I,J)
```